MECHANISTIC ANALYSIS OF THE ROLE OF FRATAXIN IN BACTERIAL AND EUKARYOTIC FE-S CLUSTER BIOSYNTHETIC PATHWAYS

A Dissertation

by

SHACHIN PATRA

Submitted to the Office of Graduate and Professional Studies of
Texas A&M University
in partial fulfillment of the requirements for the degree of

DOCTOR OF PHILOSOPHY

Chair of Committee,	David P. Barondeau
Committee Members,	Tadhg Begley
	Frank M. Raushel
	Paul A. Lindahl
Head of Department,	Simon W. North

August 2018

Major Subject: Chemistry

ABSTRACT

Iron-sulfur (Fe-S) clusters are essential cofactors and are found in all branches of life. In eukaryotes, Fe-S assembly complex is composed of NFS1, ISD11, ACP, ISCU2, and FXN subunits. NFS1 is a cysteine desulfurase that utilizes a PLP cofactor to extract sulfur from its cysteine substrate and produce a persulfide species on a cysteine residue of a mobile S-transfer loop. Sulfur is then transferred from the mobile S-transfer loop of NFS1 to ISCU2, where it is combined with ferrous iron and electrons to generate [2Fe-2S] clusters. ISD11 and ACP are critical for the stability of the Fe-S assembly complex and may modulate NFS1 function. Eukaryotic ISC pathway is characterized by low activity of SDA and significant rate enhancement by FXN in presence of ISCU2. Prokaryotic cysteine desulfurase IscS (59% identity) stable without accessory proteins and highly active. Interestingly, both FXN and homolog CyaY activates/inhibits the eukaryotic/prokaryotic Fe-S assembly respectively.

Here, we investigated the role of FXN/CyaY in each step of Fe-S biosynthesis. We found that S-transfer loop cysteine participates in cys-aldimine formation, cys-quinonoid decay, persulfide formation on itself, and transfer of this sulfane sulfur to scaffold protein. Interestingly, in eukaryotes, FXN enhances all these steps but not as fast as IscS. All these data support a model in which monomeric cysteine desulfurase architecture (such as in SDA_{ec}) promotes non-productive conformations of S-transfer loop of cysteine desulfurase resulting in low activity. FXN binding (in eukaryotic system) excludes non-productive conformations and directs the trajectory of the NFS1 mobile S-transfer loop to position the cysteine to function as a general acid, nucleophile, and sulfur delivery agent in different steps and accelerates Fe-S cluster biosynthesis. In prokaryotes, because of the closed architecture, the other subunit of cysteine desulfurase regulates S-transfer loop

trajectory (better than the FXN in eukaryotic system) and therefore have high activity even in absence of FXN. Consistent with this, $IscS^{S10Q}$ variant exhibits significantly weaker dimer interface, and concentration dependent enhancement of dimer concentration and activity. Also, data indicate that reduced FDX2 is probably not the electron source but sensitizer of persulfide on scaffold protein towards reduction by reduced glutathione.

DEDICATION

This dissertation is dedicated to my parents whose constant encouragement and support were invaluable during my Ph.D.

ACKNOWLEDGEMENTS

I would like to acknowledge my advisor Prof. David Barondeau for giving me the opportunity to do research in his lab on a really interesting project and giving me the platform to develop myself as an independent researcher. I would also I would like to thank my committee members, Prof. Tadhg Begley, Prof. Frank Raushel and Prof. Paul Lindahl for their helpful suggestions, support and guidance throughout my career at Texas A&M.

Additionally, I must also acknowledge Prof. Tadhg Begley for allowing me to use of his radio-HPLC, CD spectrometer, and stopped flow apparatus. We also thank Dr. Rung-yi Lai and Dr. Jamison P Huddleston for their assistance with the radio-HPLC and KinTek software, respectively.

I would like to thank my colleagues from the Barondeau lab, past and present, specially Dr. Deepika Das for their helpful discussions, criticism and suggestions, which were invaluable for my research.

Finally, I would like to thank my friends, family for their amazing support.

CONTRIBUTORS AND FUNDING SOURCES

This work was supervised by a dissertation committee consisting of Professor David Barondeau [advisor] and Professor Tadhg Begley, Professor Frank Raushel and Professor Paul Lindahl [committee members].

All the experiments involving iron sulfur cluster formation or transfer (monitored by CD) were conducted and analyzed by Dr. Deepika Das.

All other work conducted for the dissertation was completed by the student independently.

Graduate study was supported by NIH, NSF and Welch foundation grants.

TABLE OF CONTENTS

LIST OF FIGURES

Page

LIST OF TABLES

CHAPTER I

INTRODUCTION AND LITERATURE REVIEW

IRON SULFUR CLUSTER

Iron sulfur clusters are one of the most ancient and versatile cofactors found in nature. As the name suggests, these cofactors consist of iron and sulfur, more specifically a combination of ferrous and ferric irons and sulfide. The iron centers have tetrahedral coordination geometry and can bind a maximum of four ligands. Sulfides act as bridging ligand and can occupy 2-3 coordination sites. The rest of the coordination sites are filled by mostly protein-based ligands although small molecule ligand such as glutathione is also known to coordinate iron sulfur cluster. Most common of the protein-based ligands are cysteine, which coordinates through side-chain thiol. Other less frequently found ligands are histidine (ligation by side-chain imidazole), aspartic acid (ligation by side-chain carboxylate), serine (ligation by side-chain hydroxyl group) and even α-amino group of amino acids. The simplest of iron sulfur clusters are $[Fe_2S_2]$ and $[Fe_4S_4]$, which also happens to be the most common type. There are several other forms of iron sulfur clusters, which are more complex in nature and found only in a number of proteins. Examples include $[Fe_3S_4]^0$ (glutamate synthase), $[Fe_8S_7]$ (P-clusters of nitrogenase), $[MoFe_7S_8C]$ (M-clusters of nitrogenase) and $[NiFe_3S_4]$ (C-cluster of CODH). However, they are involved in some of the most important chemistries found in nature, such as N_2 fixation and carbon monoxide oxidation.

Iron sulfur clusters are redox cofactors capable of adopting multiple redox states and can easily perform one or two electron redox reactions. Because of the variety of iron sulfur cluster type, they come with a broad range of redox potentials. On one end of the spectrum, we have $[Fe_4S_4]^{2+/1+}$ clusters which can be highly reducing (E_m = -700 mV). On the other end of the

spectrum, we have HiPIPs ($[Fe_4S_4]^{3+/2+}$), which can be highly oxidizing (E_m = 400 mV, Ferredoxin thioredoxin reductase). Other cluster types have somewhat intermediate redox potential. Redox potential of iron sulfur clusters also depends on ligation. For example $[Fe_2S_2]^{2+/1+}$ have more reducing having redox potential (in the range of -460 mV to -200 mV) when they are coordinated with cysteine. However, in Rieske type cluster where one of the irons is coordinated with two histidine residues, the redox potential become more positive and can reach up to +300 mV. Redox potential of iron sulfur cluster also depends on solvation and the extent of hydrogen bonding. Both bridging sulfides and coordinating irons ligands are excellent candidates for hydrogen bond formation, which in turn depends on the extent of solvation. Therefore, mutation of amino acid residues near the cluster, complex formation with another protein molecules, substrate binding can change the solvation pattern around iron sulfur cluster and in turn change the redox potential of the clusters. Redox potential also depends on the geometry of both the cluster and the ligands. Any effect that can bring about a conformational change in the protein structure, can change the geometry of the ligands and thereby the redox potential of the cluster. All the above points illustrate the flexibility and tenability of redox potential of iron sulfur cluster, which makes them ideal candidates for the medium of electron transfer process.

In addition to being excellent in redox chemistry, Iron sulfur clusters can also perform several other functions, which are essential for cell viability. For example, iron sulfur clusters can function as a catalytic site for substrate binding and activation. In the $[Fe_4S_4]$ cluster of aconitase, three irons are coordinated by three cysteine residues and the remaining iron is coordinated by water. This iron (called unique Fe site) provides the coordination site for substrate binding, which is followed by dehydration/hydration chemistry. Radical SAM enzymes also provide excellent examples of substrate binding by iron sulfur cluster. Here methionine amino acid binds that unique

Fe site bidentately via α-amino and α-carboxilato groups. Iron sulfur clusters have also been utilized as a mechanism for iron storage. Methanogenic archaea champion this by expressing polyferredoxin, which contain up to 12 [Fe_4S_4] clusters in tandemly repeated 8-Fe ferredoxin like domain[1-2]. Iron sulfur clusters are also used as a substrate. Examples include biotin biosynthesis, lipoic acid biosynthesis. Iron sulfur clusters especially [Fe_4S_4] are very susceptible towards oxidative damage, which degrades them primarily to [Fe_2S_2]. This usually is accompanied by a large conformation change. This property has been utilized by proteins to act as a sensor of oxidative stress (example FNR). All these make iron sulfur cluster one of nature's most versatile and important cofactor.

BIOSYNTHETIC PATHWAYS OF IRON SULFUR CLUSTER

NIF pathway

In earlier days of evolution, the world used to be anaerobic and iron and sulfur were abundant in their reduced form (ferrous iron and sulfide). This vast pool of sulfide and ferrous iron were probably utilized to make iron sulfur clusters. However, this process is not efficient. It requires a lot of material and the production of the desired iron sulfur cluster cannot be controlled. Under laboratory conditions, the combination of ferric iron with sulfide often leads to a much larger polymeric species with an unspecific stoichiometry of iron and sulfur. This polymeric species is not soluble and therefore if produced, will be deposited in the cell and this, in turn, will interfere with the normal cellular process. It is no surprise that a biosynthetic mechanism has evolved, which will give rise to desired iron sulfur cluster species under controlled conditions with minimum side products.

Iron sulfur cluster biosynthesis machinery was first identified in nitrogen-fixing bacterium *Azotobacter vinelandii*. A systematic analysis of the genes co-expressed with the structural components (*nif*H, *nif*D, *nif*K) of nitrogenase led to the discovery of the nitrogen-fixation-specific (*nif*) gene cluster (*nif*USVWZM)[3-4]. Later on, inactivation of individual genes in the nif gene cluster led to a very interesting observation. Except for nifU and nifS, all other gene inactivation resulted in defects of either P-cluster or M-cluster. However, deletion of either nifU or nifS caused a substantial loss of activity of both P-protein and MoFe-protein. As both P-cluster and M-cluster are more complex iron sulfur cluster, it was concluded that both NifU and NifS function in the formation of small and simple iron sulfur clusters unit, which then can be combined by P-cluster and M-cluster specific maturation genes to produce P-cluster and M-cluster respectively[5]. Subsequent purification and biochemical analysis revealed that (1) NifS contains PLP cofactor, (2) NifS takes up L-cysteine as substrate and produces L-alanine and under reducing conditions also produces sulfide, (3) an active site cysteine is essential for its activity, mutation or alkylation of this cysteine leads to inactivation of the enzyme and (4) it contains persulfide after incubation with cysteine. This led to the conclusion that NifS catalyzes desulfurization of cysteine and hence NifS was termed as cysteine desulfurase. Similar biochemical analysis of NifU revealed that it can accommodate the formation of a transient iron sulfur cluster and thereafter designated as scaffold protein[6].

ISC pathway

The incomplete loss of nitrogenase activity upon deletion of NifS and NifU suggested that there might be some house-keeping iron sulfur cluster biosynthetic pathway operating at a very slow rate under nitrogen-fixing condition. Therefore, a search under non-nitrogen-fixing

conditions with nifS deleted strain led to the discovery of another cysteine desulfurase. Further genetic experiments[7] revealed that this newly found cysteine desulfurase gene is a part of an operon[8], which was named as ISC (Iron Sulfur Cluster) operon indicating their involvement in iron sulfur cluster biosynthesis pathway[7]. This operon contained nine genes, now designated as cysE2, IscR, IscS, IscU, IscA, hscB, hscA, fdx and iscX. Except for cysE2, expressions of all other genes are regulated by iscR. Subsequent biochemical and genetic studies demonstrated that isc genes are involved in the biosynthesis of iron sulfur clusters in general[9] and thereby act as a housekeeping system. IscR turned out to be a transcription regulator that regulates the expression of all the genes in isc operon including itself except cysE2. CysE2 was found to be involved in cysteine biosynthesis and separately regulated. IscS is a PLP dependent cysteine desulfurase[10] that bears considerable sequence identity with first identified cysteine desulfurase NifS. IscU has a high sequence similarity with the first domain of NifU and acts as a scaffold protein. IscA has been postulated to be an alternate scaffold[11] and a site for converting two [Fe_2S_2] clusters into [Fe_4S_4] cluster by two-electron reduction coupling[12-15]. HscB and HscA share sequence identity with DnaJ and DnaK, which acts as chaperon. This prompted to hypothesize that HscB and HscA might act as co-chaperon and chaperon respectively and helps in cluster delivery to target protein by bringing about a conformational change in either cluster bound IscU or apo-target protein in an ATP dependent manner[16-18]. Interestingly isc operon encodes for fdx gene[19] that expressed a [Fe_2S_2] containing ferredoxin, which has been shown to be essential and speculated to take part in electron delivery during iron sulfur cluster biosynthesis. IscX has been shown to inhibit iron sulfur cluster biosynthesis and may have some regulatory role. Later on, genome-wide search revealed *isc* operon to be a part of many other bacterial genomes, solidifying its role as the housekeeping iron sulfur cluster biosynthetic pathway.

SUF pathway

Consistent with their housekeeping role, deletion of IscS and IscU in *Azotobacter vinelandii* proved to be fatal. However, when IscS and IscU were deleted, the resulting strain of *E. coli* remained viable. This observation led to the discovery of another iron sulfur cluster biosynthesis pathway, called SUF system (Sulfur Utilization Factor). In *E. coli suf* operon consist of *sufA, sufB, sufC, sufD, sufS* and *sufE*. SUF system was found to be involved in biosynthesis, protection and repair of iron sulfur clusters under the condition of oxidative stress or iron starvation.

IRON SULFUR CLUSTER BIOSYNTHETIC PATHWAYS IN EUKARYOTES

In eukaryotes, iron sulfur cluster assembly takes place mainly in mitochondrial matrix space and involves about 10 proteins. The members of this pathway are – NFS1[20], ISD11[21], ACP, ISCU2, FXN, FDX2[22], FDXR[23], HSC20[24], HSP75, GRX5, ISCA1/2[25] and ABC7[20, 26]. Most of these proteins bear high sequence identity to the proteins encoded by bacterial *isc* operon and therefore this mitochondrial iron sulfur cluster biosynthetic pathway was defined as ISC pathway. The genes involved in this process are nuclear encoded and imported into mitochondria using mitochondrial-targeting sequence (MTS) as a guide. Proteins first get unfolded and enter mitochondria. MTS is then cleaved by mitochondrial processing peptidases and the resultant mature proteins are folded back to their active form in a chaperon-mediated pathway. As expected, mitochondrial ISC pathway is more complex than bacterial and involves several eukaryotic specific proteins or proteins of bacterial origin that now has a new function.

NFS1 is the cysteine desulfurase[27] required in this process. It is a 47 kD homo-dimer and bears 59% sequence identity with *E. coli* IscS. It contains a PLP cofactor and reacts with cysteine as substrate to produce alanine and a persulfide on the active site cysteine, which is situated on a mobile loop. NFS1 by itself is very unstable and readily precipitated when recombinantly expressed in *E. coli*. ISD11 is a three-helix bundle eukaryotic specific protein with a molecular weight of 11 kD. It is positively charged at physiological pH (estimated pKa = 10.73) and has conserved Leucine-Tyrosine-Arginine (LYR) motif at the N-terminus, which makes it a member of the LYR family of proteins. Knockout and knockdown studies confirmed that ISD11 is essential[21, 28-29] for viability and has function in mitochondrial iron sulfur cluster biosynthetic pathway. It forms a stable complex with NFS1, called **SD** (NF**S**1 + IS**D**11) and has been proposed to stabilize NFS1. Additionally, ISD11 has also been proposed to activate the mobile loop cysteine on NFS1[30-32]. Acyl Carrier Protein (ACP), a small 10 kD protein known for its requirement in type II fatty acid synthesis (FAS), has recently been characterized to have a moonlighting function in iron sulfur cluster biosynthesis through complex formation with NFS1 and ISD11 with a final stoichiometry of 1:1:1. This three-protein complex **SDA** (NF**S**1 + IS**D**11 + **A**CP) has been characterized as the functional cysteine desulfurase unit for iron sulfur cluster biosynthesis. ACP has a 4'-phosphopentethiene (4'-PPT) prosthetic group covalently bound to a conserved serine residue. This 4'-PPT forms a thioester linkage with fatty acid during fatty acid synthesis (FAS). In the crystal structure of SDA complex, a 16-carbon long fatty acid covalently bound to ACP through 4'-PPT was found to be inserted into the hydrophobic core of ISD11 created by the unusual conformation of the three helixes. At the end of this hydrophobic core, there is a conserved phenylalanine residue that is connected to the active site of NFS1 through hydrogen bonding. It

was proposed that ACP might regulate iron sulfur cluster biosynthesis by regulating cysteine desulfurase activity by varying the chain length of the bound fatty acid[33].

ISCU2 is the scaffold protein, which is 70% identical with *E. coli* IscU. ISCU2 has three cysteine residues (C35, C61 and C104) which are conserved in all organisms and required for coordination with the [Fe_2S_2]. ISCU2 binds with SDA in 1:1 stoichiometry to form SDAU complex.

There are two A-type proteins in human mitochondria, ISCA1 and ISCA2, which function in maturation of [Fe_4S_4] along with IBA57 (**I**ron sulfur cluster assembly factor for **b**iotin synthase and **a**conitase-like mitochondrial protein, molecular weight 57 kD)[34-35]. ISCA2 is similar to ISCA1 except a 21-residue insert, which makes their function non-redundant. *E. coli* homolog IscA can complement for ISCA1 but not for ISCA2. ISCA has also been shown to bind one iron (0.86 ± 0.24) per dimer with an association constant of at least 2 x 10^{19} M^{-1}, which is comparable with E. coli IscA (1 x 10^{19} M^{-1}) and human transferrin (4.7 x 10^{20} M^{-1})[36-37].

HSP70 and HSC20 are homologous to *E. coli* HscA and HscB respectively. This chaperon/co-chaperon system has been shown to accelerate [Fe_2S_2] transfer from ISCU2 to GRX5. However, details of this transfer process is still unknown. GRX5 is a monothiol glutaredoxin homologous to Grx4 in *E. coli* and has been shown to act as an intermediate during iron sulfur cluster delivery to different apo-acceptor. ABC7 is an ABC transporter, specific to eukaryotes and absolutely critical for cell viability, is present in the mitochondrial outer membrane. It has been postulated that it acts as a gate for an unknown sulfur compound, which needs to be released from mitochondria into the cytosol for further iron sulfur biosynthesis process, known as CIA pathway. Although postulated as a second iron sulfur cluster biosynthetic pathway in eukaryotes, its

dependence on mitochondrial pathway raises question if the CIA pathway should be considered a separate pathway or an extension of mitochondrial ISC pathway.

FRIEDREICH'S ATAXIA (FRDA) AND FRATAXIN

Friedreich's ataxia (also called FRDA) is an autosomal recessive neurodegenerative disorder and most common form of ataxia. It has been estimated in Europe one in 50,000 people suffer from this disease and one in every 120 people are deduced carrier. Symptoms of this disease include gait, limb ataxia, lack of tendon reflexes and sense of position and hypertrophic cardiomyopathy. Symptoms first appear usually around puberty and by the age of 20 the patient becomes confined in a wheelchair and wait for a slow and painful death, as there is no cure. A gene called X25 was identified at chromosome 9q13 –q21.1, had an abnormally long GAA triplet repeats in the first intron and impaired transcription profile most likely because of the abnormal intronic expansion. This gene contained 5 exons and encoded 210 amino acid proteins, which was named frataxin[38]. Normally there are 7-40 repeats of GAA triplet. However, for some FRDA patients the repeat can reach up to 1700.[39] It was later established that the number of repeats inversely correlated with expression levels of the protein frataxin.[40] Larger the repeat, lower is the expression. This confirmed that loss of frataxin would cause FRDA. More than 95% FRDA patient are homozygous i.e. both the allele contains abnormal GAA triplet repeat. However, a small fraction of FRDA patient patients were found to be heterozygous i.e. one allele contains abnormally GAA triplet repeat and the other allele contains missense or nonsense mutation[41].

This breakthrough in FRDA research led to extensive biochemical characterization of the frataxin gene. First by tagging a GFP protein, frataxin was found to be targeted towards mitochondria[42]. Expansion of this study to human, mouse and yeast revealed frataxin function in

mitochondria and this is universal phenomenon[43]. Proteins targeted to mitochondria generally contain a highly arginine and lysine-rich positively charged targeting sequence. Amino acid sequence revealed that frataxin also has one and it is 55 amino acids long. After frataxin enters mitochondria, the first 40 residues of this mitochondrial targeting sequence are cleaved by a mitochondrial processing peptide (MPP)[44]. The resultant polypeptide (41 – 210) undergoes a second truncation step to yield the final mature form, which contains residues 82 – 210[45-47]. This mature form is however unfolded during mitochondrial entry and efficiently refolded with the help of Tim44 and mtHSP70 proteins[48].

Function of frataxin and its involvement in FRDA has been the center of debate for a long time. Frataxin has been proposed to be a regulator of iron homeostasis in mitochondria as its deletion resulted into severe impairment of iron flux[49-50]. Excessive iron accumulation in mitochondria in frataxin-deleted strains led to the proposal of frataxin being an iron storage protein[51]. Genome-wide analysis of gene expression has shown frataxin deficiency results in elevated levels of proteins, especially iron uptake proteins that are under control of iron sensing transcription factors such as ATF1/ATF2[52-54]. The fact that these transcription factors are induced under low cytosolic iron condition led to the proposal that frataxin is involved in maintaining the efflux of iron from mitochondria into cytosol. One common side effect of excess iron accumulation in frataxin-deficient cells has been damaged by reactive oxygen species (ROS). Therefore, frataxin has also been proposed to have a function in ROS detoxification[55-56]. Frataxin deficiency also resulted in deficiency of mitochondrial iron sulfur protein such as aconitase[57]. However, as it was known that ROS could damage aconitase [Fe4S4] cluster, it was not known for sure if the deficiency in iron sulfur protein was because of oxidative damage from ROS or because absence of frataxin impaired. Later on, it was conclusively shown that indeed frataxin play an important

role in iron sulfur cluster biosynthesis in mitochondria[58-60] and all other phenotype could be explained by this. Iron-binding properties of yeast frataxin[61] and impaired iron homeostasis in frataxin-deficient mitochondria later led to the proposal of frataxin being iron chaperon[62-63] and iron donor[64] during iron sulfur cluster biosynthesis. However, iron binding of frataxin is not stoichiometric and depending on the source, frataxin can bind 0-16 iron suggesting iron binding can be an artifact of the carboxylic acid patch of frataxin[64-67]. Indeed, iron donor and iron storage role of frataxin is later refuted convincingly[68].

A paradigm shift in frataxin function discovery occurred when frataxin was found to form a complex with cysteine desulfurase complex (SDA) in presence of ISCU2[69-71] and act as an allosteric activator[70] of the cysteine desulfurase[72]. Frataxin were able to accelerate the rate of cysteine desulfurase activity by 5 times and in the presence of ferrous iron, the rate went up to about 10 times. In vitro iron sulfur cluster formation assay showed an equivalent acceleration for SDAUF complex compared to SDAU, establishing acceleration of cysteine desulfurase activity by frataxin was sufficient to explain the role of frataxin in iron sulfur cluster biosynthesis. Later on, it was found that frataxin variants found in FRDA patients had weaker binding to cysteine desulfurase complex and also failed to accelerate cysteine desulfurase activity to same extent as wild-type frataxin[73-74]. This further solidified frataxin's function as an allosteric activator. However, about same time frataxin homolog in *E. coli* CyaY were found to an inhibitory effect on iron sulfur cluster biosynthesis despite not having any impact on cysteine desulfurase activity[75]. This puzzle was solved after a very interesting discovery that acceleration or inhibition by frataxin/CyaY was dependent on the cysteine desulfurase[76]. So, with IscS both CyaY and frataxin inhibited iron sulfur cluster biosynthesis whereas with SDAU, both CyaY and frataxin accelerated iron sulfur cluster biosynthesis. To account for the allosteric activator function of frataxin research

was focused in mainly two areas – 1) it was tested if frataxin can accelerate persulfide formation on the mobile loop cysteine of NFS1 and 2) if frataxin can accelerate the transfer of sulfane sulfur from mobile loop cysteine of NFS1 to ISCU2 or small molecule thiols. Cysteine binding ability of the active site PLP was tested in presence and absence of frataxin and it was found that frataxin increased the amount of cysteine bound to PLP and thereby concluded that frataxin facilitates cysteine binding to the active site[31]. It has also been proposed that frataxin helps orienting the mobile loop of NFS1 and thereby accelerate C-S bond cleavage of the cysteine substrate, which in turn results in increased rate of persulfide generation on mobile loop cysteine. However, any kind evidence has not been presented till date in support of the above-mentioned hypothesis. Evidence for frataxin's function as accelerator of sulfur transfer first emerged when radioactive ^{35}S was incubated with SDAUF and found increased radioactivity on ISCU2[77]. However, presence of excess thiol which can act as sulfur transfer agent and increased radioactive labeling on NFS1 raised doubt if enhanced radioactive labeling on ISCU2 is because of acceleration of sulfur transfer step or as a downstream effect of enhanced cysteine desulfurase activity. Later on, similar result was obtained in another elegant study. However, the extent of increase in persulfide content on ISCU2 compared to NFS1 clearly showed that it could not be explained by acceleration of cysteine desulfurase activity alone and frataxin must accelerate sulfur transfer step[78]. The same study also showed accelerated reduction of NFS1 persulfide by DTT in presence of frataxin[78]. Therefore, it was concluded that frataxin accelerates iron sulfur cluster biosynthesis by accelerated release of sulfide which is utilized in making iron sulfur cluster. After all these years of rigorous research, still there has not been a unanimous conclusion about the function of frataxin.

FRATAXIN BYPASS

Frataxin function discovery drew a considerable attention of the scientific community mostly because of the prospect of drug discovery for Friedreich's Ataxia. A serendipitous discovery of a variant of Isu protein in yeast, which could alleviate the phenotype of frataxin deletion in absence of frataxin, also became very interesting. While experimenting with a frataxin-deleted yeast strain, it was observed that some of the colonies out-grew others. A followed-up detailed genetic analysis revealed that a single amino acid residue (M107) on Isu underwent a spontaneous mutation to different amino acids such as isoleucine, leucine, and valine and that single mutation was responsible for the observed frataxin bypass phenomena[79]. It was later shown in an *in vitro* experiment that M107I variant of Isu in yeast could increase cysteine binding to PLP, just like frataxin[31]. This gave rise to the hypothesis that M107I variant of Isu (M106I in human ISCU2) acts like frataxin and can replace frataxin. Frataxin was hypothesized to cause a conformational change in wild-type ISCU2 that activated cysteine desulfurase and M106I variant of ISCU2 was postulated to be already in that conformation and therefore activated cysteine desulfurase even in absence of frataxin.

MECHANISM OF IRON SULFUR CLUSTER BIOSYNTHESIS

Although we have a pretty good idea about the functions of the proteins involved in iron sulfur cluster, there is not much known about the chemistry that happens during iron sulfur cluster biosynthesis. We know cysteine reacts with the PLP cofactor of NFS1 to generate a persulfide on the mobile loop cysteine. A mechanism of cysteine desulfurase activity had been proposed based on the work with NifS. However, no further work has been done to prove or disprove that mechanism. It is well known with PLP-dependent enzymes that amino acid residues surrounding

PLP cofactor play important role in protonation and deprotonation of PLP that has a profound effect on the activity of the enzyme. No systematic analysis of residues in cysteine desulfurase has been done to evaluate their effect on cysteine desulfurase activity, which in turn could help to figure out the exact mechanism of cysteine desulfurase activity.

There has been a considerable amount of debate whether or not sulfur transfer from NFS1 mobile loop cysteine to ISCU2 is actually a part of iron sulfur cluster biosynthesis pathway. ISCU2 has their conserved cysteines – C35, C61 and C104 (C37, C63 and C106 in *E. coli* IscU). Evidence has been produced for all three cysteines residue to be the acceptor of sulfane sulfur by different groups[77, 80-81]. Not only that, these cysteine residues were shown to contain polysulfide. However, all the experiments were carried out in excess of cysteine. Therefore, the observations could be explained by a thiol-mediated sulfur transfer event where cysteine (or other small molecule thiols) can cleave NFS1 persulfide to generate cysteine persulfide, which now can distribute that sulfane sulfur to any available thiol. The finding that frataxin can accelerate sulfur transfer to small thiols such as DTT even led to the proposal that thiol-mediated sulfur transfer is actually the physiological way if iron sulfur cluster biosynthesis[78]. However, DTT being a non-physiological molecule raised the possibility than this is a DTT dependent phenomena and physiological thiol such as cysteine and glutathione may behave differently. Also, so far nobody has demonstrated under similar condition using physiological thiol one pathway is faster that other one. There had been another debate on whether or not the iron sulfur cluster biosynthesis followed iron-first mechanism or sulfur first mechanism i.e. whether ISCU2 obtains the sulfur before it binds iron (sulfur-first) or after it binds iron (iron-first). The fact that elevated levels of persulfide is formed on ISCU2 in presence of frataxin and in absence of iron settled the debate in favor of sulfur-first mechanism[77].

[Fe_2S_2] gets both sulfurs from cysteine via a persulfide intermediate on NFS1. To generate two sulfide molecules from two persulfides requires four electrons. Since ferrous iron is used as substrate[82] and in the final cluster it is found in +3 oxidation state, we can assume that two of the required four electrons come from two ferrous irons. The source of the remaining two electrons has not been conclusively proven. Ferredoxin (both in *E. coli* and yeast) has been shown to be required for iron sulfur cluster biogenesis[22, 83-85]. Therefore, it was postulated that ferredoxin along with ferredoxin reductase and NADPH delivers the remaining two electrons. Evidence has been provided with both *E. coli* and human system in support of electron donating ability of NADPH-ferredoxin reductase-ferredoxin system[85-86]. However, the overall rate and the amount of [Fe_2S_2] bound ISCU2 produced in that reaction has been very small when compared with thiols (cysteine or glutathione) as reducing system. Chemically reduced ferredoxin (both in *E. coli* and human) has also been shown to be able to reduce persulfide on the mobile loop cysteine of cysteine desulfurase[87-88]. One would expect a stoichiometric transfer of electrons from reduced ferredoxin to persulfide to generate sulfide i.e. one equivalent of sulfide production from two equivalents of reduced ferredoxin. However, the experiment generated much more sulfide than one would expect from the amount of reduced ferredoxin used. Also, this experiment did not provide any account of what happens to ISCU2 persulfide up on treatment with reduced ferredoxin. In a different experiment, using a novel gel-based assay to detect persulfide bound to protein, reduced ferredoxin was shown not to be able to cleave persulfide on both NFS1 and ISCU2[78]. Additionally, ferrous iron alone and together with reduced ferredoxin also failed to reduce persulfide on both NFS1 and ISCU2[78].

Another unknown, related to the mechanism of iron sulfur cluster biosynthesis is the stoichiometry of ISCU2 when it has a [Fe_2S_2] cluster. ISCU2 has been shown to exist as a monomer

or dimer with one [Fe_2S_2] cluster per monomer or dimer respectively[89]. ISCU2 dimer has also been proposed to be the physiological iron sulfur cluster source for all iron sulfur protein in mitochondria although the evidence is weak. The major problem with the idea of ISCU2 monomer as a scaffold is the lack of a fourth ligand. All of the conserved cysteines have been shown through mutational analysis to be essential for iron sulfur cluster synthesis on ISCU2 and therefore they were hypothesized to form three of the four available coordination to [Fe_2S_2] cluster. Different residues had been proposed as the fourth ligand, which includes H107, D37 and even the mobile loop cysteine of cysteine desulfurase[90]. The fact that the D37A mutation on IscU produces an even more stable cluster rule out D37 as the fourth ligand[91]. Resonance Raman analysis of [Fe_2S_2] bound IscU showed a higher stretching frequency than normally found for thiol (cysteine) ligation. It was interpreted, as the fourth ligand must be smaller than sulfur i.e. either oxygen or nitrogen. H107 is in proximity and can ligate through imidazole side chain. However, if imidazole coordinates, the stretching frequency will be even lower as the whole imidazole moiety acts as a single unit and not just a nitrogen atom[92]. Considering proximity to the cluster oxygen ligation is the only explanation for the fourth ligand. However, no such residue has been identified to date that fits these criteria.

CHAPTER II

MECHANISM FOR ACTIVATION AND BYPASS OF FRATAXIN IN HUMAN FE-S CLUSTER BIOSYNTHESIS

INTRODUCTION

Iron sulfur (Fe-S) clusters are ubiquitous protein cofactors that are required for critical cellular processes [93-94]. Fe-S clusters exist in a variety of stoichiometries, most often as [2Fe-2S]$^{2+/1+}$ and [4Fe-4S]$^{2+/1+}$ species, and commonly function in substrate activation and in electron transfer. Fe-S clusters are synthesized and distributed to apo target proteins by conserved biosynthetic pathways. In humans, an assembly complex located in the mitochondrial matrix is responsible for synthesizing Fe-S clusters. The structural core of this assembly complex consists of cysteine desulfurase (NFS1), eukaryotic-specific LYR protein (ISD11), and acyl carrier protein (ACP) subunits and is referred to as the SDA complex [33, 95]. The ISD11 and ACP subunits are required for function, stabilize NFS1, and favor different quaternary interactions for NFS1 than its prokaryotic homologs [33, 96-99]. NFS1 uses a pyridoxal 5'-phosphate (PLP) to convert L-cysteine to L-alanine and generate a persulfide intermediate on a cysteine residue of a mobile S-transfer loop (**Figure II-1, step 1**). Sulfur is then transferred from NFS1 to a cysteine residue on the scaffold protein ISCU2 (**Figure II-1, step 2**). ISCU2 combines sulfane sulfur with Fe^{2+} and electrons to produce [2Fe-2S]$^{2+}$ clusters [72, 77, 100] (**Figure II-1, step 3**) in a poorly understood process. To complete catalytic turnover, intact [2Fe-2S] cluster intermediates on ISCU2 are transferred to a cluster carrier protein, such as the monothiol glutaredoxin GRX5 (**Figure II-1, step 4**), as a part of the cluster distribution network.

Although eukaryotes require frataxin (FXN) for the synthesis of Fe-S clusters [59, 101-102], the precise role of FXN remains controversial. The loss of *FXN* is linked to the fatal neurodegenerative disease Friedreich's ataxia (FRDA) [103], which results in decreased activity for Fe-S cluster enzymes, accumulation of iron in the mitochondria, and susceptibility to oxidative stress [50, 104]. Identifying the role of FXN has been complicated by the existence of isoforms of different lengths. The longer form, $FXN^{\Delta 1-55}$, can undergo an iron-dependent oligomerization to produce a species reminiscent of ferritin that may function in iron storage [105-109]. The truncated form, $FXN^{\Delta 1-80}$, is widely considered to be the functional form *in vivo*; truncated FXN is monomeric even in the presence of iron [110], interacts with the NFS1-ISD11-ISCU2 complex [70, 72, 102, 111-112], and rescues cells challenged with *FXN* depletion [113]. Early studies revealed that $FXN^{\Delta 1-80}$ has a modest binding affinity for iron (3-55 μM) and led to the proposal that FXN accelerates Fe-S cluster synthesis by functioning as a chaperone that donates iron [61-63, 112, 114-119]. More recently, multiple studies provide evidence that FXN functions as an allosteric activator that enhances cysteine desulfurase activity and the subsequent rate of Fe-S cluster assembly on the scaffold protein [31, 70, 72, 77, 120]. FXN has been proposed to affect the sulfur chemistry by enhancing cysteine binding to the PLP cofactor of the cysteine desulfurase [31], and increasing sulfur transfer to the scaffold protein [77, 120] and small molecule thiols [70, 120]. Conflicting results indicate that FXN does [31, 77] or does not [120] affect persulfide formation on NFS1. Interestingly, a suppressor mutant on *Saccharomyces cerevisiae* Isu1 (homolog of human ISCU2; $Isu1^{M107I}$ also known as $Isu1_{Sup}$) was identified that rescues the depletion of *S. cerevisiae* Yfh1 (homolog of human FXN) [79, 121]. Initial studies have suggested that $Isu1^{M107I}$ increases the accumulation of persulfide species on Nfs1 similar to the addition of FXN [31, 77]; however, additional kinetic studies are required to probe details of the mechanism and

determine the specific chemical steps FXN and Isu1^{M107I} accelerate in promoting Fe-S cluster biosynthesis.

In this manuscript, new assays were developed to probe how FXN and human ISCU2^{M106I} (equivalent to Isu1^{M107I}) affect the kinetics of individual steps in Fe-S cluster biosynthesis. We found that the addition of either FXN or substitution of ISCU2 with ISCU2^{M106I} increased the overall rate of cluster synthesis and transfer to GRX5. Further, these studies provide compelling evidence that FXN accelerates reactions involving the NFS1 mobile S-transfer loop that result in an increased rate of [2Fe-2S] cluster assembly on ISCU2. In contrast, ISCU2^{M106I} primarily affects the transfer rate of intact [2Fe-2S] clusters from ISCU2 to GRX5. Overall, our results provide new mechanistic insight into Fe-S cluster biosynthesis and indicate FXN and ISCU2^{M106I} function at distinct stages of this pathway.

RESULTS

Both the ISCU2^{M106I} substitution and FXN accelerate the formation of [2Fe-2S] clusters on GRX5. Our initial objective was to test if the substitution of human ISCU2 with the ISCU2^{M106I} variant functions analogously to FXN and stimulates Fe-S cluster biosynthesis. A circular dichroism (CD) assay was developed to monitor an entire Fe-S cluster assembly and transfer reaction (**Figure II-1, step 1-4**) to better reproduce the *in vivo* biosynthetic pathway than previously reported assays that only monitor partial reactions. This assay takes advantage of the positive ellipticity from [2Fe-2S]-GRX5 and low ellipticity from [2Fe-2S]-ISCU2 at 450 nm (**Figure II-2**). The reaction conditions contained the recombinantly expressed human NFS1-ISD11 complex that co-purified with *Escherichia coli* ACP (SDA_{ec}) [33, 122], with the addition of recombinant human ISCU2 ($SDA_{ec}U$), ISCU2^{M106I} ($SDA_{ec}U^{M106I}$), or ISCU2 and FXN

($SDA_{ec}UF$). Reactions were initiated with the addition of L-cysteine and glutathione, which is required for binding the Fe-S cluster to GRX5. All complexes exhibited final CD spectra consistent with [2Fe-2S]-GRX5 (**Figure II-3**). Similar overall rates were observed for the $SDA_{ec}UF$ and $SDA_{ec}U^{M106I}$ complexes (**Fig. II-4A and Table II-1**), which were about 3 times greater than the $SDA_{ec}U$ complex. The results from this *in vitro* Fe-S cluster biosynthetic assay are consistent with both the stimulation of activity by FXN and the bypass of FXN by $ISCU2^{M106I}$.

FXN and $ISCU2^{M106I}$ operate at different steps in Fe-S cluster biosynthesis. We tested the effect of adding FXN to the $SDA_{ec}U^{M106I}$ complex in complete cluster assembly and transfer reactions (**Figure II-1, step 1-4**). The $SDA_{ec}U^{M106I}F$ complex had a rate that was faster than $SDA_{ec}U$ (nearly 7-fold greater) and was about twice the rate of either the $SDA_{ec}UF$ or $SDA_{ec}U^{M106I}$ complex (**Fig. 1A and Table II-1**). This additive result in the Fe-S assembly assay hints that the stimulatory effects of FXN and $ISCU2^{M106I}$ occur at different steps in Fe-S cluster biosynthesis. As FXN was previously shown to increase the rates of partial reactions, including the Fe-S cluster assembly reaction on ISCU2 and the cysteine desulfurase activity of $SDA_{ec}U$ [33, 70, 123], we tested whether $ISCU2^{M106I}$ also affected those steps of Fe-S cluster biosynthesis.

The $ISCU2^{M106I}$ variant was tested for its ability to mimic FXN and increase the rate of [2Fe-2S] cluster formation on ISCU2 (**Figure II-1, step 1-3**). We used CD to monitor [2Fe-2S] cluster formation on ISCU2 and $ISCU2^{M106I}$ by following changes in ellipticity at 330 nm, similar to a previously reported assay [123]. Here, the addition of FXN to the $SDA_{ec}U$ complex was shown to accelerate Fe-S cluster formation on ISCU2 (2.8 fold greater) under a comparable set of conditions (**Figure II-4B and Figure II-5; Table II-1**). The $SDA_{ec}U^{M106I}$ complex exhibited 1.5 times greater cluster synthesis activity compared to the native $SDA_{ec}U$ complex, but only about

half the activity of $SDA_{ec}UF$. Addition of FXN to the $SDA_{ec}U^{M106I}$ complex further enhanced the activity (1.5 fold greater), consistent with FXN stimulation of the native system.

We also tested the effect of substituting the $ISCU2^{M106I}$ variant for ISCU2 in cysteine desulfurase activity assays. SDA_{ec} was previously shown to exhibit a low k_{cat} (0.60 min^{-1}) for the cysteine desulfurase reaction [33], which was not affected by the addition of ISCU2, but showed a stimulation by an order of magnitude upon the addition of both ISCU2 and FXN (**Table II-1**) [33, 70]. The $SDA_{ec}U^{M106I}$ complex exhibited kinetic parameters highly similar to the $SDA_{ec}U$ complex with a k_{cat} 10-fold lower than the $SDA_{ec}UF$ complex (**Table II-1 and Figure II-6**). Moreover, the addition of FXN to the $SDA_{ec}U^{M106I}$ complex stimulated k_{cat} in a manner reminiscent of the wild-type system. Overall, the additive effect in the complete synthesis and transfer assays coupled to the inability of $ISCU2^{M106I}$ to replace FXN in partial Fe-S cluster assembly and cysteine turnover reactions are consistent with FXN and $ISCU2^{M106I}$ affecting different steps of Fe-S cluster biosynthesis.

The $ISCU2^{M106I}$ substitution accelerates cluster transfer to GRX5. Since ISCU2 acts as a scaffold for [2Fe-2S] cluster synthesis and functions as an intermediate to transfer these clusters to target proteins, we evaluated the ability of FXN and $ISCU2^{M106I}$ to affect the transfer of the [2Fe-2S] cluster intermediate from ISCU2 to GRX5 (**Figure II-1, step 4**). The $SDA_{ec}U$ and $SDA_{ec}U^{M106I}$ complexes were incubated with L-cysteine and ferrous iron in the absence of GRX5 and the development of the characteristic [2Fe-2S]-ISCU2 CD spectrum was observed (**Figure II-7**). After completion of the [2Fe-2S]-ISCU2 formation reaction, apo-GRX5 (with or without FXN) was added under anaerobic conditions, and the cluster transfer reaction from ISCU2 to GRX5 was followed by monitoring the increase in ellipticity at 450 nm (**Figure II-4C and Figure II-8**). The

rates of cluster transfer for the native complex with and without FXN were the same within error (Table 1), establishing that FXN does not have a role in cluster transfer under these conditions. In contrast, Fe-S assembly complexes containing the ISCU2^{M106I} substitution almost doubled the rate of cluster transfer to GRX5 compared to those with wild-type ISCU2.

Next, we tested whether the dissociation of [2Fe-2S]-ISCU2 or [2Fe-2S]-ISCU2^{M106I} from the SDA_{ec} complex, which is thought to be necessary to facilitate cluster transfer, impacts cluster exchange reactions with GRX5. Fe-S clusters were chemically reconstituted on ISCU2 and ISCU2^{M106I} in the absence of the SDA_{ec} complex. After purification, ISCU2 and ISCU2^{M106I} each bound approximately two iron atoms and two sulfide atoms per protein. The [2Fe-2S]-bound proteins were reacted with GRX5 and shown to have similar initial kinetics but different overall extents of transfer (**Figure II-4D and Figure II-9**). The ellipticity change for ISCU2^{M106I} was approximately 4 times greater than that for native ISCU2, suggesting that the ISCU2^{M106I} substitution alters the cluster-binding equilibrium compared to native ISCU2 and favors the cluster-bound GRX5 species. One possible explanation for this result is that the [2Fe-2S] cluster bound to ISCU2^{M106I} is less stable leading to enhanced transfer to GRX5. To test this possibility, a DTT extrusion assay was used to examine the susceptibility of ISCU2 and ISCU2^{M106I} to loss of their [2Fe-2S] clusters. [2Fe-2S] clusters were enzymatically generated on ISCU2 (or ISCU2^{M106I}) and the proteins were combined with DTT (**Figure II-10**). Both samples lost a majority of their cluster-dependent CD signal within 30 min. The similar rates of cluster loss (within 15% of one another; **Figure II-10A**) indicates the much greater extent of [2Fe-2S] cluster transfer from the ISCU2^{M106I} sample to GRX5 (**Figure II-4D**) involves more than just a change in cluster stability. Overall, these studies indicate that the ISCU2^{M106I} substitution, but not FXN, affects the Fe-S cluster transfer reaction from ISCU2 to GRX5.

FXN accelerates persulfide formation on NFS1 and ISCU2. Our next objective was to further define how FXN accelerates Fe-S cluster synthesis. To probe the effect of FXN on the rates of sulfur accumulation on NFS1 and ISCU2 (**Figure II-1, step 1 & 2**), a rapid acid quench assay was developed that couples HPLC separation with radiolabeled sulfur detection. In this assay, various Fe-S assembly complexes are reacted with L-[^{35}S]-cysteine substrate, quenched with acid after different reaction times, and applied to a reverse phase HPLC column for analysis of protein content (absorbance) and persulfide label (radioactivity). The ability to rapidly protonate thiolate nucleophiles, which inhibits sulfur transfer reactions [124], and analyze proteins for ^{35}S incorporation under quench conditions are critical aspects of this assay. Control experiments established conditions to separate proteins in the SDA$_{ec}$UF complex that contain cysteine residues (NFS1 and ISCU2; **Figure II-11 and Figure II-12**). The effectiveness of acid in quenching sulfur transfer from NFS1 to ISCU2 was established by reactions under normal and quench conditions (**Figure II-13**). Initial studies with excess L-[^{35}S]-cysteine substrate resulted in labeling of multiple cysteine residues on NFS1 and ISCU2 (**Figure II-14**). Some of these labeled cysteine residues, especially on NFS1 (C158, C163, C353, and C426), are likely due to side-reactions of the SDA$_{ec}$U complex that occur with excess cysteine substrate, long incubation times, and no additional reductant or iron; these conditions likely permit sulfur transfer reactions from persulfide species to excess cysteine and subsequent scrambling of the radiolabel.

The rates of persulfide formation on NFS1 and ISCU2 were determined using a stoichiometric amount of substrate. The SDA$_{ec}$U and SDA$_{ec}$UF complexes were combined with L-[^{35}S]-cysteine, quenched after different reaction times, and the proteins were separated under quench conditions. Plotting the amount of radiolabel as a function of time revealed saturation between 0.20-0.25 labels per NFS1 (**Figure II-15A and II-15B**) and ISCU2 (**Figure II-15C and**

II-15D) for the $SDA_{ec}U$ and $SDA_{ec}UF$ complexes. Interestingly, the amount of label on NFS1 did not decrease at longer times as one might expect for sequential irreversible reactions using limited amounts of substrate (**Figure II-1, step 1 & 2**). Persulfide formation on NFS1 and ISCU2, which were fit simultaneously, matched well with an equilibrium sulfur transfer model with a second cysteine turnover (**Figure II-15E and II-16**). Models that lack the equilibrium step (k_{-2}) or second cysteine turnover (k_3) did not adequately fit the data. The rates of persulfide formation on NFS1 were constrained to be the same for the $SDA_{ec}U$ (or $SDA_{ec}UF$) complex with or without a persulfide-bound ISCU2 ($k_1 = k_3$). Under these conditions, the slow step for both $SDA_{ec}U$ and $SDA_{ec}UF$ complexes was the formation of the persulfide species on NFS1 (**Table II-1 and Figure II-15**). FXN accelerated both the rate of persulfide formation on NFS1 (6.5 fold greater) and sulfur transfer from NFS1 to ISCU2 (30 fold greater). This kinetic model suggests the persulfide transfer reaction from NFS1 to ISCU2 is reversible with an equilibrium constant near one for both complexes. These experiments strongly support the proposed role of FXN as an allosteric activator that accelerates sulfur transfer chemistry [70, 77, 120].

FXN affects the rate of persulfide cleavage by free cysteine. Pulse-chase experiments were designed to evaluate the ability of FXN to labialize persulfide species and facilitate sulfur transfer chemistry. The cysteine desulfurase substrate, L-cysteine, was tested for its ability to cleave persulfide species associated with the $SDA_{ec}U$ and $SDA_{ec}UF$ complexes. A stoichiometric amount of L-[^{35}S]-cysteine was first incubated with the individual complexes. The labeled complexes were then combined with non-radioactive L-cysteine for various times, quenched with acid, and analyzed as described above. For the $SDA_{ec}U$ complex, spiking the sample with non-radioactive cysteine resulted in the loss of most of the labeled sulfur on both NFS1 and ISCU2, which occurred

at similar rates (**Figure II-17A and II-17B; Table II-1**). Intriguingly, the addition of FXN resulted in an approximate 5-fold increased rate of sulfur loss from NFS1, but almost no loss of label from ISCU2. To rationalize these results with the above equilibrium kinetic model (**Figure II-15E**), we suggest that cleavage of the [^{35}S]-label occurs primarily from the mobile S-transfer loop of NFS1 and not from ISCU2 (**Figure II-17C**). After NFS1 persulfide cleavage, slow cysteine turnover for the $SDA_{ec}U$ complex results in re-equilibration of the label through interprotein sulfur transfer from ISCU2, explaining the similar persulfide depletion rates for NFS1 and ISCU2 (**Table II-1 and Figure II-17**). In contrast, the $SDA_{ec}UF$ complex is proposed to repopulate the mobile S-transfer loop of NFS1 through rapid enzymatic cysteine turnover rather than re-equilibration, reconciling the apparent protection by FXN of the [^{35}S]-label on ISCU2. Overall, these radiolabeling studies coupled to previous cysteine desulfurase assay results suggest that FXN accelerates PLP-associated chemistry and sulfur transfer reactions from NFS1 to thiol-containing molecules (ISCU2, DTT, and L-cysteine).

FXN accelerates the decay of the PLP quinonoid intermediate for NFS1. To determine how FXN accelerates persulfide formation on NFS1, the PLP chemistry associated with the cysteine desulfurase reaction was directly probed using stopped-flow kinetics (**Figure II-1, step 1**). The proposed cysteine desulfurase mechanism includes sequential formation of cys-aldimine, cys-quinonoid, and cys-ketimine intermediates (**Figure II-18A**) [125-127], which have distinct absorbance maxima. The $SDA_{ec}U$ and $SDA_{ec}UF$ complexes were combined with L-cysteine and changes in absorbance were monitored. A high substrate concentration (10 mM) was used to increase the accumulation of PLP-based intermediates in the reaction. The first observed event is a rapid increase in absorbance at 410 nm (**Figure II-19**), which was assigned to the cys-aldimine

intermediate [126]. The $SDA_{ec}UF$ sample developed this signal more rapidly (the formation occurred during the dead time of the instrument) compared to the $SDA_{ec}U$ sample and accumulated approximately 8-fold more of this intermediate. Decay of this 410 nm species occurred at similar rates for the two complexes (**Table II-2**). The next intermediate, which absorbed maximally at 508 nm and was assigned to the cys-quinonoid species [126], developed at similar rates in the presence and absence of FXN (**Figure II-18B and Table II-1**). Interestingly, the decay rate of this cys-quinonoid intermediate was increased by a factor of four in the presence of FXN. Correspondingly, the formation of a species that absorbs at 340 nm (**Figure II-19 S14B**), which was assigned to the cys-ketimine intermediate [126], was also enhanced by the addition of FXN. We next found that addition of the bacterial homolog of FXN (CyaY) to the $SDA_{ec}U$ complex also increased the decay rate (2.4 fold greater) of the cys-quinonoid intermediate (**Figure II-18C and Table II-2**), consistent with the ability of CyaY to activate the human cysteine desulfurase complex [76]. Finally, $ISCU2^{M106I}$ was tested for its ability to mimic FXN and affect steps in the PLP chemistry of NFS1. Stopped-flow kinetics of the $SDA_{ec}U^{M106I}$ complex showed slower development and slightly faster decay kinetics (1.2 fold greater) for the cys-quinonoid intermediate compared to the native $SDA_{ec}U$ complex (**Figure II-18D and Table 1**). These stopped-flow experiments suggest that FXN, and to a smaller extent CyaY, affects the ability of NFS1 to accelerate the decay of the cys-quinonoid intermediate and generate the cys-ketimine species that is attacked by the mobile S-transfer loop during cysteine turnover.

We then tested whether the mobile S-transfer loop influences the decay kinetics of the cys-quinonoid intermediate in addition to its critical role in carbon-sulfur bond cleavage of the cys-ketimine intermediate to generate the NFS1 persulfide species. The conversion of the quinonoid intermediate to the ketimine species requires protonation at the C4' position (**Figure II-18A**). In

bacterial cysteine desulfurases, the mobile S-transfer loop cysteine is thought to be the proton donor for this step of the mechanism [126-127]. We, therefore, generated the $NFS1^{C381A}$ variant to test if the mobile S-transfer loop cysteine of NFS1 functions as the general acid for quinonoid decay in the SDA_{ec} complex. Stopped-flow kinetics for the $S^{C381A}DA_{ec}UF$ complex revealed that the quinonoid intermediate does not decay to generate the ketimine species (**Figure II-18E**), consistent with a proton donation role for C381. Overall, these results indicate FXN affects reactions associated with the NFS1 mobile S-transfer loop, which functions as a general acid, nucleophile, and sulfur transfer agent in Fe-S cluster biosynthesis.

DISCUSSION

A direct link between the *FXN* gene and the neurodegenerative disease Friedreich's ataxia (FRDA) was established in a seminal 1996 study [103]. Typical FRDA patients have lower wild-type FXN expression levels (4-36% of controls) [128-132], suggesting a threshold level of FXN is required for normal function. FXN depletion results in the loss of activity for Fe-S cluster enzymes, increased iron accumulation in mitochondria, and enhanced sensitivity to oxidative stress [104]. Strategies to treat FRDA have focused on iron chelators, antioxidants, and mechanisms to increase FXN levels [133-134]. Unfortunately, FRDA remains incurable. An alternate approach to generating a FRDA treatment is to first determine the biological role of FXN in Fe-S cluster biosynthesis and then replace or bypass that function.

An initial hypothesis was promoted that FXN functions as a chaperone that provides iron for Fe-S cluster assembly. This assignment was based on FXN depletion studies, which reveal a disruption of iron homeostasis and accumulation of iron in the mitochondria, and the lack of a designated iron chaperone for the Fe-S assembly pathway coupled to the presence of an iron-

binding patch of carboxylate residues on FXN. However, FXN has weak iron binding affinity towards ferrous iron (55 μM), which is the substrate for Fe-S cluster biosynthesis, and the iron-binding carboxylate patch residues are only semi-conserved [61-63, 112, 114-119]. Moreover, a similar iron overload phenotype is generated upon depletion of other members of the mitochondrial Fe-S assembly system [135], indicating that this phenotype is linked to loss of Fe-S clusters and not necessarily the ability to donate iron for this pathway. Furthermore, FRDA clinical variants for FXN have been identified on a region distinct from the carboxylate patch. These FRDA variants are not iron-binding residues and exhibit diminished ability to bind and activate the Fe-S assembly complex. Finally, the presence of ~150 μM labile iron pool in mitochondria could function as a feedstock for iron-containing proteins and raises the question as to whether a designated iron chaperone is even required for the Fe-S cluster biosynthetic pathway [136]. Despite these concerns, many investigators still champion an iron donor role for FXN.

More recently, much stronger evidence has been provided that supports a role for FXN in facilitating sulfur-based chemistry required for Fe-S cluster biosynthesis [31, 33, 70, 72, 77, 120, 123, 137-139]. In this manuscript, we have extended these FXN functional studies to include stopped-flow interrogation of the eukaryotic cysteine desulfurase reaction and functional assays that incorporate both synthesis of the Fe-S cluster intermediate and transfer of the cluster to an acceptor protein. We provide a stepwise analysis of the role of FXN in (*i*) the PLP-associated formation of intermediates for the cysteine desulfurase NFS1; (*ii*) the kinetics of sulfur accumulation on NFS1; (*iii*) the kinetics of interprotein sulfur transfer to the scaffold protein ISCU2; (*iv*) the rate of Fe-S cluster intermediate formation on ISCU2; and (*v*) the kinetics of [2Fe-2S] cluster transfer from ISCU2 to the monothiol glutaredoxin GRX5 (**Figure II-18A** and **Figure II-1**).

FXN accelerates steps associated with the mobile S-transfer loop of NFS1. Stopped-flow experiments revealed a clear role for FXN in accelerating the decay of the cys-quinonoid intermediate for the $SDA_{ec}U$ complex (**Figure II-18**). The transformation of the cys-quinonoid intermediate to the cys-ketimine species requires protonation at the C4' position. Substitution of the mobile S-transfer loop cysteine (C381A) of NFS1 compromised the ability to advance to the ketimine intermediate. This result is consistent with NFS1 residue C381 functioning as a general acid for this step in the mechanism, consistent with the prokaryotic cysteine desulfurases [126-127]. Radiolabeling studies revealed that FXN also accelerates the rate of persulfide formation on NFS1, which results from attack of the deprotonated mobile S-transfer loop cysteine on the cys-ketimine intermediate, and the rate of interprotein sulfur delivery from the mobile S-transfer loop cysteine of NFS1 to ISCU2 (**Figure II-15** and **Table II-1**). These enhanced rates of sulfur transfer also manifested in increased rates for the formation of [2Fe-2S] cluster intermediates on ISCU2 and in complete reactions in which [2Fe-2S] clusters were synthesized and transferred to GRX5.

In addition, we determined how human $ISCU2^{M106I}$, which is analogous to $Isu1^{M107I}$ [79, 121], is able to bypass the function of FXN and stimulate Fe-S cluster biosynthesis. $ISCU2^{M106I}$ was unable to replace FXN and affect the cysteine desulfurase kinetic parameters of the SDA_{ec} complex (**Table II-1**) and only had a minor stimulatory effect on the rate of Fe-S cluster formation on ISCU2. Consistent with this result, a recent crystal structure indicates that this $ISCU2^{M106I}$ substitution is unlikely to affect the mobile S-transfer loop of NFS1 [140]. Instead, we show that $ISCU2^{M106I}$, unlike FXN, accelerates the rate of intact [2Fe-2S] cluster transfer from ISCU2 to GRX5 (**Figure II-4C**). Further analysis indicates that the $ISCU2^{M106I}$ substitution does not affect cluster stability on ISCU2 (**Figure II-10**) but appears to affect the [2Fe-2S] cluster binding equilibrium between ISCU2 and GRX5 (**Figure II-4D**). We hypothesize that substitutions on the

scaffold protein that are capable of bypassing FXN (including the substitution of Isu1 M107 with residues that have a higher hydropathy index such as valine or isoleucine) [79] favor hydrophobic protein-protein interactions that drive the cluster transfer reaction from ISCU2 to GRX5. Stimulation of different steps by FXN and ISCU2^{M106I} is further supported by the additive effect that was observed in complete synthesis and transfer assays.

Model for the role of FXN in Fe-S cluster biosynthesis. The eukaryotic $SDA_{ec}U$ complex has an unusually low activity for a cysteine desulfurase enzyme (k_{cat} < 10% of prokaryotic IscS) and requires FXN binding to stimulate activity and approach the catalytic turnover of IscS [33, 70]. CyaY, which is the prokaryotic homolog of FXN, does not activate IscS and, instead, inhibits *in vitro* Fe-S cluster biosynthesis [141]. Swapping protein components between the prokaryotic and eukaryotic systems reveals that these activation/inhibition effects were surprisingly independent of the FXN and ISCU2 homologs, but dependent on the cysteine desulfurase [76]. A recently determined structure of the SDA_{ec} complex revealed an incomplete substrate binding site with a solvent-exposed PLP cofactor and an overall architecture in which ISD11 molecules mediate interactions between NFS1 subunits [33]. Quaternary interactions between NFS1 subunits of the SDA_{ec} complex are quite different than its prokaryotic homologs IscS, which have contributions from each subunit to the active site channel of the other subunit [142-143]. The Cory SDA_{ec} architecture provides a rationale for the essential nature of ISD11 in eukaryotes, the low basal levels of cysteine desulfurase activity for the SDA_{ec} or $SDA_{ec}U$ complex, and the stimulation of sulfur-based chemistry upon FXN homolog binding to the eukaryotic cysteine desulfurases.

In our model, the $SDA_{ec}U$ is a low activity form of the Fe-S assembly complex with an incomplete substrate binding site and a mobile S-transfer loop that occupies a primarily non-

productive conformation **(Figure II-20**). FXN functions as an allosteric activator and upon binding completes the substrate binding site and favors productive conformations for the mobile S-transfer loop cysteine. This alteration of the mobile S-transfer loop trajectory results in an acceleration of proton donation, which is necessary for advancing the cys-quinonoid intermediate, and an increased rate of persulfide formation on NFS1 and sulfur transfer to ISCU2. A role in binding and excluding non-productive conformations is further supported by the ability of the FXN homolog CyaY, which shares a mere 20% sequence identity with the human form, to impart the same effects on the cys-quinonoid decay (**Figure II-18C**) and on the cysteine desulfurase activity [76]. Although the FXN-induced stimulation of the mobile S-transfer loop reactions is relatively small (**Table II-1**; 3 to 30 fold), this may be sufficient to reach the modest *in vivo* activity threshold that supports Fe-S cluster biosynthesis and mitochondrial function. The incorporation of ISD11/ACP into the eukaryotic Fe-S cluster biosynthetic pathway is thereby a mechanism to integrate FXN as an activity control element or regulator that drives sulfur chemistry. Overall, these results provide new insights into FXN function and suggest strategies to replace (exclude non-productive mobile S-transfer loop conformations) or bypass FXN function (facilitate Fe-S cluster transfer from ISCU2) and provide potential new mechanisms to treat FRDA.

MATERIALS AND METHODS

Protein Preparations. Plasmids containing human NFS1 (Δ1-55) and ISD11 (pZM4) were generously provided by S. Leimkuhler [144]. The NFS1 and ISD11 plasmids were transformed into *E. coli* strain BL21(DE3) cells and copurified with the bacterial ACP (ACP_{ec}) as the SDA_{ec} complex [33]. Human ISCU2 (Δ1-35) and FXN (Δ1-55) were separately expressed and purified as previously described [70]. The spontaneous conversion of Δ1-55 FXN to the truncated form was

confirmed by SDS-PAGE [70]. The QuikChange protocol (Agilent) was used to introduce the M106I point mutation into the *ISCU2-pET11a* plasmid [70] and the C381A point mutation into the *NFS1-pET15b* plasmid [144]. The protein sequence numbering for the M106I variant does not include the ISCU2 signal sequence to be consistent with the literature for the bacterial and yeast homologs. The MEGAWHOP [145] method was used to substitute human *GRX5* for *FDX* in the *pHis-GFP-TEV-FDX* plasmid [146] and produce *pHis-GFP-TEV-GRX5*. Sequences were confirmed by the Gene Technologies Lab (Texas A&M University).

The *pHis-GFP-TEV-GRX5* plasmid was transformed into Rosetta (DE3) cells (VWR). The cells were grown in LB media (VWR) at 37 °C until the OD_{600} reached 0.5 and then β-D-1-thiogalactopyranoside (IPTG) was added to a final concentration of 0.5 mM. The temperature was decreased to 16 °C and the cells were grown for an additional ~16 h. The harvested cell pellets were resuspended in Buffer A (50 mM Tris and 250 mM NaCl at pH 7.5) with 5 mM imidazole and lysed by sonication (Branson sonifier 450). The soluble fraction was loaded on a Ni-NTA column (5 mL; GE Life Sciences) and the his-GFP-TEV-GRX5 fusion was eluted using Buffer A and a linear gradient between 5 and 500 mM imidazole. The green fractions were combined and dialyzed into Buffer B (50 mM Tris, pH 7.5). The sample was then incubated overnight at room temperature with TEV protease (1:50 molar ratio of protease to fusion protein). The cleaved material was then loaded onto an anion exchange column (27 mL; 16 mm × 13.5 cm, POROS HQ 50) and eluted with Buffer B and a linear gradient from 0 to 1 M NaCl. The GRX5 fractions were concentrated and loaded onto a 26/60 Sephadex 100 column (GE Life Sciences) equilibrated with 50 mM HEPES and 150 mM NaCl at pH 7.5. Monomeric fractions with > 96% purity were concentrated, frozen in liquid nitrogen and stored at −80 °C. Unless otherwise stated, all protein manipulations and reactions were carried out in an anaerobic glove box (MBRAUN; maintained

at ~14 °C with O_2 < 1 ppm). Protein concentrations were estimated using the following extinction coefficients: SDA_{ec} using 10.9 $mM^{-1}cm^{-1}$ at 420 nm, ISCU2 using 8490 $M^{-1}cm^{-1}$ at 280 nm, FXN using 26030 $M^{-1}cm^{-1}$ at 280 nm, and GRX5 using 17780 $M^{-1}cm^{-1}$ at 280 nm [70, 147]. Protein variants were assumed to have the same extinction coefficient as the native proteins.

Complete Fe-S cluster synthesis and transfer reactions. The complete reaction assays included 0.5 µM SDA_{ec}, 20 µM ISCU2 (or $ISCU2^{M106I}$), 20 µM (or 0 µM) FXN, 40 µM GRX5, and 400 µM $Fe(NH_4)_2(SO_4)_2$ and Buffer C (50 mM HEPES, 150 mM KCl and 10 mM $MgCl_2$ at pH 7.5). The reactions were initiated by the addition of 100 µM L-cysteine and 10 mM GSH. Cluster formation on GRX5 was then measured for $SDA_{ec}U$, $SDA_{ec}UF$, $SDA_{ec}U^{M106I}$ and $SDA_{ec}U^{M106I}F$ by monitoring the ellipticity change at 450 nm using a Chirascan circular dichroism (CD) spectrometer (Applied Photophysics). Cuvettes (1 cm path length) were sealed with a rubber septum and electrical tape in a glove box. The kinetic data were fit to an exponential rise equation ($[y=y_0+A_0*(1 - \exp(-k*t))]$ where the k is the apparent rate of cluster formation on GRX5) using Kaleidagraph (Synergy Software, Reading, PA).

Fe-S cluster assembly reactions on ISCU2. Fe-S assembly reactions on ISCU2 contained 10 µM SDA_{ec}, 30 µM ISCU2 (or $ISCU2^{M106I}$), 30 µM FXN (when added), 400 µM $Fe(NH_4)_2(SO_4)_2$ and Buffer C. The reactions were initiated with 1 mM L-cysteine. The formation of [2Fe-2S] clusters was monitored by the change in ellipticity at 330 nm [123]. The initial increase in ellipticity was plotted with time and fit a linear equation (R^2 values ≥ 0.97) using Kaleidagraph.

Cysteine desulfurase activity measurements. Cysteine desulfurase activities were measured for each complex using a slightly modified methylene blue assay [70, 148]. Protein complexes were generated with final concentrations of 0.5 μM SDA_{ec}, 1.5 μM ISCU2 (or $ISCU2^{M106I}$), and 1.5 μM FXN (when included). The complexes were combined with 4 mM D,L-DTT and incubated for 15 min anaerobically on a heating block at 37 °C. Different concentrations of L-cysteine were added, incubated for 6 min, and quenched with 20 mM *N*,*N'*-diphenyl-*p*-phenylenediamine (DPD) (in 7.2 M HCl) and 30 mM $FeCl_3$ (in 1.2 M HCl). After 20 min, the samples were centrifuged and the absorbance was measured at 670 nm. The amount of sulfide produced was determined for each data point using a standard curve. Rates ($[S^{2-}]$/([NFS1]*min)) were plotted against the amount of L-cysteine added and fit to the Michaelis-Menten equation using Kaleidagraph.

[2Fe-2S] cluster transfer reactions from enzymatic and chemically reconstituted ISCU2 to GRX5. Clusters were enzymatically generated on ISCU2 (or $ISCU2^{M106I}$) using 0.5 μM SDA_{ec}, 20 μM ISCU2 (or $ISCU2^{M106I}$), and 400 μM $Fe(NH_4)_2(SO_4)_2$ and Buffer C. The reactions were initiated with of 100 μM L-cysteine and 10 mM GSH. After 160 min, the enzymatic formation of [2Fe-2S] clusters appeared to be completely based on the lack of changes in ellipticity at 450 nm. A solution containing 40 μM GRX5 (with or without 20 μM FXN) was then injected with an air-tight syringe into the sealed cuvette to initiate the transfer reactions. The change in ellipticity was plotted with time and fit a linear equation with Kaleidagraph (R^2 values ≥ 0.97).

[2Fe-2S] clusters were chemically generated on ISCU2 (or $ISCU2^{M106I}$) by reacting 30 μM of apoprotein with 600 μM ferric ammonium citrate, 600 μM Na_2S and 10 mM D,L-DTT for an hour. DTT and the excess iron and sulfide were then removed with a desalting column (5 mL, GE Healthcare) equilibrated in Buffer C. Iron was quantitated with the ferrozine assay (extinction

coefficient of 28,000 $M^{-1}cm^{-1}$ at 562 nm) [149] and sulfide was quantitated using a methylene blue assay with an additional pre-treatment of the protein with NaOH and zinc acetate to release bound sulfide [150]. The protein concentration was determined using the Bradford assay. Chemically reconstituted ISCU2 had 2.1 ± 0.3 iron and 2.0 ± 0.6 sulfide atoms per protein, whereas $ISCU2^{M106I}$ had 1.9 ± 0.5 iron and 2.2 ± 0.1 sulfide atoms per protein. Cluster transfer reactions were initiated by combining [2Fe-2S]-ISCU2 or [2Fe-2S]-$ISCU2^{M106I}$ with 60 µM GRX5 and 10 mM GSH. Transfer reactions were monitored by the change in ellipticity at 450 nm.

[2Fe-2S] cluster extrusion assay. [2Fe-2S] clusters were assembled on 30 µM ISCU2 (or $ISCU2^{M106I}$) in the presence of 10 µM SDA_{ec}, 100 µM L-cysteine, 400 µM $Fe(NH_4)_2(SO_4)_2$ and 10 mM GSH. 4 mM D,L-DTT was added to the samples to initiate the cluster extrusion reaction, which was followed by the loss of ellipticity at 330 nm. The extrusion rates were determined by fits to a linear equation.

Protein separation and ^{35}S quantification for sulfur transfer reactions. L-[^{35}S]-cysteine (PerkinElmer, 10.2 µM, 1.00796 mCi) was diluted 50 times by non-radioactive L-cysteine to generate a 1 mM stock solution (final concentration of L-[^{35}S]-cysteine was 204 nM). Proteins from Fe-S assembly complexes (SDA_{ec} and ISCU2) were applied to a reverse phase C4 column (Waters) attached to a HPLC (1260 Infinity, Agilent Technologies) and separated using a gradient from either 0 to 100% or from 30% to 70% Buffer D (0.1 % TFA in water, pH 2.0) with the remainder of the composition made up of Buffer E (60% CH_3CN, 40% isopropanol, 0.1% TFA). Both the absorbance (diode array detector) and, after mixing with scintillation cocktail (BioCount 111182), the [^{35}S] signal (Model 5C β-RAM radio-HPLC detector, LabLogic) were recorded for

the eluted proteins. The retention time of NFS1 (ISD11 and ACP_{ec} do not contain cysteine residues required for persulfide formation) was determined by reacting a 25 µL aliquot of the SDA_{ec} complex (37.5 µM) with 25 µL of L-[^{35}S]-cysteine (final concentration of 500 µM) for 30 min. The reaction was stopped by addition of 50 µL quenching solution and the proteins were separated under quench conditions. The quenching solution was made by mixing 1 volume of concentrated HCl with 4 volumes of 6 M guanidine hydrochloride (pH < 1). The retention time for ISCU2 was determined using absorbance or reaction of the $SDA_{ec}U$ complex with L-[^{35}S]-cysteine and comparison to the SDA_{ec} complex. Note that FXN, like ISD11 and ACP_{ec}, lacks cysteine residues needed to form a persulfide intermediate. To demonstrate that the quench solution inhibits sulfur transfer, labeled NFS1 was first generated by reacting the SDA_{ec} complex (30 µM) with L-[^{35}S]-cysteine (400 µM final concentration, 45 µl total reaction volume) for 30 min. The labeled NFS1 was either (*i*) incubated with ISCU2 (80 µM, 5 µL) for 30 min, followed by the addition of 50 µL quenching solution; or (*ii*) first combined with 50 µL quenching solution and then incubated with ISCU2 (80 µM, 5 µL) for 30 min. Samples were analyzed by a reverse phase chromatography under quench conditions. NFS1Data collection and analysis were performed with Laura software (LabLogic). To quantitate the amount of persulfide associated with the peak, the area under the scintillation curve (in CPM) was converted into a [^{35}S] concentration using a standard curve generated from known amounts of L-[^{35}S]-cysteine and then multiplied by the dilution factor (unlabeled / labeled L-cysteine = 4901.96).

Assays for monitoring persulfide formation and decay. For the persulfide formation and decay assays, 30 µM SDA_{ec} and 30 µM ISCU2 were combined to generate the $SDA_{ec}U$ complex, which was converted to the $SDA_{ec}UF$ complex by the addition of 75 µM FXN. The $SDA_{ec}U$ and

$SDA_{ec}UF$ complexes were reacted with either 30, 200, or 600 μM cysteine (0.0204% [^{35}S]-cysteine), incubated at 37°C for different lengths of time (30 sec to 1 h), and diluted 4-fold into the quenching solution described above. The amount of persulfide associated with NFS1 and ISCU2 was calculated as described above, plotted against time, and fit to a reaction scheme (see below) using KinTek software (KinTex Corporation, Austin, TX). To determine which cysteine residues were labeled with persulfide species, the $SDA_{ec}U$ complex was combined with 300 μM L-cysteine, incubated at 37 °C for 30 min, and quenched with concentrated HCl. The sample was digested with pepsin (100:1 sample:pepsin based on concentration in mg/mL) at 22 °C for 30 min and subjected to LC/MS/MS analysis (Center for Mass Spectrometry (CMS) at Texas A&M University).

Pulse-chase experiments were conducted by first reacting the $SDA_{ec}U$ and $SDA_{ec}UF$ complexes (30 μM SDA_{ec}, 30 μM ISCU2, with or without 75 μM FXN) with 30 μM [^{35}S]-cysteine for 40 min (the amount of label maximized after 10-20 min) to generate radiolabeled NFS1 and ISCU2. Next, we added a final concentration of 1 mM non-radioactive L-cysteine to the samples and then diluted 4-fold into the quenching solution at various times. The number of residual persulfide labels on NFS1 and ISCU2 were determined and fit to an exponential decay equation [$y=y_0+A_0*\exp(-k*x)$] using Kaleidagraph, where the k value gives the apparent rate of persulfide loss.

Validation of data fitting for persulfide formation kinetics. The data were fitted to a simulated mechanism according to the reaction scheme (Fig. 2E) using KinTek software. The estimation of error was determined by FitSpace confidence contour analysis. FitSpace determines the goodness of the fit by measuring the dependence of the sum of square errors (SSE) on each pair of parameters

while all other parameters were varied. The confidence interval of all the fitted parameters was constrained by χ^2 threshold values of 0.99 and 0.997 for the $SDA_{ec}U$ and $SDA_{ec}UF$ data, respectively. These thresholds indicate that varying the parameter within the confidence interval would not increase the χ^2 value more than 1% ($SDA_{ec}U$) and 0.3% ($SDA_{ec}UF$) from the minimum χ^2 (χ^2_{min}) value, which represents the best fit. Confidence contour plots are provided that indicate well-defined regions determined by χ^2 threshold values (red colored patches).

Stopped-flow kinetics for cysteine desulfurase reaction. 100 µM $SDA_{ec}U$ (100 µM SDA_{ec} + 100 µM ISCU2) or 100 µM $SDA_{ec}UF$ (100 µM SDA_{ec} + 100 µM ISCU2 + 100 µM FXN) in assay buffer (50 mM HEPES, 250 mM NaCl, pH 7.5) was placed in one of the syringes of the stopped-flow apparatus (KinTek Corporation). The other syringe contained 10 mM L-cysteine. The samples were mixed by simultaneously pressing both syringes. Formation of the aldimine, quinonoid, and ketimine intermediates were followed by monitoring changes in absorbance at 410, 508 and 340 nm, respectively. For the aldimine and quinonoid kinetics, traces monitored at 410 nm and 508 nm with time were fitted with Origin software (OriginLab) to a consecutive B equation [$y = y_0 + (k_1*[A]_0/(k_2-k_1))*(\exp(-k_1*t)-\exp(-k_2*t))$], where k_1 and k_2 are rate constants of the formation and decay of intermediates respectively. The ketimine kinetics could not be adequately fit using a consecutive B equation.

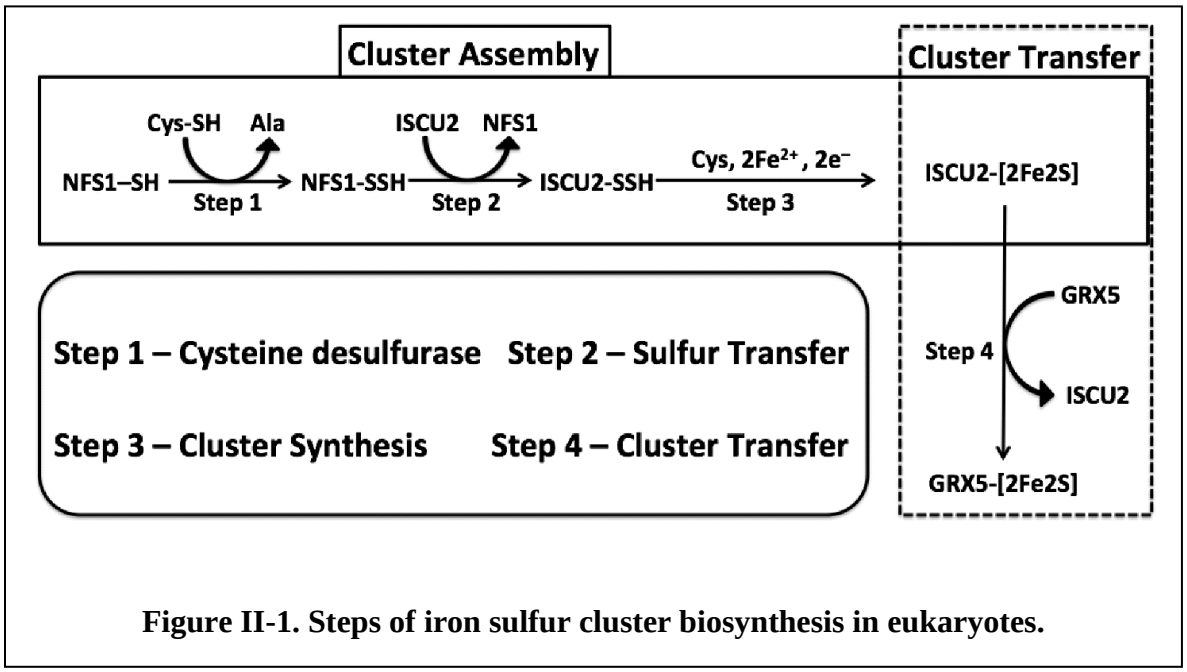

Figure II-1. Steps of iron sulfur cluster biosynthesis in eukaryotes.

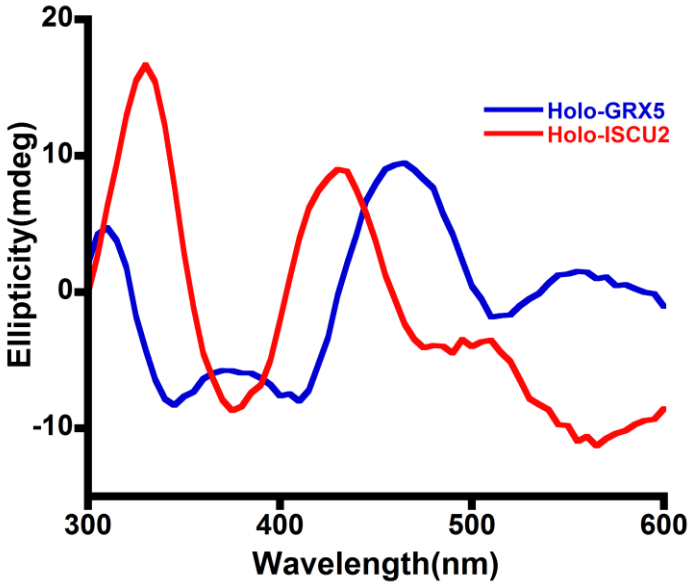

Figure II-2. Visible CD spectra for holo-ISCU2 and holo-GRX5 have distinct features. CD spectra were recorded for 25 µM [2Fe-2S]-ISCU2 (red) and 30 µM [2Fe-2S]-GRX5 (blue).

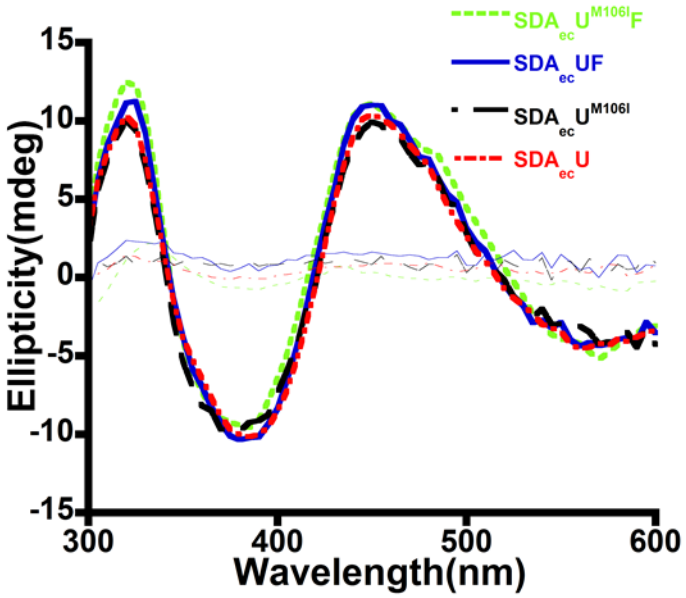

Figure II-3. Final CD spectra for complete Fe-S assembly and transfer reactions resemble [2Fe-2S]-GRX5. [2Fe-2S] cluster synthesis and transfer reactions to GRX5 for the $SDA_{ec}U$ (red), $SDA_{ec}UF$ (blue), $SDA_{ec}U^{M106I}$ (green) and $SDA_{ec}U^{M106I}F$ (black) complexes. Spectra are shown before the reaction is initiated (fine lines) and at end points of assay (bold lines; see **Figure II-4A**).

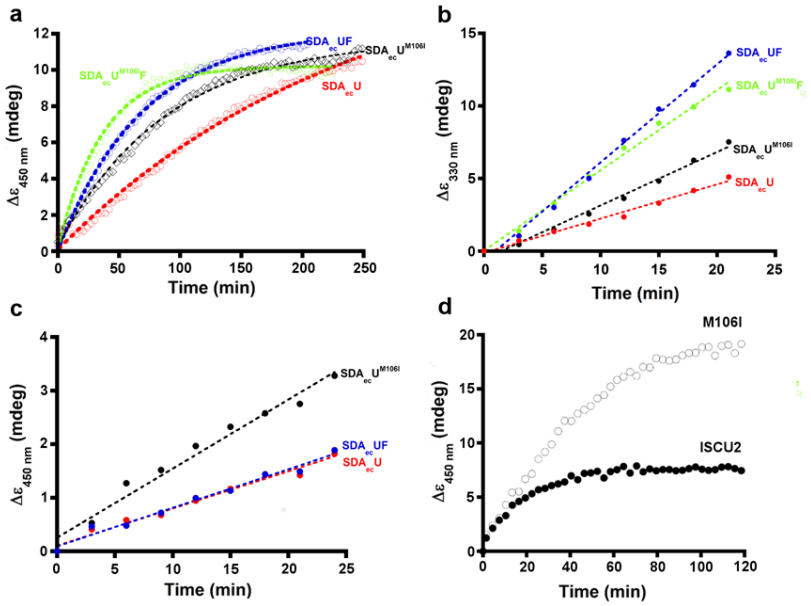

Figure II-4. FXN and the ISCU2^{M106I} substitution accelerate different steps in Fe-S cluster biosynthesis. A) Kinetics of Fe-S cluster synthesis and transfer to GRX5 were monitored for different assembly complexes by the change in ellipticity at 450 nm. The average change in ellipticity (n = 3; maximum error of 1.8 in ellipticity) is plotted and fit with an exponential rise equation. The final CD spectra are shown in **Figure II-3. B**) Fe-S cluster assembly reactions on ISCU2 were monitored for assembly complexes by the change in ellipticity at 330 nm. The average change in ellipticity (n = 3; maximum error of 1.8 in ellipticity) is plotted and fit with a linear equation. The complete time course of the reactions and final CD spectra are shown in **Figure II-5. C**) Kinetics of cluster transfer from pre-formed holo-ISCU2 to apo-GRX5 were monitoring by the change in ellipticity at 450 nm. Reactions were initiated (time = 0) by the anaerobic injection of GRX5 (with or without FXN). The average change in ellipticity (n = 3; maximum error of 0.8 in ellipticity) is plotted and fit with a linear equation. The CD spectra before addition of GRX5 and the complete time course of the reaction are shown in **Figure II-6 and II-7. D**) Chemically reconstituted ISCU2 (or ISCU2^{M106I}) was reacted with GRX5 and the [2Fe-2S] cluster transfer was monitored by the increase in ellipticity at 450 nm. Full spectra are shown in **Figure II-9.** Color scheme: SDA$_{ec}$U (red), SDA$_{ec}$UF (blue), SDA$_{ec}$U^{M106I} (black) and SDA$_{ec}$U^{M106I}F (green).

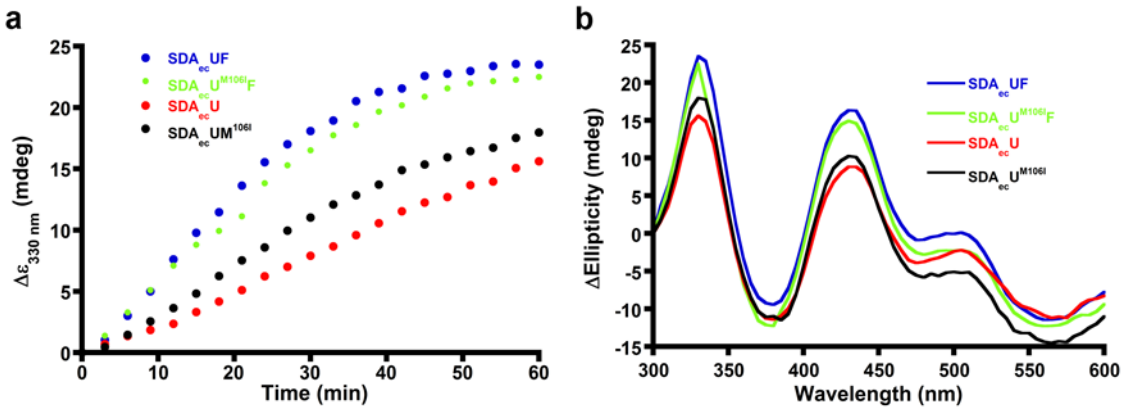

Figure II-5. Full time course and final CD spectra for Fe-S cluster synthesis reactions on ISCU2. A) Fe-S assembly intermediate formation on ISCU2 were monitored by the change in ellipticity at 330 nm and shown for different assembly complexes. **B**) The overall similarity in the final CD spectra (after 60 min) for the different complexes indicates the formation of analogous Fe-S clusters. The complexes are indicated by their color in the figure: $SDA_{ec}U$ (red), $SDA_{ec}UF$ (blue), $SDA_{ec}U^{M106I}$ (black) and $SDA_{ec}U^{M106I}F$ (green).

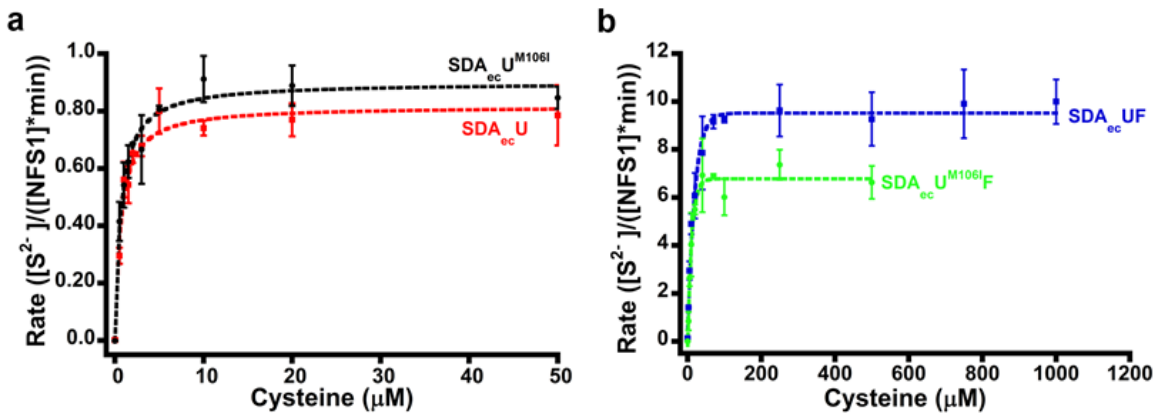

Figure II-6. Fe-S assembly complexes containing native ISCU2 or ISCU2^{M106I} exhibit similar kinetic parameters for the cysteine desulfurase reaction. Cysteine desulfurase activities for complexes **A**) without ($SDA_{ec}U$ in red and $SDA_{ec}U^{M106I}$ in black) and **B**) with FXN ($SDA_{ec}UF$ in blue and $SDA_{ec}U^{M106I}F$ in green) at different concentrations of L-cysteine. Lines through the data are the fits to the Michaelis-Menten equation. Experiments were performed in triplicate.

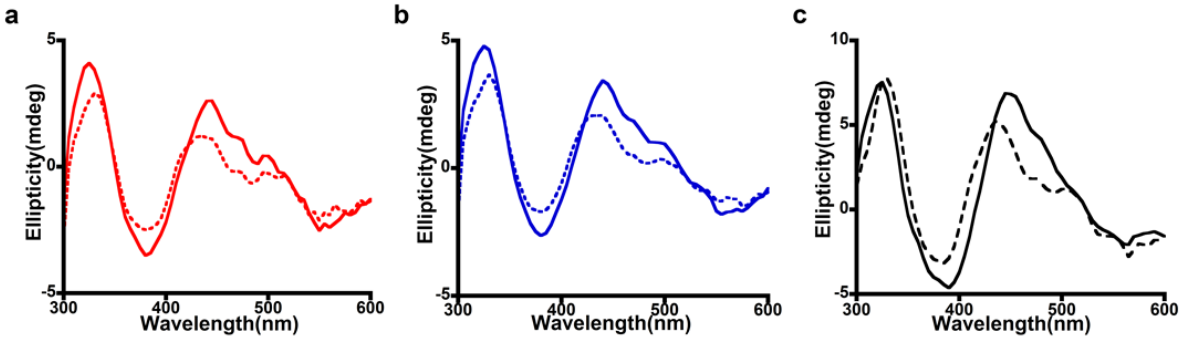

Figure II-7. CD spectra of Fe-S cluster bound species in transfer reaction from ISCU2 to GRX5. Fe-S clusters were synthesized *in situ* on ISCU2 (or ISCU2^{M106I}) for **A**) SDA$_{ec}$U (red), **B**) SDA$_{ec}$UF (blue) and **C**) SDA$_{ec}$U^{M106I} (black) complexes. CD spectra are recorded (dotted lines) after 160 min from initiation of the reaction. The samples were then spiked with 40 µM GRX5 (with or without 20 µM FXN) and the CD spectra was recorded 20 min later (solid line) later. Kinetic traces monitored at 450 nm are shown in **Figure II-8**.

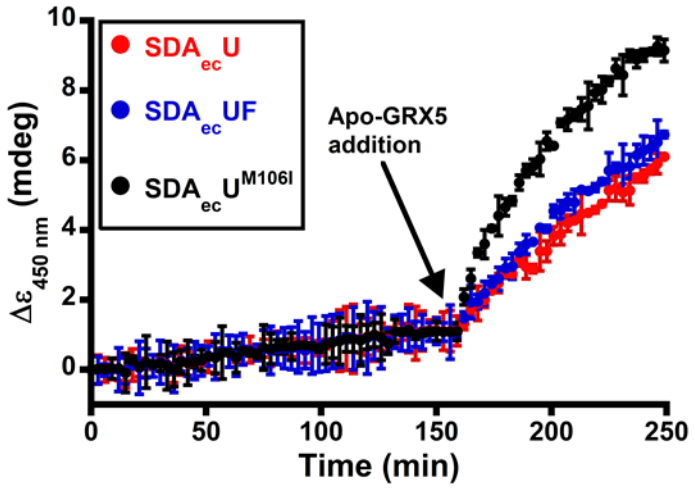

Figure II-8. Incorporation of the ISCU2^{M106I} substitution increases the cluster transfer rate from ISCU2 to GRX5. Fe-S clusters were synthesized on ISCU2 in reactions described in **Figure II-7**. The ellipticity at 450 nm was monitored for the SDA$_{ec}$U (red), SDA$_{ec}$UF (blue) and SDA$_{ec}$U^{M106I} (black) complexes. Samples were spiked with GRX5 (with or without FXN) 160 min after the reaction was initiated. Experiments were performed in triplicate.

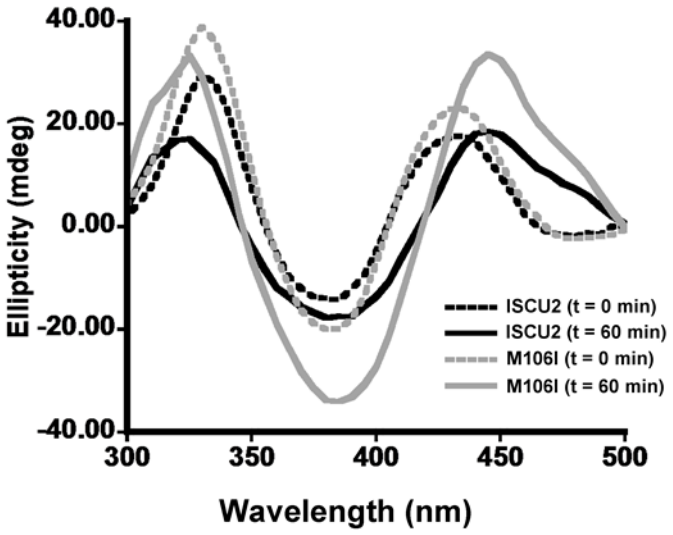

Figure II-9. Cluster transfer from chemically reconstituted ISCU2 and ISCU2^{M106I} to GRX5. 30 µM [2Fe-2S] cluster bound ISCU2 (black) or ISCU2^{M106I} (grey) before (dashed line) and after (solid line) reaction with 60 µM GRX5 in the presence of 10 mM GSH.

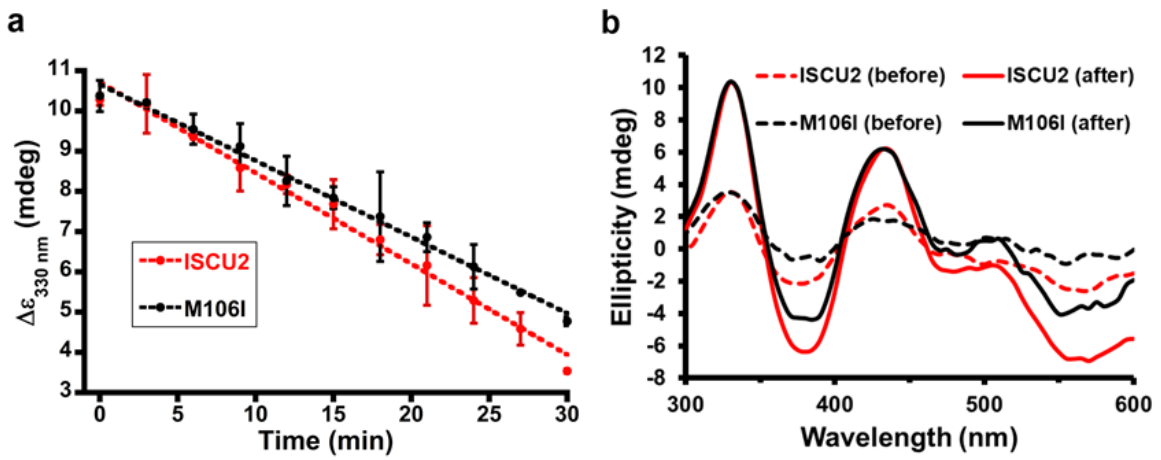

Figure II-10. [2Fe-2S] clusters bound to ISCU2 and ISCU2^{M106I} have comparable stabilities. A) [2Fe-2S] clusters were enzymatically assembled on ISCU2 (red) or ISCU2^{M106I} (blue). The addition of DTT initiated the cluster extrusion reaction, which was followed by the loss of ellipticity at 330 nm. The extrusion rates (0.22 mdeg/min for ISCU2 and 0.19 mdeg/min for ISCU2^{M106I}) were determined by fits to a linear equation. Experiments were performed in duplicate. **B**) Complete CD spectra are shown for the ISCU2 (red) and ISCU2^{M106I} (blue) before (solid line) and 30 min after (dashed line) the addition of DTT.

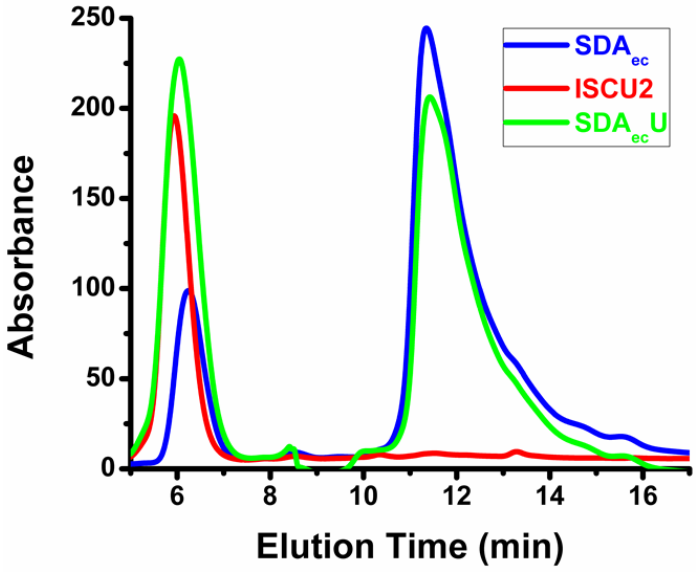

Figure II-11. Separation of subunits for the SDA$_{ec}$U complex. Assembly complex subunits were separated on a reverse phase column (gradient composed of CH_3CN, isopropanol and TFA; see Methods). ISCU2 (140 µM, red) eluted with a retention time of ~6 min. The SDA$_{ec}$ sample (45 µM, blue) had two peaks with retention times of ~6 min and ~12 min. The SDA$_{ec}$U sample (45 µM SDA$_{ec}$ plus 140 µM ISCU2, green) had increased peak intensity with a retention time at ~6 min, consistent with the presence of ISCU2.

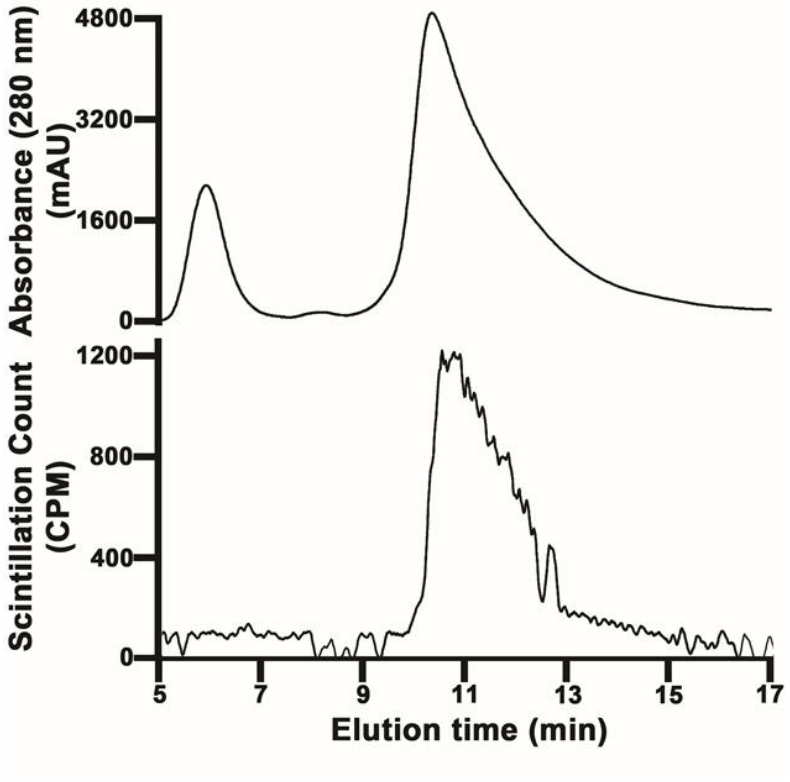

Figure II-12. Separation and detection of [^{35}S]-labeled NFS1. The SDA_{ec} complex was reacted with L-[^{35}S]-cysteine, quenched with acid, and the proteins were separated on a reverse phase column under quench conditions. The retention time for NFS1 (~11 min) was identified by the radioactivity peak (bottom panel). The band at ~6 min in the top panel was assigned to ISD11 and/or ACP_{ec}.

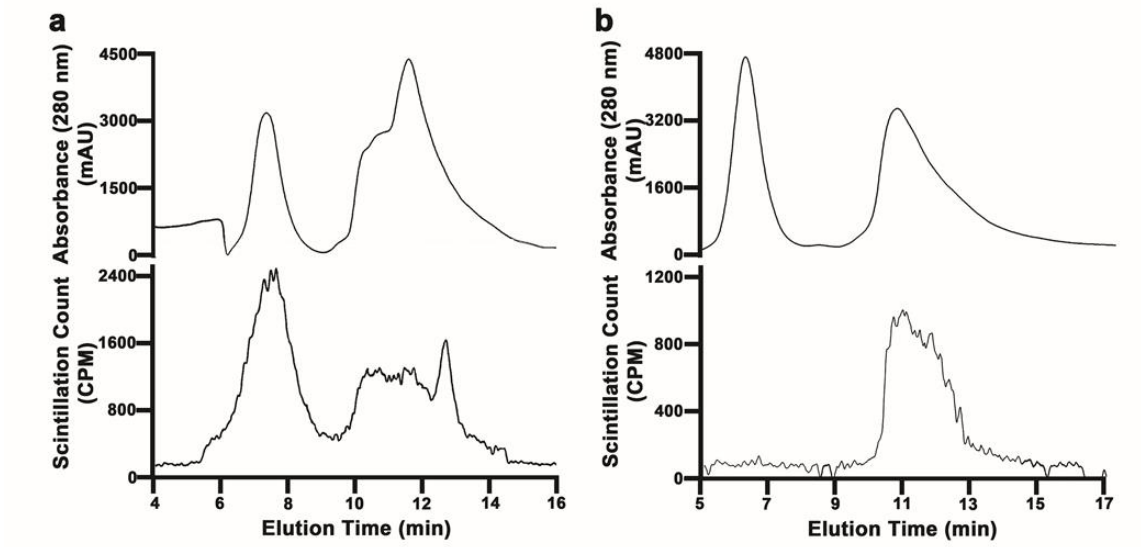

Figure II-13. Evidence that acid quenching inhibits interprotein sulfur transfer. NFS1 was labeled by combining the SDA_{ec} complex with L-[^{35}S]-cysteine for 30 min. **A**) The labeled NFS1 was incubated with ISCU2 for 30 min, followed by the addition of the quenching solution. The [^{35}S] label was associated with both the NFS1 (peak at ~12 min) and ISCU2 (peak at ~7 min). **B**) The labeled NFS1 was first combined with quenching solution and then incubated with ISCU2 for 30 min. The [^{35}S] label was associated with NFS1 (peak at ~12 min) but not ISCU2 (peak at ~7 min). Samples were analyzed by a reverse phase chromatography similar to **Figure II-11** and **II-12**. Note that the peaks for $ISD11/ACP_{ec}$ coincides with ISCU2 but have no cysteine residues that could form a persulfide species.

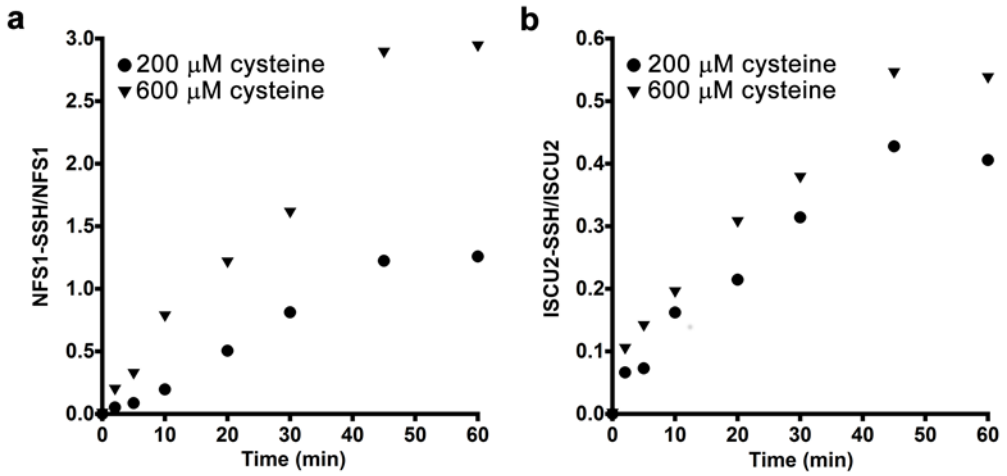

Figure II-14. Reactions with excess cysteine result in multiple persulfide species on NFS1 and ISCU2. The $SDA_{ec}U$ complex (30 μM SDA_{ec} and 30 μM ISCU2) was reacted with 200 or 600 μM L-[^{35}S]-cysteine at 37 °C and quenched at various times. The protein subunits were separated by reverse phase chromatography and the amount of radioactivity was quantitated for **A**) NFS1 and **B**) ISCU2.

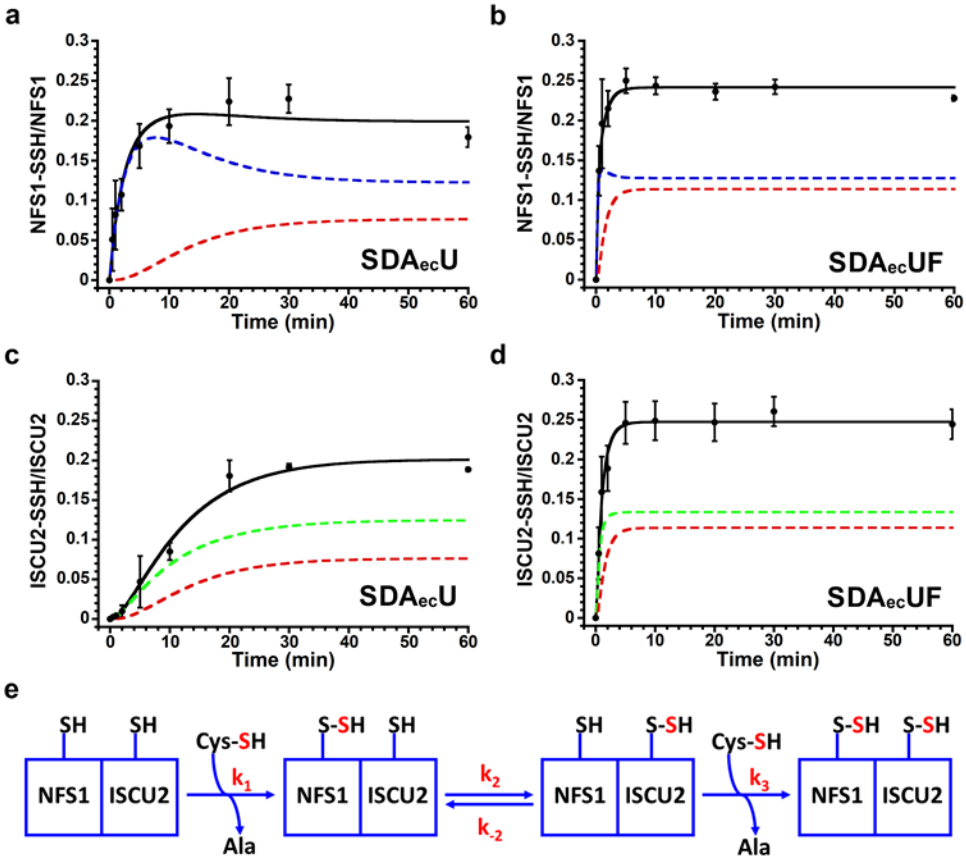

Figure II-15. **FXN accelerates the persulfide formation kinetics on both NFS1 and ISCU2.** $SDA_{ec}U$ and $SDA_{ec}UF$ complexes were reacted with a stoichiometric amount of L-[^{35}S]-cysteine, quenched with acid, and the proteins were separated using conditions similar to **Figure II-11**. Formation of [^{35}S]-persulfide was quantitated and plotted for **A**) NFS1 ($SDA_{ec}U$), **B**) NFS1 ($SDA_{ec}UF$), **C**) ISCU2 ($SDA_{ec}U$), and **D**) ISCU2 ($SDA_{ec}UF$). **E**) Best-fit kinetic model ($k_1 = k_3$) for persulfide accumulation on cysteine residues of NFS1 and ISCU2. The data for $SDA_{ec}U$ or $SDA_{ec}UF$ were fit simultaneously with KinTek and the fits were validated using FitSpace (**Figure II-16**). Blue, green, and red dashed lines represent the simulated amounts of persulfide on NFS1, ISCU2, or both NFS1 and ISCU2, respectively. Black lines indicate the total amount of simulated persulfide on NFS1 or ISCU2.

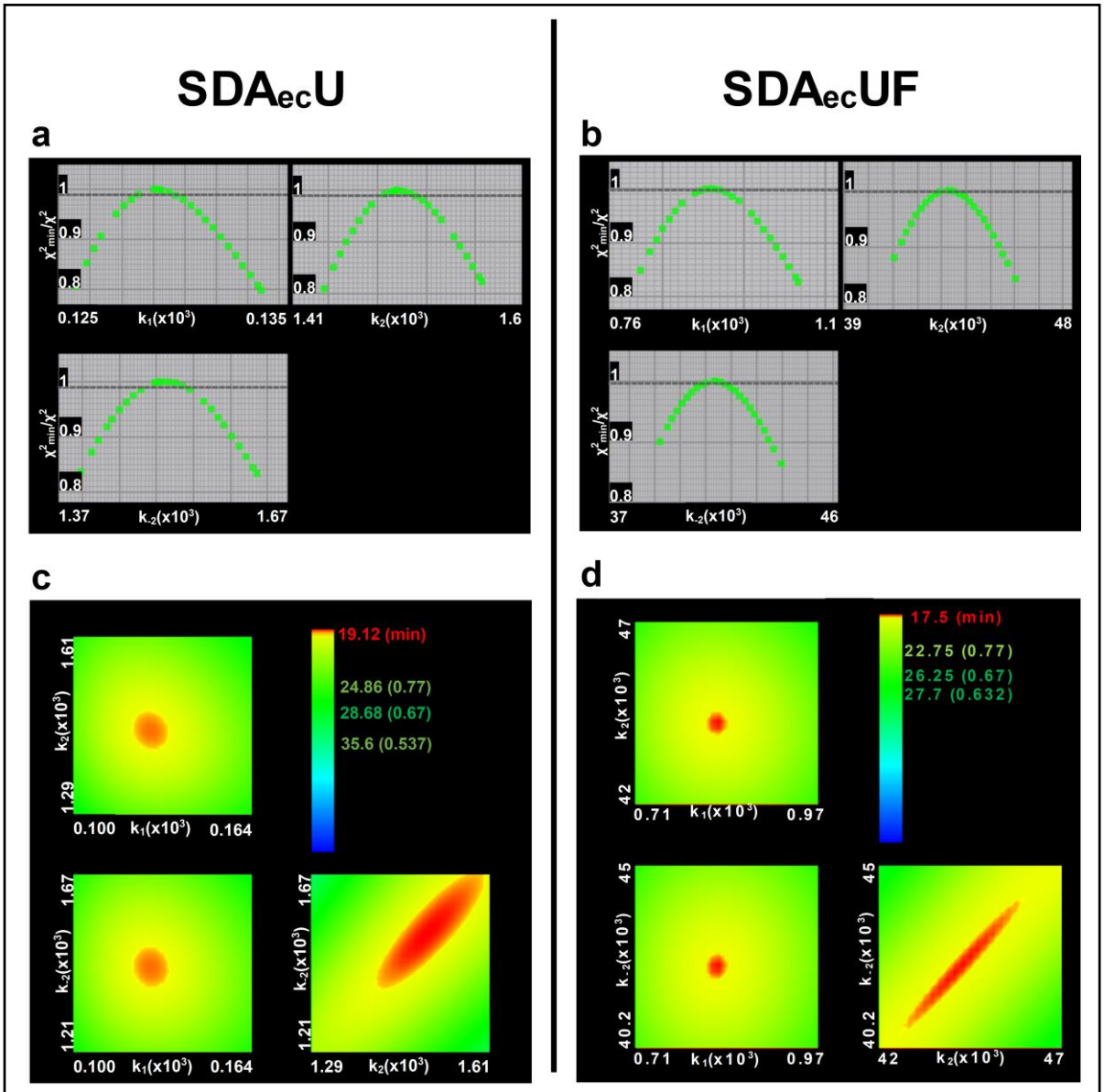

Figure II-16. Analysis of goodness of fit for persulfide formation model by FitSpace. Calculation of the (χ^2_{min}/χ^2) when k_1, k_2 and k_{-2} were varied individually for the **A**) $SDA_{ec}U$ and **B**) $SDA_{ec}UF$ complexes. For the best fit parameter value, (χ^2_{min}/χ^2) approaches one. Deviation from the best fit parameter value increase χ^2 for the fit and, in turn, decreases the (χ^2_{min}/χ^2) value. Heatmap describing 2D confidence contour (see Materials and Methods) for the **C**) $SDA_{ec}U$ and **D**) $SDA_{ec}UF$ complexes indicate that all the parameters are well constrained.

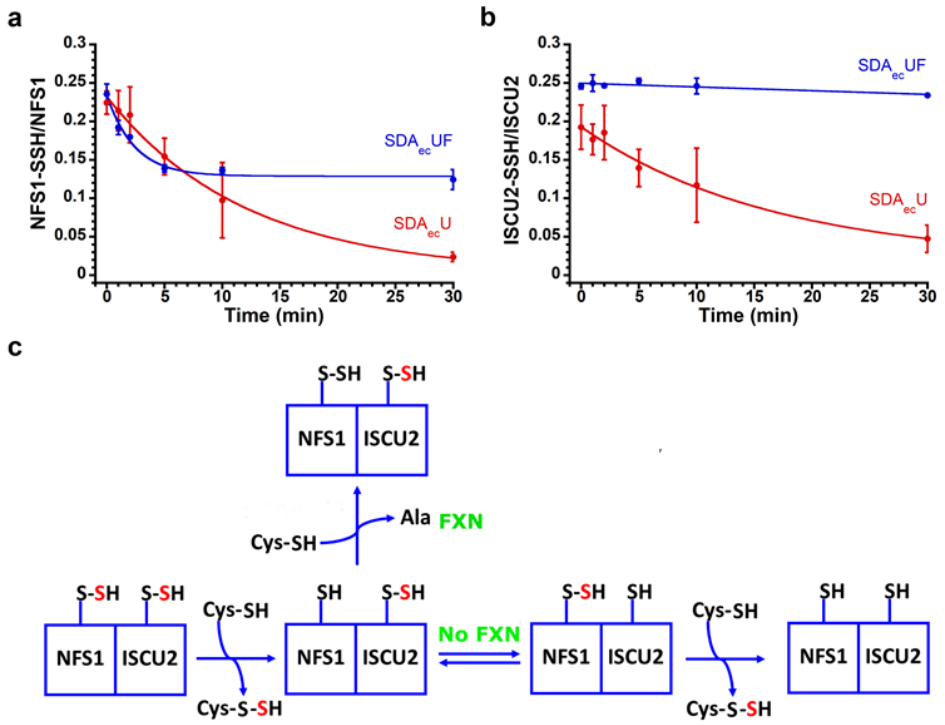

Figure II-17. **FXN accelerates the persulfide decay kinetics from NFS1.** $SDA_{ec}U$ (red) and $SDA_{ec}UF$ (blue) complexes were reacted with stoichiometric amounts (30 μM) L-[^{35}S]-cysteine for 40 min and then chased with 1 mM non-radioactive L-cysteine. Samples were then quenched with acid at various times and the amount of remaining [^{35}S]-label on **A**) NFS1 and **B**) ISCU2 were determined. The data were fit to an exponential decay or linear (loss of ISCU2 label from $SDA_{ec}UF$ complex) equation. **C**) Model for the effect of FXN on persulfide decay from the $SDA_{ec}U$ and $SDA_{ec}UF$ complexes. The NFS1 persulfide is proposed to be the primary species cleaved during the chase experiment. In the presence of FXN, the persulfide on NFS1 is rapidly regenerated by turnover with non-radioactive L-cysteine. In the absence of FXN, slower cysteine desulfurase turnover results in re-equilibration (transfer) of the ISCU2 radiolabeled sulfur (atom colored red) to NFS1 and subsequent cleavage.

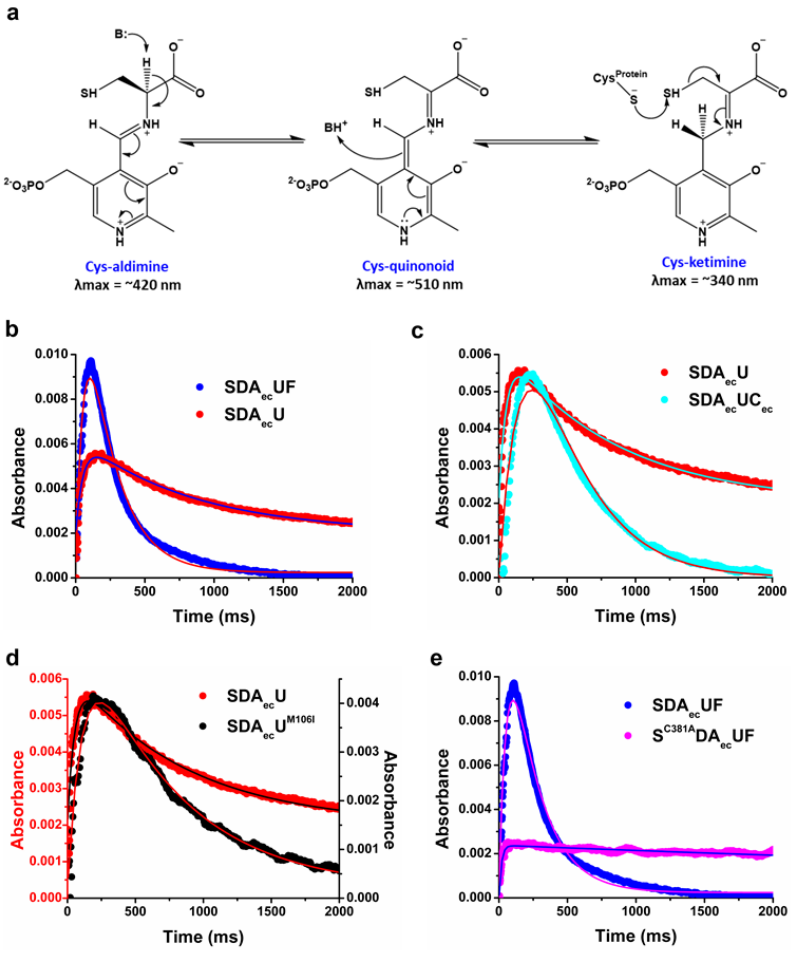

Figure II-18. FXN accelerates the decay of the quinonoid intermediate. A) Scheme showing steps of PLP chemistry that leads to C-S bond cleavage and persulfide formation on the mobile loop cysteine (NFS1-SSH). Stopped-flow kinetics for the cis-quinonoid decay of **B**) $SDA_{ec}U$ and $SDA_{ec}UF$ complexes, **C**) $SDA_{ec}U$ and $SDA_{ec}UC_{ec}$ (includes *E. coli* FXN homolog CyaY), **D**) $SDA_{ec}U$ and $SDA_{ec}U^{M106I}$ and **E**) $SDA_{ec}UF$ and $S^{C381A}DA_{ec}UF$. The traces are an average of three independent experiments. The rates for the development and decay of the quinonoid intermediate were obtained by nonlinear regression analysis (solid lines).

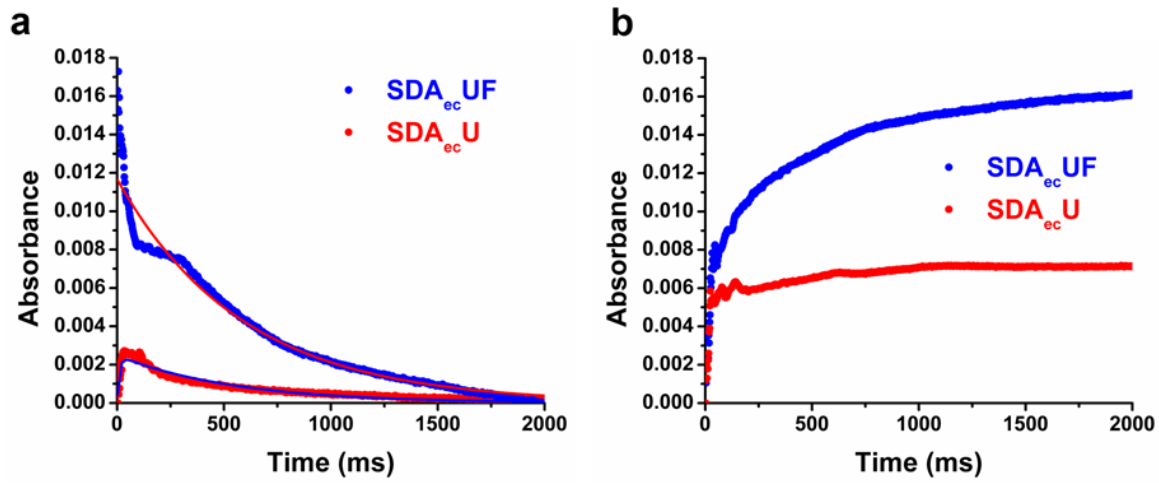

Figure II-19. Effect of FXN on the cys-aldimine and cys-ketimine formation and decay kinetics. The $SDA_{ec}U$ (red) and $SDA_{ec}UF$ (blue) complexes were reacted with 10 mM L-cysteine and the absorbance at **A**) 410 nm (assigned to the cys-aldimine intermediate) and **B**) 340 nm (assigned to the cys-ketimine intermediate) were recorded as a function of time in a stopped-flow experiment. The lines through the data in **A**) is a fit to a consecutive B equation (see Methods). The data in **B)** could not be meaningfully fit a rate equation.

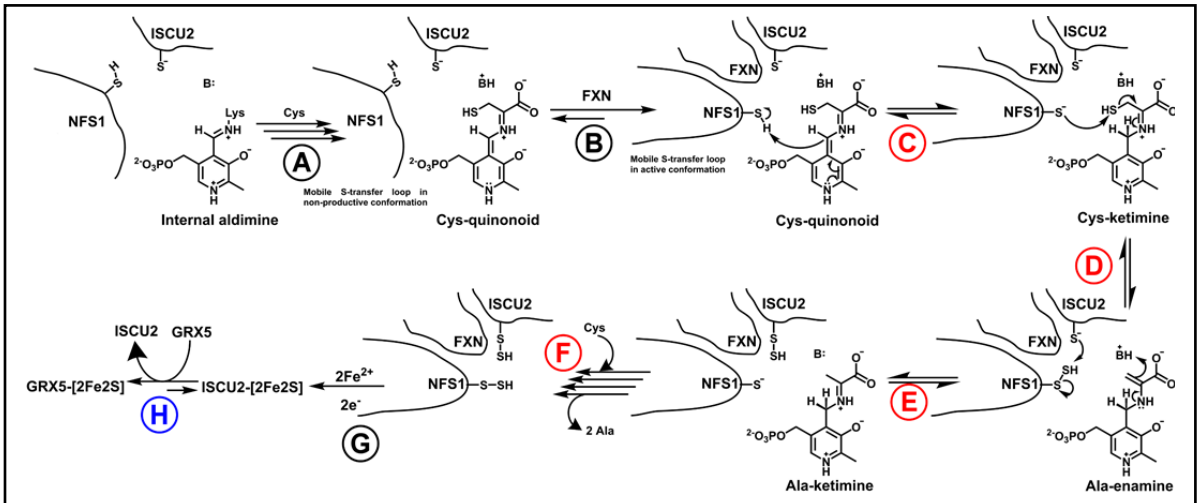

Figure II-20. Model for how FXN and the FXN bypass variant accelerate Fe-S cluster biosynthesis. A) Cysteine binding to NFS1 generates the Cys-quinonoid intermediate. **B**) In the absence of FXN, the NFS1 mobile S-transfer loop exists primarily in a non-productive conformation. FXN binding favors the active conformation. **C**) The FXN promoted conformation of the S-transfer loop allows its cysteine to function as a general acid and accelerate the decay of the cys-quinonoid intermediate. **D**) The deprotonated cysteine of the S-transfer loop nucleophilically attacks the cys-ketimine intermediate to generate a persulfide intermediate on NFS1 (NFS1-SSH). **E**) FXN favors the appropriate trajectory to deliver sulfur and produce a persulfide species on ISCU2 (ISCU2-SSH). **F**) A second cysteine turnover generates the NFS1-SSH ISCU2-SSH intermediate. **G**) Incorporation of ferrous iron and electrons generates the [2Fe-2S] intermediate on ISCU2. **H**) The [2Fe-2S] cluster is transferred to the apo acceptor GRX5. Steps labels in red are accelerated by FXN. Steps labeled in blue are accelerated by the ISCU2^{M106I} bypass variant.

Table II-1. Kinetic data for Fe-S assembly complexes (human).

						Relative Rate with respect to $SDA_{ec}U$	
		$SDA_{ec}U$	**$SDA_{ec}U^{M106I}$**	**$SDA_{ec}UF$**	**$SDA_{ec}U^{M106I}F$**	**$SDA_{ec}U^{M106I}$**	**$SDA_{ec}UF$**
Cysteine desulfurase activity	k_{cat} (min^{-1})	0.82 ± 0.03[a]	0.90 ± 0.02	10.07 ± 0.15[a]	7.34 ± 0.34	1.1	12.3
	K_M (μM)	0.62 ± 0.11[a]	0.65 ± 0.09	11.61 ± 0.92[a]	8.0 ± 2.0		
Complete reaction	Cluster synthesis & transfer to GRX5 (mdeg/min $X10^{-3}$)	4.1 ± 0.3	11.3 ± 0.2	14.4 ± 0.2	27.2 ± 0.9	2.8	3.5
Cluster transfer	Cluster transfer ISCU2 to GRX5 (mdeg/min X 10^{-3})	70 ± 0.5	130 ± 1	68 ± 5	ND	1.9	1.0
Cluster synthesis	Cluster formation on ISCU2 (mdeg/min X 10^{-2})	24 ± 1	37 ± 2	68 ± 2	55 ± 1	1.5	2.8
Sulfur transfer reactions with [^{35}S]-Cys (min^{-1} X 10^{-2})	Persulfide formation on NFS1 (k_1 and k_3)	0.8 (0.75 – 0.81)[b]	ND	5.2 (5.1 – 5.2)[b]	ND	–	6.5
	Persulfide transfer NFS1 to ISCU2 (k_2)	8.6 (8.5 – 9.6)[b]	ND	266 (252 – 282)[b]	ND	–	30.9
	Persulfide back transfer ISCU2 to NFS1 (k_{-2})	8.4 (8.2 –10.0)[b]	ND	254 (241 – 270)[b]	ND	–	30.2
Pulse-chase experiments (min^{-1} X 10^{-2})	Persulfide decay for NFS1	8 ± 1[c]	ND	42 ± 7[c]	ND	–	5.3
	Persulfide decay for ISCU2	6 ± 2[c]	ND	0.048 ± 0.0015[c,d]	ND	–	0.008
PLP Chemistry	Cys-quinoid formation (s^{-1})	19.5 ± 0.5	9.3 ± 0.1	17.5 ± 0.4	ND	0.5	0.9
	Cys-quinoid decay (s^{-1})	1.19 ± 0.03	1.47 ± 0.01	4.80 ± 0.07	ND	1.2	4.0

[a]Data from reference 4, [b]The values in parentheses denotes the lower and upper limit of the best fit value (rate constant). These were calculated at 99% and 99.7% confidence contours for $SDA_{ec}U$ and $SDA_{ec}UF$ complexes, respectively. [c]Spiked with 1 mM non-radioactive L-cysteine. [d]Determined with linear fit. ND – Not determined.

Table II-2. Rates for individual steps in the cysteine desulfurase reaction for Fe-S assembly complexes.

	Rate of Cys-aldimine Formation ($mAU.s^{-1}$)	Rate of Cys-aldimine Decay ($mAU.s^{-1}$)	Rate of Cys-quinonoid Formation ($mAU.s^{-1}$)	Rate of Cys-quinonoid Decay ($mAU.s^{-1}$)	Relative rate of cys-quinonoid decay
$SDA_{ec}U$	96 ± 15	1.82 ± 0.05	19.5 ± 0.5	1.19 ± 0.03	1
$SDA_{ec}U^{M106I}$	–	–	9.3 ± 0.1	1.47 ± 0.01	1.2
$SDA_{ec}UF$	–	1.70 ± 0.01	17.5 ± 0.4	4.80 ± 0.07	4.0
$SDA_{ec}UC_{ec}$	–	–	5.6 ± 0.2	2.9 ± 0.1	2.4

CHAPTER III

CYAY INHIBITS IRON SULFUR CLUSTER BIOSYNTHESIS IN PROKARYOTES BY INHIBITING SULFUR TRANSFER FROM ISCS TO ISCU

INTRODUCTION

Iron sulfur clusters are essential protein cofactors for most living organisms in all three domains of life[93]. They play crucial roles in electron transport, catalysis, regulation of gene expression, iron homeostasis etc[151-152]. Hence, iron sulfur cluster biosynthesis needs to be very tightly regulated. In prokaryotes, three iron sulfur cluster biosynthesis pathways are known – 1) Nitrogen fixation (NIF)[3-4], 2) Iron sulfur cluster assembly (ISC)[7-9] and 3) Sulfur Formation pathway (SUF)[153]. Among these, ISC pathway is the housekeeping pathway and operates under 'normal' growth conditions. On the other hand, NIF and SUF are more specialized systems. NIF is used exclusively to synthesize iron sulfur clusters on nitrogenases whereas SUF is used to make iron sulfur cluster under oxidative stress and limited iron conditions[154]. ISC pathway is also the only pathway that is shared between prokaryotes and eukaryotes. Therefore, the proteins involved in ISC pathway are highly conserved. In *E. coli*, ISC operon encodes genes for IscR (iron sulfur cluster containing transcriptional regulator), IscS (cysteine desulfurase)[10], IscU (scaffold protein)[89, 92], IscA (alternate scaffold/iron donor)[11, 155-156], HscB (co-chaperone)[17-18], HscA (chaperone)[18, 157], Fdx (putative electron donor)[86, 158] and IscX (effector)[159-160].

The mechanism of iron sulfur cluster biosynthesis is also very well conserved across prokaryotes and eukaryotes. IscU is the scaffold protein on which the cluster is assembled. IscS is a PLP dependent cysteine desulfurase that provides the sulfur to scaffold protein IscU in the form of a persulfide via an absolutely conserved mobile loop cysteine assisted conversion of cysteine to

alanine. That sulfane sulfur then reacts with ferrous iron and electrons provided most likely from reduced Fdx to form a $[2Fe2S]^{2+}$ on IscU in a process that is still very poorly understood. The scaffold protein then transfers the cluster to Grx4 in a reaction accelerated by HscA-HscB pair in an ATP dependent manner. Grx4 then transfers the clusters downstream to terminal acceptors like Fdx, Rieske etc.

Frataxin (FXN), a eukaryotic protein, has been shown to act as an allosteric activator of the eukaryotic cysteine desulfurase[70]. It activates iron sulfur cluster biosynthesis in eukaryotes by accelerating cys-aldimine formation, cys-quinonoid decay, persulfide formation on cysteine desulfurase NFS1 and sulfur transfer from NFS1 to scaffold protein (ISCU2) (CHAPTER II). Absence of this activation in absence of FXN such as in neurodegenerative disease Friedreich's Ataxia (FRDA)[38, 40] leads to impairment of iron sulfur cluster biosynthesis, severe iron overload in mitochondria and subsequent elevated oxidative stress that cause severe damage to the cell leading to cell death[39, 57, 161]. In stark contrast to eukaryotic system, CyaY (bacterial homolog of FXN) has been shown to inhibit iron sulfur cluster assembly on scaffold protein *in vitro*[75]. It was later shown that FXN also inhibits iron sulfur cluster biosynthesis on *E. coli* IscU and that the inhibitory effect of CyaY/FXN is dependent on cysteine desulfurase (prokaryotic vs. eukaryotic)[76]. However, the exact mechanism of how CyaY inhibits iron sulfur cluster biosynthesis on IscU is still unknown. Deletion of CyaY did not produce any of the phenotypes associated with FXN deletion most likely because under normal growth conditions, iron sulfur cluster biosynthesis is not required to be slowed down/inhibited[162]. However, it was recently shown that CyaY is required for cellular fitness under oxidative stress and limited iron conditions and has an overall positive role[160, 163-164]. Along the same line, a single mutation (I108M) on IscU was shown to make the cell

dependent on CyaY by somehow slowing down iron sulfur cluster biosynthesis creating condition of oxidative stress[165].

In this study, we aimed to determine how CyaY inhibits iron sulfur cluster biosynthesis on IscU and whether the inhibition translates to a slower rate of cluster delivery to terminal targets. We also investigated in detail the effect of I108M mutation on *E. coli* IscU on the rate of cluster assembly on IscU in presence and absence of CyaY. Using a combination of stopped-flow experiments, a novel persulfide formation assay and CD spectroscopy, we determined that CyaY slows down iron sulfur cluster formation on IscU by inhibiting sulfur transfer from IscS to IscU and that the inhibitory effect is indeed translated to slower rate of cluster delivery to Grx4 which functions as an intermediate cluster carrier. Moreover, we did not see any effect of $IscU^{I108M}$ mutation in presence or absence of CyaY.

RESULTS

Both CyaY and $IscU^{I108M}$ do not affect quinonoid decay. It has been shown that FXN, as well as CyaY, accelerate quinonoid decay for eukaryotic cysteine desulfurase resulting in a facilitated production of persulfide on mobile loop cysteine of NFS1. This is in accordance with previously published result that both FXN and CyaY act as allosteric activators of eukaryotic cysteine desulfurase. To determine whether or not CyaY slows down quinonoid decay of prokaryotic cysteine desulfurase IscS, we monitored the formation and decay kinetics of quinonoid intermediate using stopped-flow. For this, we first determined the λ_{max} (wavelength of maximal absorbance) for the quinonoid, aldimine and ketimine intermediates by scanning a 100 nm window in the range of 300 nm to 700 nm every 2 ms for 2 s (see methods). This gave us λ_{max} of quinonoid and aldimine intermediate at 508 nm and 410 nm respectively (**Figure III-1**). Unfortunately, we

did not see a peak around 340 nm for ketimine intermediate in any of our runs. We decided to use 340 nm to monitor the kinetics of ketimine intermediate nevertheless as this wavelength has been previously used to monitor ketamine intermediate[126]. As can be seen in **Figure III-2a, b, c and d**, quinonoid decay kinetics looks very similar for all the complexes and the rates of quinonoid decay were found to be very similar when fitted to consecutive B equation (**Table III-1**) with no effect of CyaY or $IscU^{I108M}$ on quinonoid decay. We also followed aldimine and ketimine formation kinetics by monitoring 410 nm and 340 nm respectively for SU and SUC complex. The kinetics were found to be similar in presence and absence of CyaY (**Figure III-3**).

CyaY inhibits sulfur transfer from IscS to IscU but does not affect persulfide formation on IscS. Next, we wanted to see if CyaY has any effect on persulfide formation on IscS and IscU which is the next downstream step after PLP chemistry. We incubated IscS and IscU in presence and absence of CyaY with cysteine that contains trace amount of radioactive ^{35}S-cysteine. We then quenched the reaction at different time points, separated proteins using HPLC (**Figure III-4a**) and quantified the amount of radioactivity via scintillation counting. The amount of radioactivity associated was then converted to the amount of persulfide on each protein using a standard curve. As can be seen in **Figure III-4b**, overall kinetics of persulfide formation on IscS in presence and absence of CyaY looked very similar but the extents of reaction completed were different. This corresponds really well with our previous observation that CyaY does not affect PLP chemistry, which directly results in persulfide formation on IscS. Contrary to this, CyaY significantly slowed down sulfur transfer from IscS to IscU **(Figure III-4c**). Interestingly, this contrasts with the effect of FXN on the human system where FXN accelerates sulfur transfer from NFS1 to ISCU2.

Both CyaY and IscU^{I108M} do not affect cysteine desulfurase activity. Cysteine desulfurase activity for all four complexes (SU, SUC, SU^{I108M}, SU^{I108M}C) was measured according to previously published protocol. Cysteine desulfurase activity was comparable for all four complexes (**Figure III-5**). The absence of an inhibitory effect of CyaY is consistent with the lack of any effect on quinonoid decay and persulfide formation on IscS.

CyaY inhibits iron sulfur cluster formation on scaffold protein while IscU^{I108M} has no effect. Iron sulfur cluster formation rates on scaffold protein (IscU or IscU^{I108M}) in presence and absence of CyaY were determined using CD spectroscopy by monitoring the ellipticity change at 330 nm. Consistent with previously published results, CyaY was observed to strongly inhibit iron sulfur cluster formation on scaffold protein (**Figure III-6 and Figure III-7**). This inhibition can be explained as a direct consequence of inhibited sulfur transfer to scaffold protein. On the other hand, contrary to literature, the rates were comparable for SU and SU^{I108M} in absence of CyaY. Moreover, CyaY did not accelerate iron sulfur cluster synthesis in the case of IscU^{I108M} as had been suggested in the literature.

CyaY does not affect iron sulfur cluster transfer from IscU to Grx4. Next, we wanted to explore if CyaY has any other effect(s) on cluster biosynthesis process in addition to inhibition of cluster assembly on scaffold protein IscU. To determine if CyaY has any effect on cluster transfer step, we reconstituted IscU (**see methods**) followed by addition of apo-Grx4 to initiate the reaction. The cluster transfer reaction was monitored using CD spectroscopy by monitoring ellipticity change at 450 nm (where Holo-Grx4 has much larger contribution compared to Holo-IscU). The rates were found to be comparable with and without CyaY (**Figure III-8 and Figure III-9**). This shows that CyaY does not affect cluster transfer from holo-IscU to apo-Grx4.

CyaY inhibits one-pot cluster synthesis on Grx4 while IscU^{I108M} has no effect. We further tested whether or not the inhibitory effect of CyaY on sulfur transfer step and consequently iron sulfur cluster assembly on scaffold protein results in inhibition of holo-Grx4 synthesis in a one-pot reaction where Holo-IscU is not pre-formed and cluster assembly on Grx4 is monitored by recording ellipticity change at 450 nm. CyaY strongly inhibited cluster synthesis on Grx4 (**Figure III-10 and Figure III-11**). On the other hand, IscU^{I108M} had no effect. This is in stark contrast to the effect of opposite mutation on human ISCU2^{M106I} which has been shown to accelerate cluster transfer from ISCU2 to GRX5.

DISCUSSION

CyaY does not affect PLP chemistry and persulfide formation on IscS and cysteine desulfurase activity, unlike FXN. Although it has been well known for a long time that CyaY inhibits iron sulfur cluster synthesis on scaffold protein IscU[75-76, 166], mechanism of the inhibition remained unknown. More specifically, it remained to be discovered which upstream step(s) is specifically inhibited by CyaY. Using a step-wise detailed analysis of the effects of CyaY on each and every upstream step and one downstream step, we sought to pinpoint the step(s) affected by CyaY. To accomplish this, we divided the whole pathway into four major steps – 1) persulfide formation, 2) sulfur transfer, 3) cluster synthesis and 4) cluster transfer (**Figure III-9**). We were aware that FXN activates persulfide formation on NFS1 by accelerating quinonoid decay. Therefore, we first tested if CyaY affects quinonoid decay. Using stopped-flow, we found that contrary to the effect of FXN in the human system, CyaY does not affect quinonoid decay of IscS both in presence and absence of IscU. Next, we examined if CyaY inhibits persulfide formation on IscS. Using the persulfide formation assay, we found that CyaY does not affect persulfide

formation on IscS unlike the effect of FXN on the human system where FXN was shown to accelerate persulfide formation on NFS1. This is consistent with our observation that CyaY does not accelerate quinonoid decay, which directly translates into persulfide formation. Therefore, this suggests that unlike in the case of FXN based activation of human cysteine desulfurase, CyaY does not perturb mobile loop trajectory of IscS. Again, consistent with lack of any effect of CyaY on persulfide formation on IscS, CyaY only had a minor inhibitory effect on cysteine desulfurase activity of IscS in presence of IscU (Also consistent with previous literature)[76].

CyaY slows down persulfide formation on IscU and subsequently iron sulfur cluster biosynthesis on IscU. In the same persulfide formation assay, we also found that in the presence of CyaY, persulfide formation on IscU was ~4 times slower. This is exactly opposite to the effect of FXN which, has been shown to accelerate persulfide formation on ISCU2. So how does CyaY inhibits persulfide formation on IscU. As we deduced earlier that CyaY does not perturb either mobile loop trajectory, we think CyaY may be causing a small conformational change in IscU, which results in misalignment of mobile loop trajectory and the cysteine residue on IscU that accepts sulfane sulfur. In absence of crystal structure of SUC complex it is extremely difficult to determine if this is the case. It is also possible that CyaY binds in the cleft between IscS and IscU and sterically prevents mobile loop cysteine from reaching to IscU and prevents sulfur transfer. The latter scenario has already been predicted using an in-silico study[167]. As expected, consistent with previous literature, CyaY was also found to strongly inhibit iron sulfur cluster formation on IscU. This shows that inhibition of sulfur transfer to scaffold protein directly translate into the inhibition of iron sulfur cluster biosynthesis on scaffold protein IscU and therefore provides

evidence in support of IscU persulfide being kinetically competent intermediate in iron sulfur cluster biosynthesis.

Inhibitory effect of CyaY propagates further downstream to holo-Grx4 formation. After successfully determining sulfur transfer as the step that is primarily inhibited by CyaY resulting in slower iron sulfur cluster formation on IscU, we went further to determine - 1) if CyaY has any further role down-stream and 2) if this inhibitory effect translates to a slower rate of cluster synthesis on downstream acceptors. We found that CyaY does not affect cluster transfer from Holo-IscU to apo-Grx4 but inhibits one-pot cluster synthesis on Grx4. This shows that the inhibitory effect of CyaY on IscU cluster assembly slows down overall cluster biosynthesis process.

The enigma: is CyaY an inhibitor or activator of iron sulfur cluster biogenesis? All the above results clearly showed that CyaY indeed inhibits iron sulfur cluster biosynthesis. This inhibitory effect originates in sulfur transfer step and propagated up to holo-Grx4 formation, which is an intermediate in cluster transfer pathway and distributes cluster to apo-targets (**Figure III-12**). This leads us to an important question - how does this inhibitory effect affect the fitness of an organism? We can predict that in absence of CyaY, an organism will produce iron sulfur cluster at a much faster rate. However, this also means transcriptional regulator IscR will also get iron-sulfur cluster faster and will start repressing protein translation to prevent overproduction of iron sulfur cluster i.e. iron sulfur cluster production will remain normal in absence of CyaY and there would not be any usual phenotype such as growth defect, unusual activity of iron sulfur cluster containing proteins etc. That is exactly what has been reported for CyaY deleted strain when grown in normal rich media[160, 162]. However, a number of recent publications also reported that CyaY

deletion affects organism's fitness under specific conditions and proposed that CyaY has a positive role in iron sulfur cluster biosynthesis. However, those reports did not discuss the inhibitory effect of CyaY *in vitro* and how this inhibitory effect may make CyaY important under those conditions. It has been shown that when YggX and ApbC genes were deleted together or separately, the presence of CyaY becomes crucial. YggX has been shown to sequester Fe(II) from participating in Fenton chemistry while keeping it available for iron-dependent cellular processes and thereby preventing oxidative damage[168-169]. ApbC is a member of MinD protein family and takes part in iron sulfur cluster metabolism process[170-173]. Understandably, absence of ApbC results in iron sulfur cluster metabolism defect and subsequent oxidative stress. When cells were grown in presence of H_2O_2, NO or paraquat, deletion of CyaY inhibited growth and this inhibition was exacerbated when YggX was also deleted[163]. Considering these results, CyaY definitely seems to have a positive effect on the fitness of organism under oxidative stress conditions. Interestingly, IscR deletion strain which cannot regulate iron sulfur production through transcriptional inhibition becomes hypersensitive to oxidative stress just like CyaY deletion strain[174]. It seems as if iron sulfur cluster acts as fuel for reactive oxygen species. Taken together, overproduction of iron sulfur cluster seems to be detrimental to the fitness of an organism in the event of oxidative stress and the inhibitory effect of CyaY on iron sulfur cluster production can explain the apparent positive effect of CyaY. At present, there is no direct evidence that overproduction of iron sulfur cluster can exacerbate oxidative stress by acting as fuel for it but if that is the case, it will change our understanding significantly.

I108M variant of IscU behaves like wild-type. It had been shown by Dancis and co-workers that a single point mutation (M → I) on scaffold protein in yeast can rescue all FXN

deletion phenotypes via bypassing FXN i.e. M → I mutation on scaffold protein in eukaryotes can make the organism FXN independent[79, 175]. As deletion of CyaY has no effect under normal growth condition, *E. coli* is CyaY independent. This led to study by Roche *et al.* to determine if the reverse mutation I → M would render *E. coli* CyaY-dependent[165]. They showed that cellular iron sulfur cluster level decreased for I → M mutation in *E. coli* and was even worse in absence of CyaY. Recently we determined that ISCU2^{M106I} bypasses FXN by accelerating cluster transfer to GRX5 in the human system. Here, we did a similar step-wise analysis to study the effect of IscU^{I108M} on each step in the presence and absence of CyaY. More specifically, we tested if IscU^{I108M} slows down any step and whether CyaY rescues the rate. We found that IscU^{I108M} variant behaved just like wild type in all the steps and the effect of CyaY on cluster assembly of scaffold protein was also similar for IscU^{I108M} and wt-IscU i.e. inhibitory rather than accelerating. Therefore, at present we still don't have a mechanism that explains the effect of I → M mutation on scaffold protein of *E. coli in vivo*.

S-transfer loop cysteine does it all: A common mechanism of *E. coli* and human cysteine desulfurase with differential regulation by FXN/CyaY. It was known that S-transfer loop cysteine in human cysteine desulfurase NFS1 acts as a proton donor for quinonoid decay. We, therefore, tested if the S-transfer loop cysteine of *E. coli* cysteine desulfurase IscS can also act as a proton donor for the quinonoid decay step. We found that mutation of mobile loop cysteine to alanine abolished quinonoid decay (**Figure III-3e, III-3f)** and indeed serves as the proton donor for quinonoid to ketimine conversion in IscS and that a similar mechanism is in operation across all cysteine desulfurases. Furthermore, we reasoned that if quinonoid decay is inhibited in C328A variant of IscS, there should be an accumulation of quinonoid intermediate. Instead, we see a very

small quantity of quinonoid. A similar result was also obtained for the human system where $S^{C381A}DA_{ec}UF$ had a very small quinonoid accumulation but was comparable to $IscS^{C328A}$. We later realized this apparent anomaly is, in fact, the norm when we compared the total quinonoid accumulation with the rate of quinonoid decay of both *E. coli* and human cysteine desulfurases (**Figure III-13**). To explain that we reasoned that the s-transfer loop cysteine must also be facilitating some upstream step, most likely aldimine formation. When aldimine formation was monitored for $IscS^{C328A}$ and $S^{C381A}DA_{ec}UF$, we found that the extent of aldimine formation is very low consistent with S-transfer loop cysteine's participation in this step (**Figure III-14 and III-15**). Moreover, when we monitored ketimine formation for $IscS^{C328A}$ and $S^{C381A}DA_{ec}UF$, we found very little accumulation of ketimine intermediate, which is again consistent with very slow quinonoid decay (**Figure III-14 and III-15**). Overall this reveals a common cysteine desulfurase mechanism in which S-transfer loop cysteine is doing everything – 1) facilitated aldimine formation, 2) accelerated quinonoid decay by acting as proton donor, 3) cleaved C-S bond of substrate cysteine by nucleophilic attack and generates persulfide on S-transfer loop cysteine and lastly 4) transfer sulfane sulfur in the form of persulfide to different sulfur acceptors. Further, we can speculate the nature of s-transfer loop cysteine's participation in aldimine formation. As we understand, a facilitated gem-diamine formation requires nucleophilic attack of substrate cysteine α-amino group to electrophilic PLP. An absorption peak at 420 nm indicates PLP is protonated at pyridine and imine nitrogens and therefore, sufficiently electrophilic. Hence, we speculate s-transfer loop cysteine may be acting as a general base and facilitates deprotonation of the α-amine moiety of incoming substrate cysteine. As we have seen previously, all these steps that are facilitated by s-transfer loop cysteine, are also accelerated by FXN whereas only the inter-protein sulfur transfer is inhibited by CyaY. This information reinstate the model of FXN based activation in which S-

transfer loop is very flexible and adopts mostly non-productive loop trajectories in human monomeric cysteine desulfurase (SDA_{ec} or $SDA_{ec}U$) architecture. FXN binding limits the non-productive loop trajectories and thereby accelerates all four steps affected by s-transfer loop cysteine. On the other hand, *E. coli* IscS is dimeric and here the other subunit is limiting non-productive loop trajectories and therefore highly active in absence of FXN/CyaY. In fact, when compared rates, IscS dimer is actually much more efficient that $SDA_{ec}UF$. Furthermore, lack of any effect of FXN/CyaY on the PLP chemistry of IscS compared to activating effects of FXN/CyaY on $SDA_{ec}U$ would strongly suggest differential binding of FXN/CyaY to dimeric IscS and monomeric $SDA_{ec}U$ and establishes monomeric architecture of SDA_{ec} as physiologically relevant quaternary structure.

MATERIAL AND METHODS

Protein purification: IscS, IscU and CyaY were purified as described previously[76]. The QuikChange method (Stratagene) was used to introduce point mutation (I108M) into plasmid containing wt-IscU[75]. The mutation was confirmed by DNA sequencing (Gene Technology Lab, TAMU). $IscU^{I108M}$ was purified using the same protocol as wt-IscU. Grx4 was purified following literature procedure[176]. Unless otherwise stated, all the reactions were carried out in an anaerobic glove box (O_2 < 1 ppm).

Stopped-flow kinetics: Proteins (100 µM of each protein) were taken in one of the two syringes of the stopped-flow apparatus (KinTek Corporation). The other syringe contained 10 mM Cysteine. They were mixed together by pressing both the syringes simultaneously. Therefore, the final concentration of proteins and cysteine in the cuvette was 50 µM and 5 mM respectively. First,

λ_{max} of each intermediate was determined by monitoring the change of absorbance every 2 ms in a 100 nm window. λ_{max} for quinonoid and aldimine intermediate was found to be 508 nm and 410 nm respectively, which were later used to monitor the kinetics of the intermediates. We could not detect a sharp peak around 340 nm for ketimine intermediate. We, therefore, used 340 nm as this wavelength has been used previously[126]. Next, the formation of aldimine, quinonoid and ketimine intermediate was followed by monitoring absorbance at 410, 508 and 340 nm respectively. For quinonoid kinetics, traces of 508 nm with time were fitted with Origin software (OriginLab) to Consecutive B equation [$y = y0 + (k1*[A]_0/(k2-k1))*(\exp(-k1*t)-\exp(-k2*t))$], where k1 and k2 are rate constants of the formation and decay of cys-qiononoid intermediate respectively. The rates were compared for IscS, IscS^{C328A}, SU, SUC, SU^{I108M} and SU^{I108M}C. [R^2 values: IscS (0.99), IscS^{C328A} (0.83), SU (0.99), SUC (0.99), SU^{I108M} (0.99), SU^{I108M}C (0.99)]. Aldimine and ketimine (410 nm and 340 nm traces respectively) could not be fit adequately using Consecutive B equation as kinetics were more complex.

Separation of proteins for sulfur transfer reaction: All the proteins (IscS, IscU and CyaY) were separated using C4 column (WAT011807, Waters) on HPLC (1260 Infinity, Agilent Technologies) at pH 2.0 (0.1 % TFA in water, Buffer A) by running a gradient of Buffer B (60% CH_3CN, 40% Isopropanol, 0.1% TFA) from 30% to 70% within 40 min with 1mL/min flow rate.

Measurement and quantification of radioactivity on proteins: The amount of radioactivity and in turn persulfide on IscS and IscU were determined using a similar procedure as described previously (CHAPTER II). Briefly, [^{35}S]-cysteine (PerkinElmer, 10.2 μM, 1.00796 mCi) was diluted 50 times by 1 mM non-radioactive cysteine resulting in a 204 nM final concentration of [^{35}S]-cysteine in the stock solution and the ratio of [^{35}S]-cysteine over cold

cysteine became 0.000204. After elution, the protein was passed through a mixer where it was combined with scintillation cocktail (BioCount 111182) and the signal was recorded with β-RAM radio-HPLC detector (Model 5C, LabLogic). Data collection and analysis were done with Laura software (LabLogic). The area under the scintillation peak (in CPM) was determined for each protein and converted into [^{35}S] concentration associated with protein by using a standard curve plotted from known amounts [^{35}S]-cysteine (and determining the area under the peak corresponding to cysteine). The total amount of persulfide on protein was obtained via dividing it by the [^{35}S]-cysteine and non-radioactive cysteine ratio.

Persulfide formation assay: Protein complexes (SU and SUC) were reacted with 30 μM cysteine (contains 0.0204% [^{35}S]-cysteine) at 37°C followed by quenching at different time points starting from thirty seconds to one hour. Final protein concentrations were 30 μM IscS, 30 μM IscU and 75 μM CyaY (for SUC) with 50 μL reaction volume. The samples were quenched by mixing 150 μL quenching solution (conc. HCl and 6 M Guanidine hydrochloride (in 1:4 ratio, pH<1) to the 50 μL reaction. 150 μL of the resulting 200 μL was injected into HPLC for analysis. Amount of persulfide associated with IscS and IscU was calculated as described above and plotted against time. The data points were fitted using Origin software (OriginLab) to exponential rise equation [y=m1+m2*(1-exp (-m3*x))] where m3 value gives the apparent rate of formation. [R^2 values; IscS-SSH formation: 0.98 (SU), 0.98 (SUC); IscU-SSH formation: 0.98 (SU), 0.88 (SUC)].

Cysteine desulfurase activity: Cysteine desulfurase activities were measured for each complex (SU, SUC, SU^{I108M} and $SU^{I108M}C$) according to the published procedure (CHAPTER II). In short, a heating block was used to bring the temperature to 37°C. The proteins were mixed to a final concentration of 0.5 μM IscS, 2.5 μM IscU (or $IscU^{I108M}$), 5 μM CyaY and 2 mM DTT

followed by incubation for 15 minutes on heating block already at 37°C, cysteine was then added and the reaction was then incubated for additional 6 min before quenching the 800 µL reaction mixture with 100 µL of *N, N'*-diphenyl-*p*-phenylenediamine (DPD, in 7.2 M HCl) and 100 µL of $FeCl_3$ (in 1.2 M HCl) with final concentration of DPD and $FeCl_3$ being 30 µM and 20 µM respectively. The samples were centrifuged after 20 min incubation at 37ºC and absorbance was measured at 670 nm. The amount of sulfide produced was determined for each data point using a standard curve. Rates ($[S^{2-}]$/([SD]*min)) were plotted against the amount of cysteine added and fitted with Origin software (OriginLab) using Michaelis-Menten Equation to obtain k_{cat} and K_M values for each complex. [R^2 values: SU (0.98), SUC (0.998), SU^{I108M} (0.99), $SU^{I108M}C$ (0.99)].

CD spectroscopy: CD spectra were recorded on a Chirascan CD spectrometer (Applied Photophysics) using a 1 cm path length cuvette. Cuvettes were sealed with a rubber septum and electrical tape in a glove box (O_2 < 1 ppm). The assays were run in 50 mM HEPES, 150 mM KCl, and 10mM $MgCl_2$ (pH 7.5) at 22ºC.

Cluster assembly assay on IscU: The assay constituted 8 µM IscS, 40 µM IscU (or $IscU^{I108M}$), 50 µM CyaY, 200 µM $Fe(NH_4)_2(SO_4)_2$ and was initiated with the addition of 10 mM GSH and 100 µM cysteine using air-tight syringes. The cluster assembly rates were measured for SU, SUC, SU^{I108M}, $SU^{I108M}C$ by monitoring the ellipticity change at 330 nm over time and fitting the initial data points using Kaleidagraph (Synergy software) to linear equation ($y=m_1x+m_2$), where m_1 gives the initial rate of cluster synthesis. [R^2 values: SU (0.99), SUC (0.96), SU^{I108M} (0.99), $SU^{I108M}C$ (0.99)].

Cluster transfer assay from Holo-IscU to apo-Grx4: 20 μM IscU was re-constituted using 1 μM IscS, 40 μM CyaY, 400 μM $Fe(NH_4)_2(SO_4)_2$ and 40 μM cysteine with cysteine being the limiting reagent to inhibit any further cluster-synthesis. 40 μM Grx4 was then injected into the cuvette anaerobically using an air-tight syringe and the cluster transfer to the latter was followed by monitoring the ellipticity change at 450 nm over time and fitting the initial data using Kaleidagraph (Synergy software) to linear equation ($y=m_1x+m_2$), where m_1 gives the initial rate of cluster transfer from Holo-IscU to apo-Grx4. 450 nm was chosen as the wavelength to monitor the transfer due to minimal contribution from holo-IscU at that wavelength. The rates were compared for SU, SUC. [R^2 values: SU (0.93), SUC (0.93)].

One-pot Cluster synthesis on apo-target: 0.5 μM IscS, 20 μM IscU (or $IscU^{I108M}$), 40 μM CyaY, 40 μM Grx4, 200 μM $Fe(NH_4)_2(SO_4)_2$ and initiated by the addition of 10 mM GSH and 100 μM cysteine. Cluster formation on Grx4 was then measured for SU, SUC, SU^{I108M}, $SU^{I108M}C$ by monitoring the change of ellipticity at 450 nm over time and fitting the initial time points using Kaleida graph (synergy software) to linear equation ($y=m_1x+m_2$), where m_1 gives the initial rate of cluster formation on Grx4. [R^2 values: SU (0.99), SUC (0.94), SU^{I108M} (0.99), $SU^{I108M}C$ (0.62)].

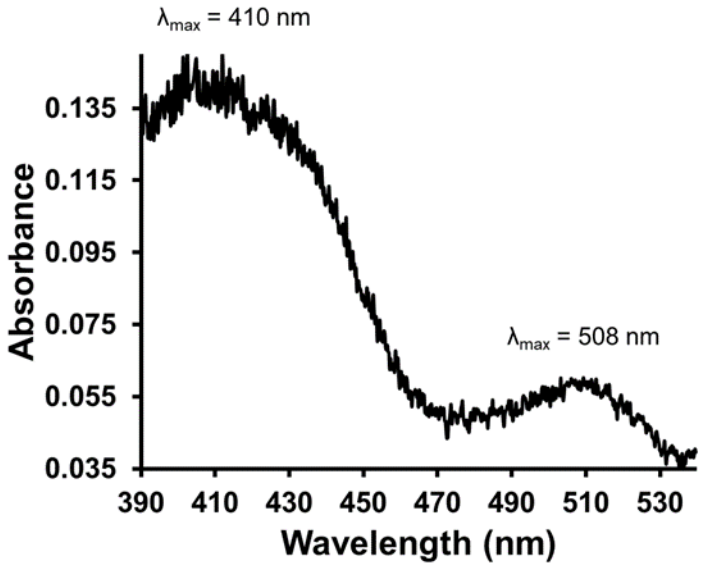

Figure III-1. Wavelengths of maximal absorbance (λ_{max}) of PLP intermediates were determined by stopped flow. Reaction contained 50 µM IscS and 5 mM cysteine (final concentration). These wavelengths were used to determine the kinetics of intermediates for all the complexes.

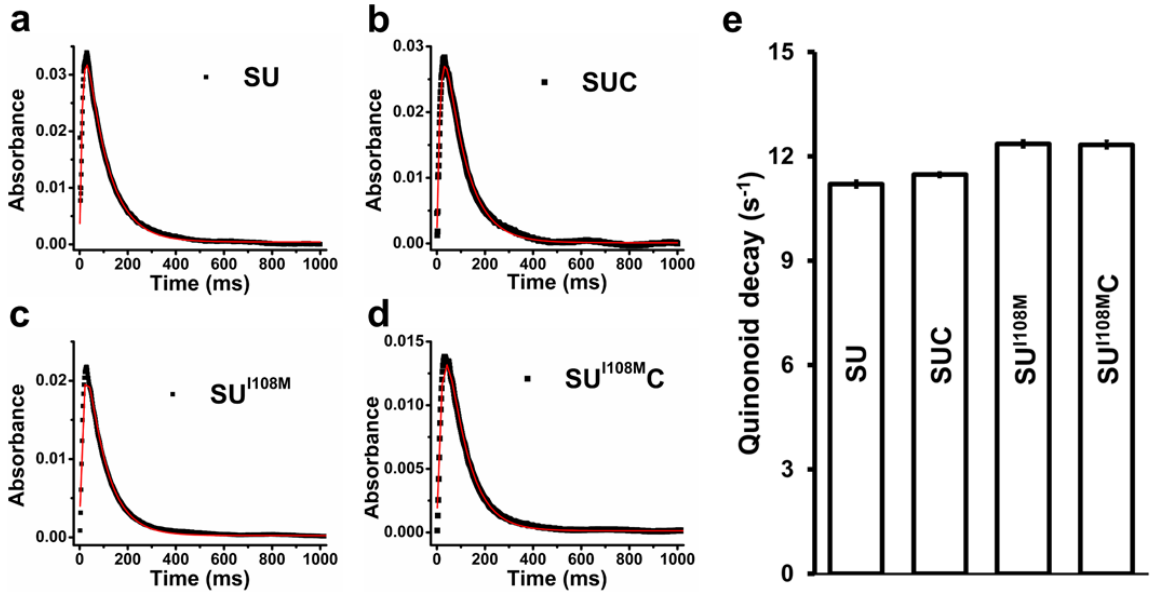

Figure III-2. Both CyaY and IscU^{I108M} does not affect the rate of quinonoid formation and decay. The formation and decay of quinonoid intermediate were monitored by stopped flow at 508 nm wavelength. Reaction contained 50 µM all the proteins (IscS, IscU/IscU^{I108M}, CyaY) and 5 mM cysteine (final concentrations). The rates were obtained by fitting the data to the equation [y=y0 + A*(m1/(m3-m2))(exp(-m2*x)-exp(-m3*x))], where m2 and m3 values give the apparent rate of formation and decay of the quinoid intermediate respectively.

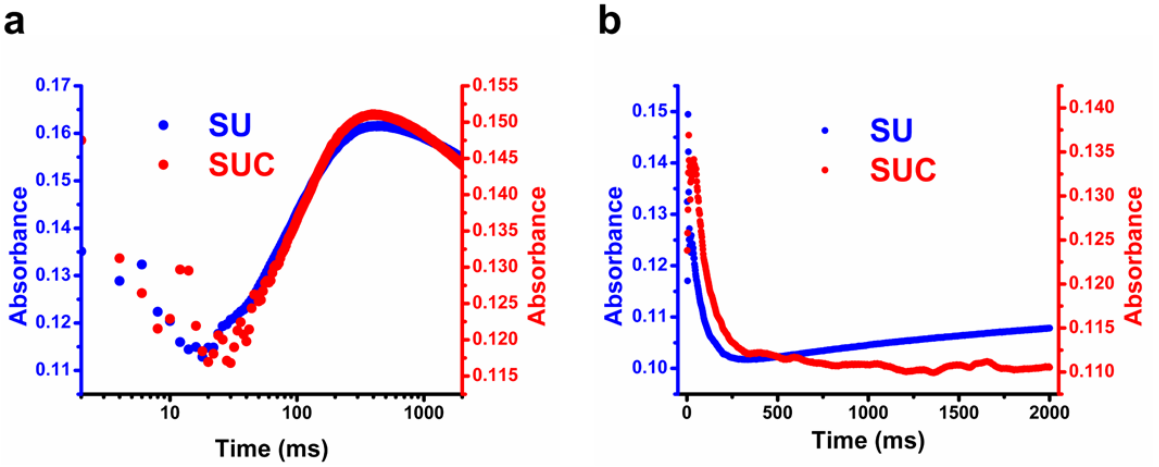

Figure III-3. CyaY does not affect the rate of aldimine and ketimine formation and decay. The formation and decay of aldimine and ketimine intermediates were monitored by stopped flow at 410 and 340 nm wavelength respectively. Reaction contained 50 µM all the proteins (IscS, IscU, CyaY) and 5 mM cysteine (final concentration). A rate constant for the formation and decay of the intermediates could not be determined as the data could not be fitted to the equation [y=y0 + A*(m1/(m3-m2))(exp(-m2*x)-exp(-m3*x))], where m2 and m3 values would have given the apparent rate of formation and decay of the intermediate respectively.

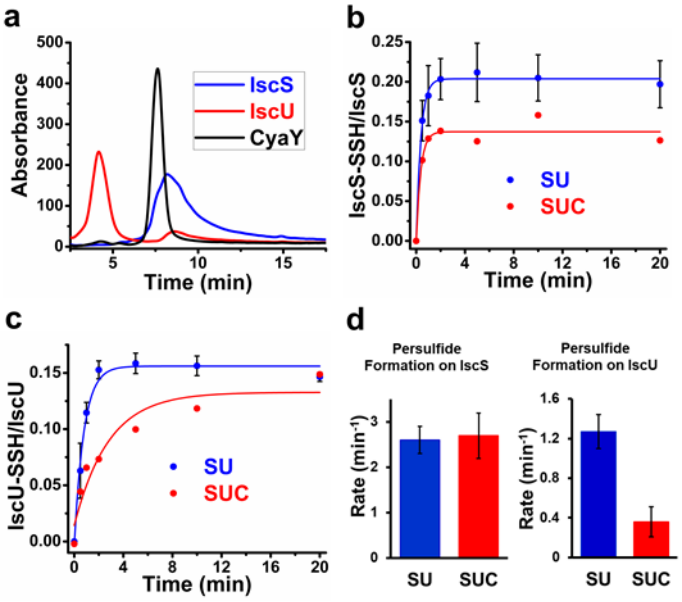

Figure III-4. CyaY does not affect the rate of persulfide formation on IscS but slows down persulfide formation on IscU. (a) Separation of proteins by HPLC. 50 µM IscS, 150 µM IscU and 50 µM CyaY were loaded onto Deltapack C4 column after diluting with quenching solution in 1:3 ratio to a final volume of 200 µL (see method). Chromatogram shows that IscS and IscU are well separated. Although CyaY co-elutes with IscS, does not affect our analysis. **(b)**, **(c)** Persulfide formation on IscS and IscU in presence and absence of CyaY was monitored by reacting 30 uM of IscS, IscU, CyaY and Cysteine (containing 0.204% ^{35}S-cysteine) at 37ºC for different time (in 0 - 20 min range). The samples were analyzed with HPLC and scintillation cocktail after quenching with quenching solution (1:4 mixture of conc. HCl and 6M guanidine hydrochloride) at given time points. The area under IscS and IscU in scintillation trace were converted into amounts of persulfide using a standard curve made from ^{35}S-cysteine standard. The data were fitted with exponential rise equation [y=m1+m2*(1-exp (-m3*x))] where m3 value gives the apparent rate of formation which is plotted in **(d)**.

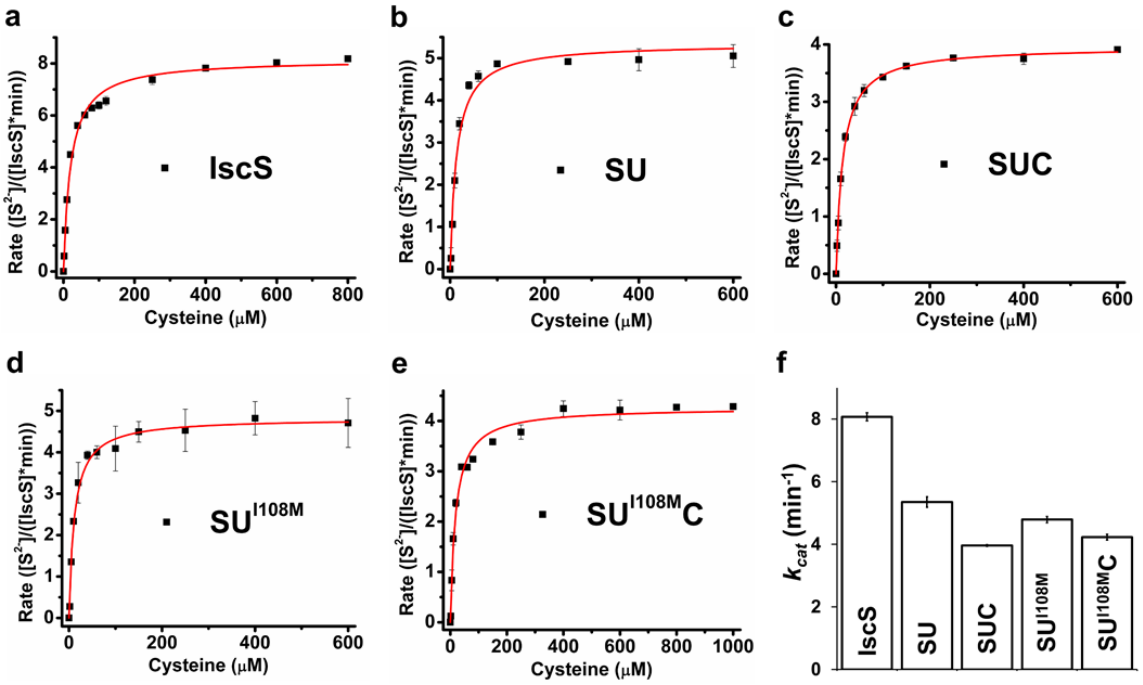

Figure III-5. Both CyaY and IscU^{I108M} does not affect cysteine desulfurase activity. The reactions contained 0.5 μM IscS, 2.5 μM IscU/IscU^{I108M}, 5 μM CyaY, 4 mM D,L-DTT. Reactions were initiated by adding cysteine and incubated for 6 min before quenching with DPD and $FeCl_3$ solution. Solutions were further incubated for 20 min. Then the samples were centrifuged and absorbances at 670 nm were measured, which were converted to concentration of sulfide using a standard curve made from known amount of sulfide. The data points were fitted to Michaelis-Menten equation (y = m1*x/(m2 + x)), where m1 and m2 are k_{cat} and K_M respectively.

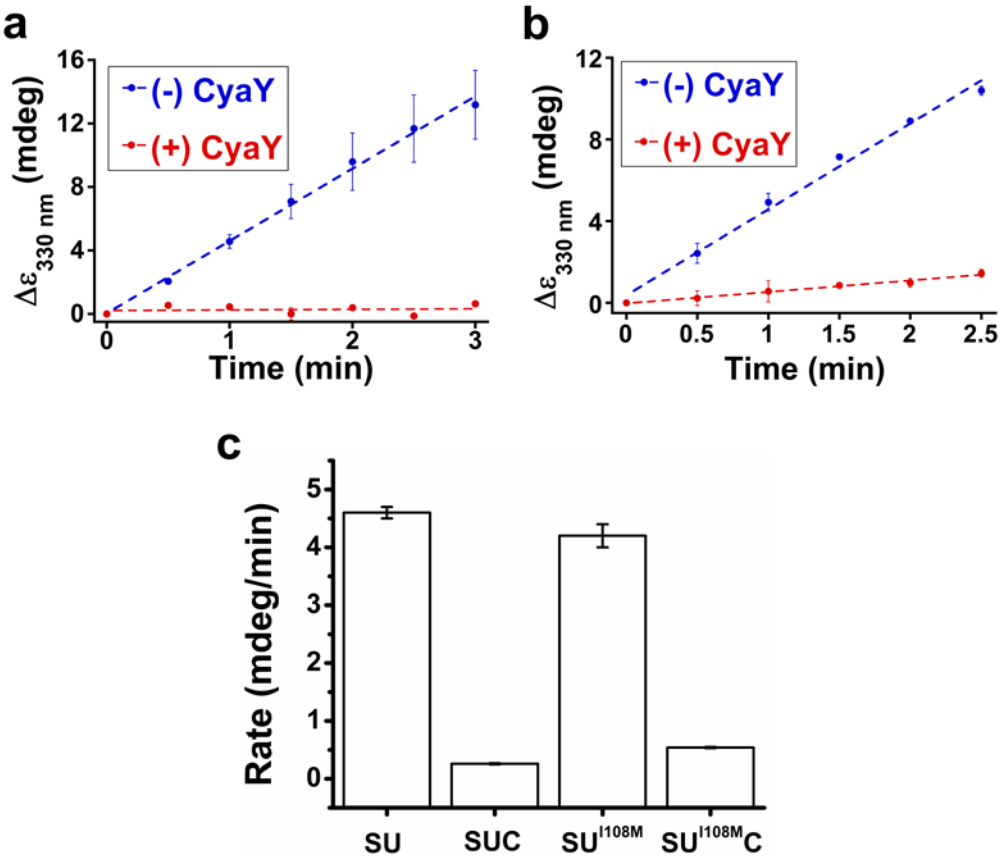

Figure III-6. CyaY inhibits cluster assembly on IscU/IscU^{I108M}. Reaction consists of 8 µM IscS, 40 µM IscU **(a)** or IscU^{I108M} **(b)**, 50 µM CyaY, 200 µM $Fe_2(NH_4)_2SO_4$ and initiated by the addition of 10 mM GSH and 100 µM cysteine. The rate is calculated by monitoring the change of ellipticity at 330 nm and fitting the initial data points to linear equation and plotted in **(c)**.

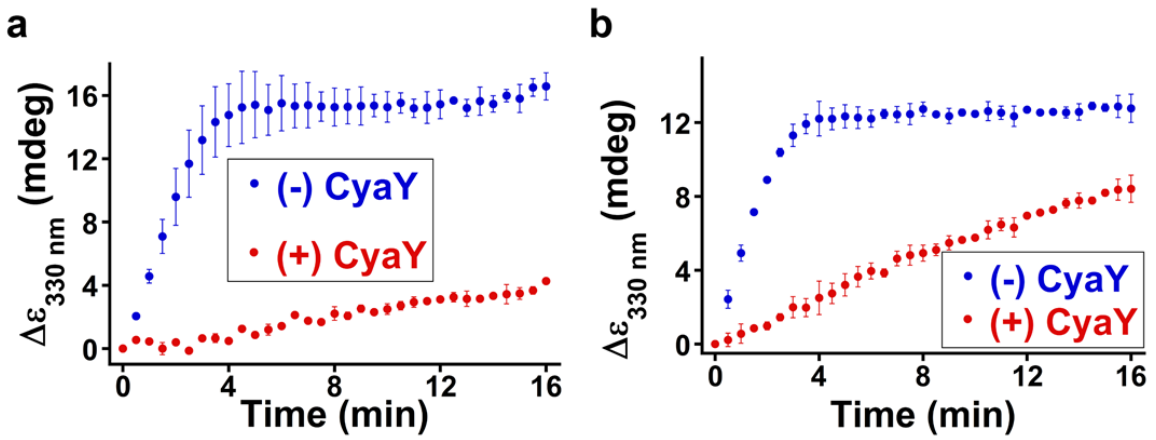

Figure III-7. Full reaction showing the effect of CyaY on cluster synthesis on either IscU or IscU^{I108M}. Reaction consists of 8 µM IscS, 40 µM IscU **(a)** or IscU^{I108M} **(b)**, 50 µM CyaY, 200 µM $Fe_2(NH4)_2SO_4$ and initiated by the addition of 10 mM GSH and 100 µM cysteine. The formation of cluster on IscU/IscU^{I108M} is monitored by the change of ellipticity at 330 nm. The fit of initial linear portion to a linear equation to determine rate is shown in **Figure III-6**.

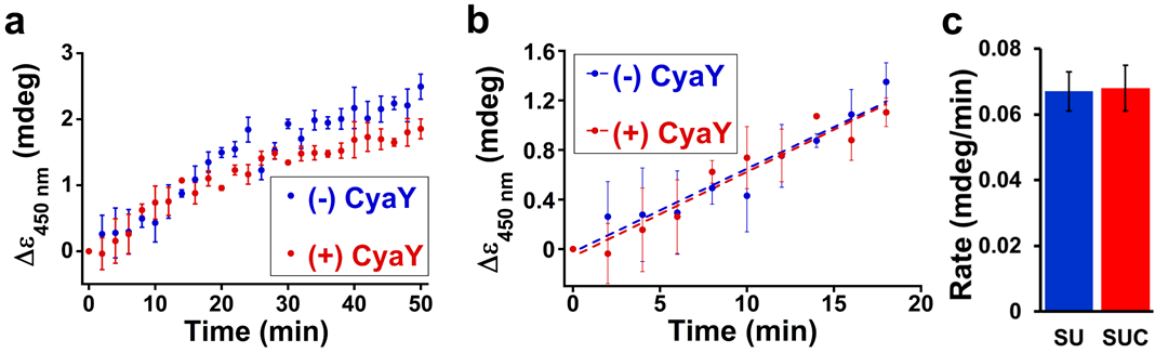

Figure III-8. CyaY does not affect the rate of cluster transfer from Holo-IscU to apo-Grx4. (a) Reaction contained 0.5 µM IscS, 20 µM Holo-IscU and 10 mM GSH and 40 µM CyaY and was initiated by the addition of 40 µM Grx4. The transfer of cluster from Holo-IscU to apo-Grx4 is measured by monitoring ellipticity at 450 nm. **(b)** The rates were obtained by fitting the initial data points to linear equation, which is plotted in **(c)**.

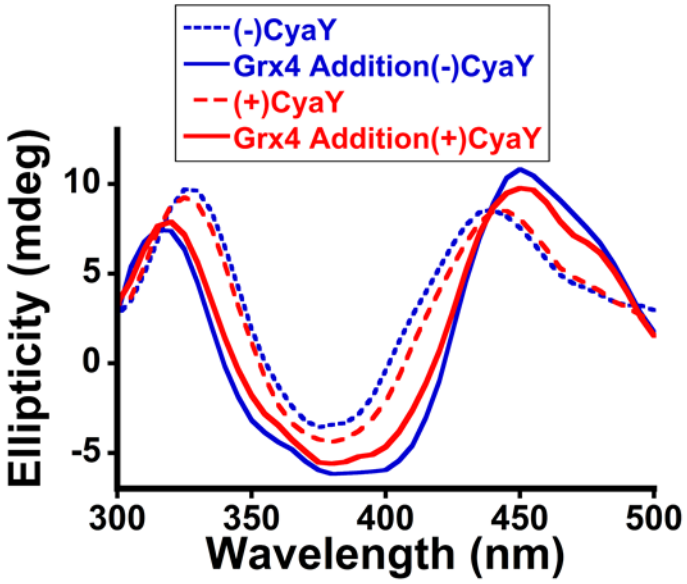

Figure III-9. Full spectra of cluster transfer reaction from holo-IscU to apo-Grx4 before and after addition of apo-Grx4. Dotted line is before apo-Grx4 addition and solid line is after apo-Grx4 addition. Blue traces are for reactions without CyaY and red traces are for reactions with CyaY.

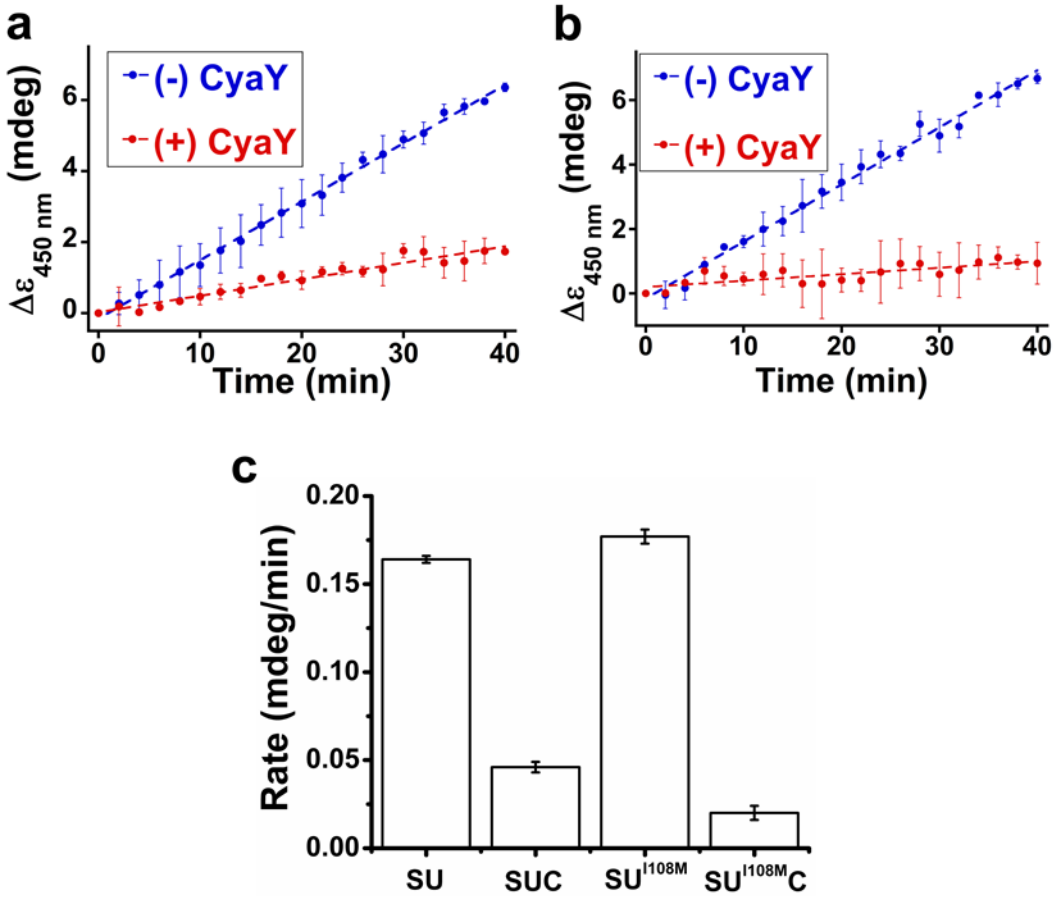

Figure III-10. CyaY inhibits one pot cluster assembly on Grx4 while IscU^{I108M} has no effect. Reactions included 0.5 µM IscS, 20 µM IscU **(a)** or IscU^{I108M} **(b)**, 40 µM CyaY, 200 µM $Fe_2(NH4)_2SO_4$ and 40 µM Grx4. The reaction was initiated with addition of 100 µM cysteine and 10 mM GSH. Cluster assembly on apo-Grx4 was measured by monitoring ellipticity at 450 nm. The rates were obtained by fitting the data to linear equation and plotted in **(c)**.

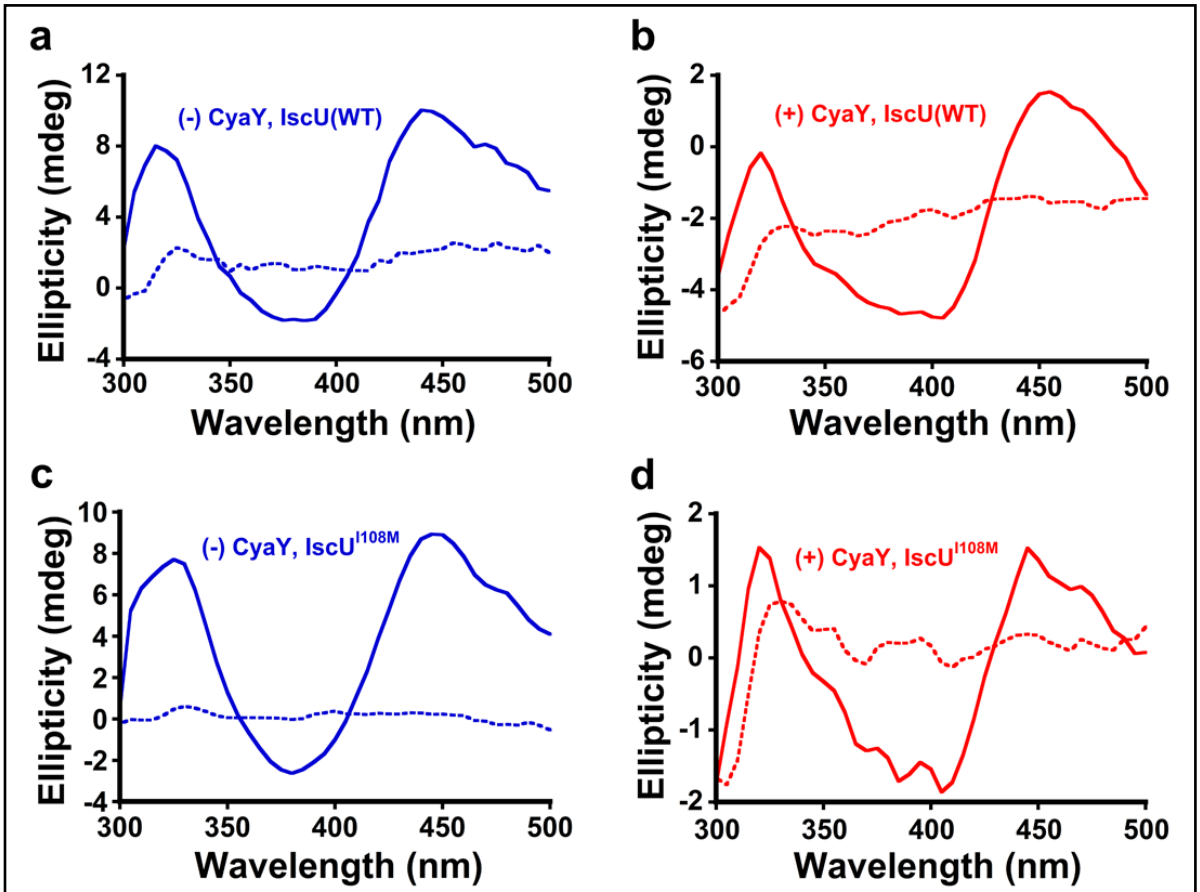

Figure III-11. Full spectra of one-pot cluster synthesis reaction on Grx4 before and after addition of (Cysteine + GSH) mixture, which was used to initiate the reaction. Dotted line is before initiation of reaction and solid line is after initiation of reaction. Blue traces are for reactions without CyaY and red traces are for reactions with CyaY. IscU (wt) was used as scaffold for **(a)** and **(b)** and IscU^{I108M} was used as scaffold for **(c)** and **(d)**.

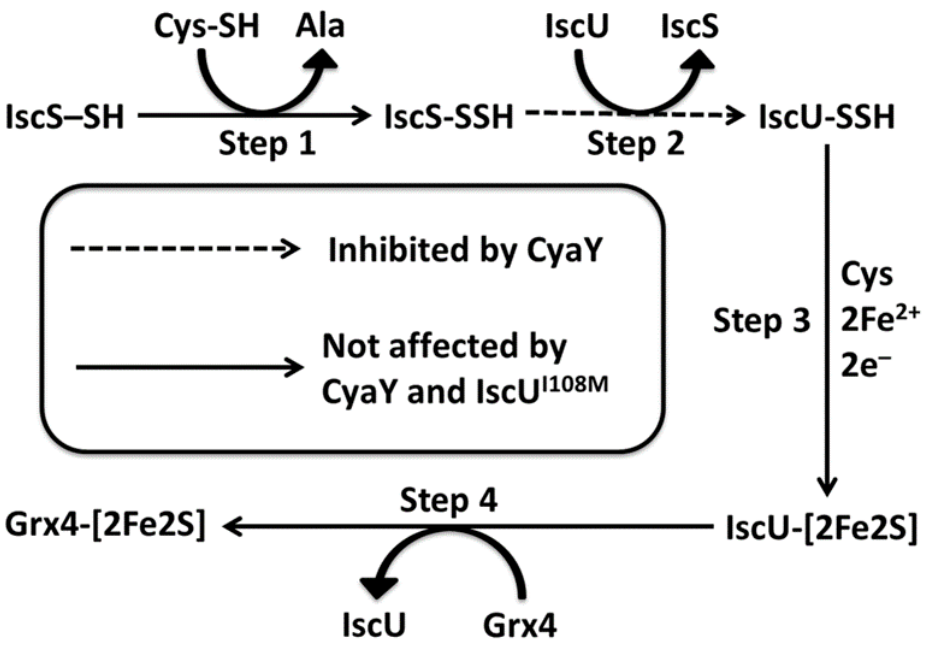

Figure III-12. Schematic diagram showing the effect of CyaY and IscU^{I108M} on each step. CyaY inhibits only sulfur transfer step and IscU^{I108M} has no effect.

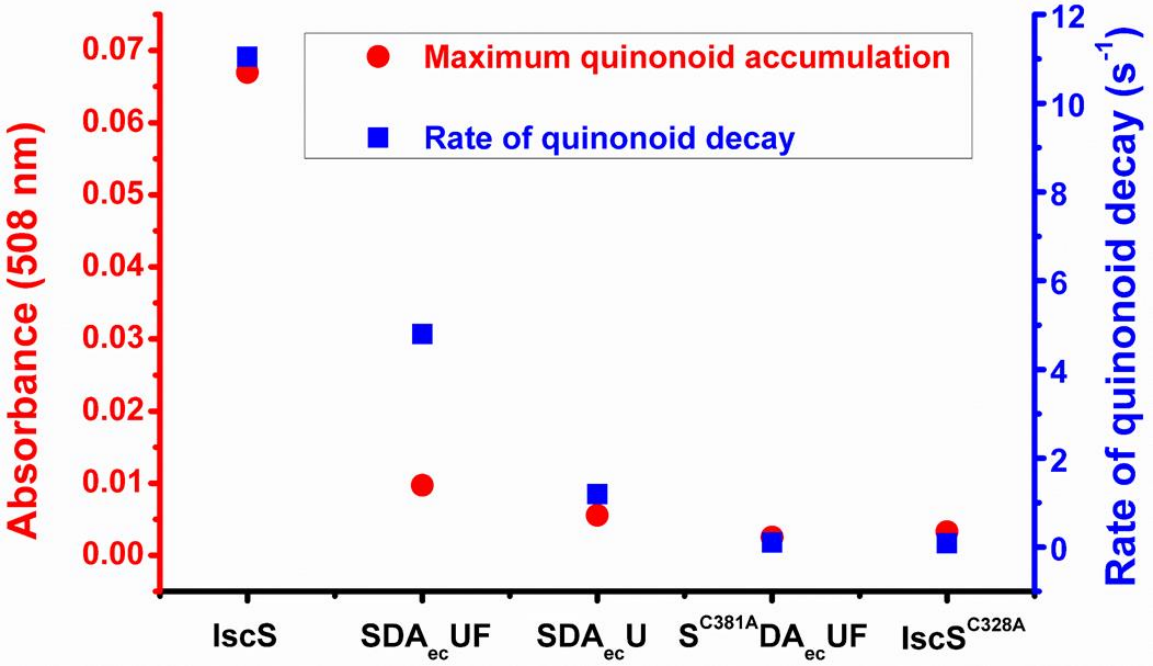

Figure III-13. Correlation between quinonoid accumulation and rate of quinonoid decay. Faster quinonoid decay strongly correlates with greater accumulation of quinonoid intermediate which is intuitively opposite. As we have shown this is due to S-transfer loop cysteine's participation in aldimine formation in the upstream step.

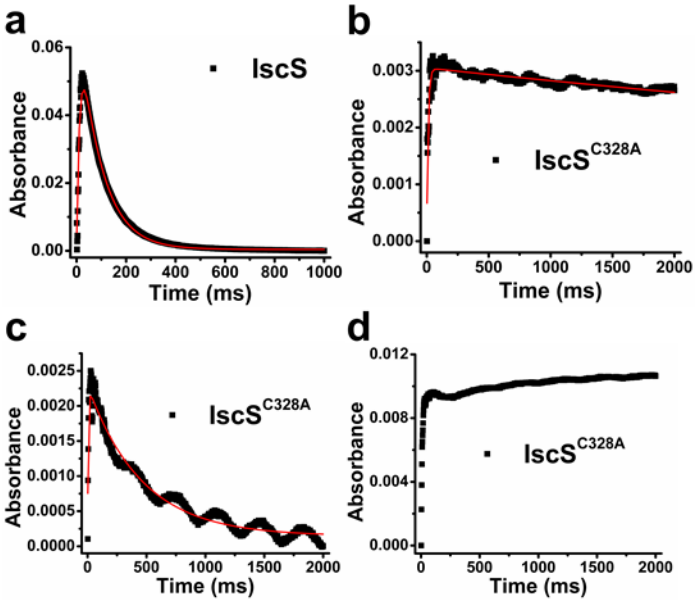

Figure III-14. S-transfer loop cysteine is the proton donor for quinonoid decay. The formation and decay of quinonoid, aldimine and ketimine intermediate were monitored by stopped flow at 508, 410 and 340 nm wavelength respectively. Reaction contained 50 µM of cysteine desulfurase (IscS or IscS^{C328A}) and 5 mM cysteine (final concentrations). The rates were obtained by fitting the data to consecutive B equation [y=y0 + A*(m1/(m3-m2))(exp(-m2*x)-exp(-m3*x))], where m2 and m3 values give the apparent rate of formation and decay of the intermediates respectively. Ketimine kinetics is too complex to fit adequately using consecutive B equation. **(a)** Quinonoid kinetics of wt-IscS. **(b)** Quinonoid kinetics of IscS^{C328A} variant. The decay of quinonoid intermediate is severely inhibited. **(c)** Aldimine kinetics of IscS^{C328A} variant. The maximum amount of aldimine formed is much smaller compared to wt-IscS. However, the rate of aldimine decay is very similar to wt-IscS. **(d)** Ketimine kinetics of IscS^{C328A} variant. Ketimine formation is very slow and consistent with very slow quinonoid decay.

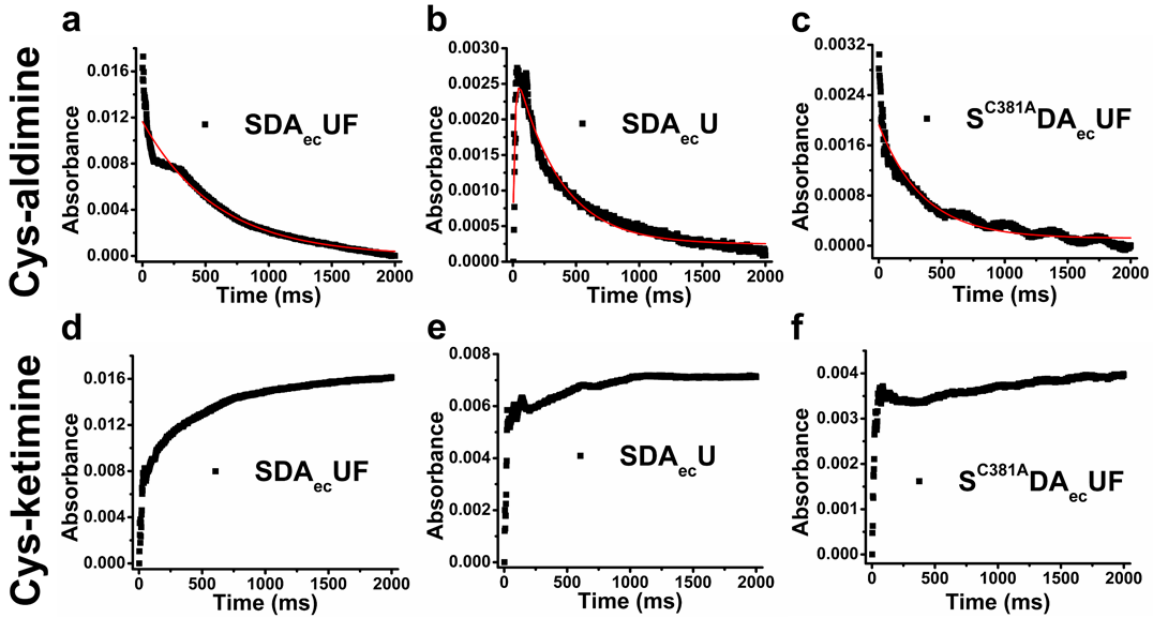

Figure III-15. S-transfer loop cysteine of NFS1 also facilitates cys-aldimine formation and accelerates cys-quinonoid decay by proton donation. (a), **(b)** and **(c)** Cys-aldimine formation takes place in the dead time of the instrument. So, we typically don't see. However, starting amount of cys-aldimine is much higher for $SDA_{ec}UF$ than that of both $SDA_{ec}U$ and $S^{C381A}DA_{ec}UF$, which are comparable. This show that s-transfer loop cysteine somehow participates in aldimine formation. In contrast, aldimine decay rates are comparable for all three complexes. Since aldimine decay is caused by C_α proton abstraction, this data shows s-transfer loop cysteine does not participate as general base for C_α proton abstraction. **(d)**, **(e)** and **(f)** Cys-ketimine if formed to a greater extent in the case of $SDA_{ec}UF$ than that of $SDA_{ec}U$ and $S^{C381A}DA_{ec}UF$, which is consistent with previously published quinonoid decay kinetics that faster quinonoid decay leads to greater accumulation of ketimine intermediate.

Table III-1. Kinetic data for Fe-S assembly complexes (*E. coli*).

						Relative Rate with respect to SU	
		SU	**SUC**	**SU^{I108M}**	**$SU^{I108M}C$**	**SU**	**SUC**
PLP Chemistry	Cys-quinoid formation (s^{-1})	79.27 ± 1.32	60.98 ± 0.64	70.96 ± 1.07	44.88 ± 0.6	1	0.77
	Cys-quinoid decay (s^{-1})	11.21 ± 0.1	11.48 ± 0.07	12.36 ± 0.1	12.34 ± 0.11	1	1.024
Persulfide formation reactions with [^{35}S]-Cys (min^{-1})	Persulfide formation on IscS	2.59 ± 0.33	2.71 ± 0.54	ND	ND	1	1.046
	Persulfide formation on IscU	1.27 ± 0.17	0.36 ± 0.15	ND	ND	1	0.283
Cysteine desulfurase activity	k_{cat} (min^{-1})	5.35 ± 0.17	3.96 ± 0.03	4.82 ± 0.09	4.26 ± 0.09	1	0.74
	K_M (μM)	14 ± 2	14.4 ± 0.6	12 ± 1	19 ± 2	1	1.029
Cluster synthesis	Cluster formation on ISCU2 (mdeg/min)	4.6 ± 0.1	0.26 ± 0.01	4.1 ± 0.2	0.54 ± 0.01	1	0.057
Cluster transfer	Cluster transfer ISCU2 to GRX5 (mdeg/min)	0.067 ± 0.006	0.068 ± 0.007	ND	ND	1	1.015
Complete reaction	Cluster synthesis & transfer to GRX5 (mdeg/min)	0.164 ± 0.002	0.046 ± 0.003	0.177 ± 0.004	0.02 ± 0.004	1	0.28

ND – Not determined.

Table III-2. Rates for individual steps in the PLP chemistry of cysteine desulfurase.

	Rate of Cys-aldimine Decay (s^{-1})	Rate of Cys-quinonoid Formation (s^{-1})	Rate of Cys-quinonoid Decay (s^{-1})	Relative rate of quinonoid decay
IscS	-	80.71 ± 1.25	11.05 ± 0.09	9.3
IscS^{C328A}	2.18 ± 0.03	77.42 ± 2.4	0.082 ± 0.003	0.069
SDA$_{ec}$U	1.82 ± 0.05	19.5 ± 0.5	1.19 ± 0.03	1
SDA$_{ec}$UF	1.70 ± 0.01	17.5 ± 0.4	4.80 ± 0.07	4.03

CHAPTER IV

DIMER TO MONOMER TRANSITION AND NOT ACTIVE SITE RESIDUES EXPLAINS LOW ACTIVITY OF NFS1

INTRODUCTION

One of the most intriguing problem in the field of iron sulfur cluster biosynthesis is the differences between prokaryotic and eukaryotic system. Prokaryotic cysteine desulfurase (IscS) does not require accessory proteins for stability as in the case of eukaryotic cysteine desulfurase (NFS1), which requires ISD11 and ACP[21, 28, 122]. Together NFS1, ISD11 and ACP form a stable cysteine desulfurase complex called SDA[33, 122, 177]. Moreover, the stable SDA complex is significantly less active (~ 8 times) than the prokaryotic counterpart (IscS)[76]. Furthermore, while eukaryotic iron sulfur cluster biosynthesis is activated by FXN[70], prokaryotic iron sulfur cluster biosynthesis is actually inhibited by CyaY[75] and the activation/inhibition mechanism is very different as previously determined. Earlier studies determined that this difference is due to the type of cysteine desulfurase used i.e. in presence of prokaryotic cysteine desulfurase both FXN and CyaY inhibits iron sulfur cluster biosynthesis whereas in presence of eukaryotic cysteine desulfurase both FXN and CyaY activates iron sulfur cluster biosynthesis[76]. The discovery of human cysteine desulfurase complex (SDA) crystal structure (PDB 5USR) revealed that although the monomer subunits are very well aligned (**Figure IV-1**), in dimer, the cysteine desulfurase subunits are arranged very differently and there is almost no interaction between the two subunits (subunits are bridged by ISD11) contrary to extensive interaction between the two IscS subunits[33, 143]. This architectural difference has provided a rationale for the inherent high activity of IscS, low activity of SDA and activation of SDA by FXN in presence of ISCU2. We hypothesize that in

open architecture (SDA architecture), S-transfer loop can adopt any number of trajectories, most of which are unproductive. In case of IscS, the other subunit provides restraint on the number of trajectories and thereby increases the probability of adopting productive loop trajectory significantly. This results in high activity of IscS. In case of SDAUF, FXN functions as pseudo-subunit of NFS1 and function similar to the other subunit of IscS although to a lesser efficiency. This hypothesis then leads to prediction that if we can manage to weaken the dimer interface of IscS by changing some dimer interface residues resulting in monomer formation, that activity of that IscS monomer will be lower (similar to SDA). If we add FXN/CyaY to the monomer we would see an increase in activity (provided they bind to the monomer). Furthermore, if we mutate the NFS1 dimer interface residues to corresponding IscS residues, we would generate and IscS type dimer of NFS1, which would have high activity similar to IscS. Alignment of IscS and NFS1 monomer structures revealed some probable residues that may be important for dimerization. We found a pair of histidine-glutamine residues (H247, Q248 of IscS) at the dimer interface and hydrogen bonds with the same residues from the other subunit (**Figure IV-2**). These residues are very well conserved among gamma-proteobacteria but absent in eukaryotes and alpha-proteobacteria (ancestors of mitochondria) where they were replaced by residues that cannot form hydrogen bond (**Figure IV-3**). Most interestingly we found a serine residue in position 10 of IscS is glutamine 64 in NFS1. This glutamine is absolutely conserved in eukaryotes. However, in prokaryotes it is mostly serine, alanine and glycine (**Figure IV-4**). In monomeric Cory architecture of NFS1 (PDB 5USR), this glutamine is hydrogen bonded to a conserved histidine that binds PLP phosphate. In IscS however, a conserved threonine (T12) hydrogen bonds with the same conserved histidine (**Figure IV-5a**). This threonine to glutamine switch results in a big conformational change in the N-terminus, which now collide with the other subunit (**Figure IV-5b**). This led up

to hypothesize that IscS^{S10Q} variant may have a week dimer interface. However, the discovery of a second crystal structure of SDA (PDB 5WGB) with IscS type architecture raised question on this monomer-dimer hypothesis specially since that material was also shown to have low activity[140]. This prompted us to look for some other ways to explain this low activity of SDA and FXN based activation. We reasoned that it is possible that some active site residue plays key role in cysteine desulfurase activity, which is positioned in an active conformation in IscS resulting in high activity but in case of SDA, it is in inactive conformation resulting in low activity. FXN binding to SDA causes a conformational change of that residue to active conformation, thereby increasing cysteine desulfurase activity. However, the active site of both IscS and NFS1 looks identical. All the residues interacting with PLP or likely to interact with cysteine substrate are identical. Only there are some minor difference in the second shell PLP interacting residues (**Figure IV-6**).

Here, we have looked at the effects of second shell PLP interacting residues and dimer interface residues on cysteine desulfurase activity. More specifically whether or not interchanging IscS and NFS1 residues would result in inter-converting IscS into NFS1. By monitoring pre-steady state kinetics using stopped flow, steady state cysteine desulfurase activity using methylene blue assay and monomer formation using analytical size exclusion chromatography (S200) we have found out that second shell PLP interacting residues do not perturb the system significantly except for C158 of NFS1, which is conserved among eukaryotes and hydrogen bonds to the conserved histidine residue that is π-stacking PLP. Mutation of this cysteine to alanine (as in IscS) results in loss of PLP during purification. S10Q variant of IscS shows weaker dimer binding and significantly low activity. Further analysis with analytical SEC shows that the activity of IscS^{S10Q} is proportional to dimer concentration, strongly indicating monomer formation as the cause of low

activity and in turn most likely the Cory-architecture (PDB 5USR) as physiologically relevant architecture.

RESULTS

2nd shell PLP interacting residues of IscS are not responsible for high activity. The effects of second shell PLP interacting residues were measured by comparing their effects on quinonoid decay and cysteine desulfurase activity. As can be seen in **Figure IV-7**, **Figure IV-8** and **Table IV-1**, there are small changes in the cysteine desulfurase activity, which corresponds nicely with the changes in rate of quinonoid decay. $S^{C158A}DA_{ec}$ was colorless after purification indicating PLP was lost during purification. Attempt to reconstitute PLP bound form resulted in twice the amount of PLP bound to protein even after extensive desalting. In presence of ISCU2 and FXN, this material showed very low activity (k_{cat}) and very high K_M indicating reconstitution with extra PLP may have compromised its function. Therefore, we cannot confidently say if C158A mutation results in low activity other that it definitely affects PLP binding. Since we don't see similar effect in IscS where this residue is alanine, it indicates may be NFS1 is monomer under reaction condition and a combination of monomeric architecture and an alanine residue is required for weaker PLP binding.

Dimer interface mutants cause low activity. When the effects of dimer interface residues were measured on quinonoid decay and cysteine desulfurase activity, it was found that there was a small decrease in quinoid decay but a significant decrease in cysteine desulfurase activity (**Figure IV-9**, **Figure IV-10**, **Table IV-2**). To determine if the lower activity was due to monomer-dimer equilibrium, the dependence of activity on enzyme concentration were measured for both IscS and $IscS^{S10Q}$. It was found that in the range of 0.25 to 5 μM, specific activity ($[S^{2-}]$/([Enzyme]*min))

remained same for IscS while increased with increasing concentration for $IscS^{S10Q}$. Fitting the observed rate (v) vs total enzyme concentration (Et) using Equation (4), binding constants were obtained at 0.01 and 1 μM for IscS and $IscS^{S10Q}$ respectively (**Figure IV-11**).

Monomerization of dimer interface mutants is the cause of low activity. Binding constant of 0.01 and 1 μM predicted that in the range of 0.5 to 10 μM, IscS will be mostly dimeric and $IscS^{S10Q}$ will have a large portion of monomer (**Figure IV-12**). In order to verify that, analytical size exclusion (S200) was used to separate monomer from dimer and estimate the percentage of the dimer. As predicted, 90% of IscS was estimated to be the dimer in all the concentrations. On the other hand, $IscS^{S10Q}$ showed increased amounts of dimed as concentrations were increased. When compared with specific activity, estimated amounts of dimer percentage from analytical SEC (S200) showed the same trend. For $IscS^{S10Q}$, as dimer percentage increased, specific activity also increased (**Figure IV-13a**). For IscS, dimer percentage remained same, specific activity also remained same (**Figure IV-13b**).

DISCUSSION

Difference between prokaryotic and eukaryotic cysteine desulfurase is an enigmatic problem. The cause is unknown and the consequences are profound. Here we have attempted to determine the cause of this dime monomer conversion. Surprisingly we found a serine residue (S10) when mutated to glutamine can weaken dimer interface significantly (K_d changed 100 timed from 0.01 μM to 1 μM). This weakened dimer interface leads to lower dimer concentration resulting in lower activity. Side by side comparison of specific activity and dimer percentage (obtained from S200) clearly showed specific activity is directly dependent on dimer concentration. This nicely fits into the idea that in monomeric architecture cysteine desulfurase

will have very low activity (basal level activity). Only when cysteine desulfurase have closed architecture (as in IscS) it becomes highly active. In case of IscS, it is a homodimer, but in case of the human system, we predict it is heterodimer with FXN playing the role of other cysteine desulfurase subunit and binding in the same surface that is normally occupied by the other subunit. We also found that second shell PLP interacting residues do not affect cysteine desulfurase activity significantly, demonstrating monomerization is the sole cause of low activity of NFS1. However, in our present study, we were not able to make monomeric IscS exclusively. From activity assay, we found the other dimer interface mutant pair (H247P, Q248L) lowered the k_{cat} value to half of wild-type. This strongly indicates that this pair also contributes towards dimer stability (not to the same extent as of S10Q). We, therefore, predict if we make a triple mutant, dimer interface will be even weaker and we may be able to achieve monomeric IscS exclusively. It will also be interesting to see if this low activity monomer can be activated by FXN/CyaY and if can be, whether or not the activation depends on the presence of ISD11. At present we know nothing about ISD11 other than that it is absolutely required for NFS1 stability. Why NFS1 became entirely dependent on ISD11 during evolution is still a mystery. We are hopeful this monomer-dimer interconversion experiments will provide significant insight into active cysteine desulfurase complex formation along with the exact function of each of members of the complex and lastly a sneak peek into the past.

MATERIALS AND METHODS

Protein Preparations. All the proteins were purified as described previously. The QuikChange protocol (Agilent) was used to introduce the point mutations. Protein variants were purified similarly to wild types. Unless otherwise stated, all reactions were carried out in an

anaerobic glove box (MBRAUN; maintained at ~14 °C with O_2 < 1 ppm). Protein concentrations were estimated using the following extinction coefficients: IscS and SDA_{ec} (wt and variants) using 6.6 $mM^{-1}cm^{-1}$ at 388 nm (in 0.1 M NaOH), ISCU2 using 8490 $M^{-1}cm^{-1}$ at 280 nm, FXN using 26030 $M^{-1}cm^{-1}$ at 280 nm, Protein variants were assumed to have the same extinction coefficient as the native proteins.

Cysteine desulfurase activity measurements. Cysteine desulfurase activities were measured for each complex using a slightly modified methylene blue assay.[70, 148] Protein complexes were generated in assay buffer (50 mM HEPES, 250 mM NaCl, pH 7.5) with final concentrations of 0.5 µM cysteine desulfurase [IscS or NFS1 (as SDA_{ec}) or their variants], 1.5 µM ISCU2, and 1.5 µM FXN (when included). The complexes were combined with 4 mM D,L-DTT and incubated for 15 min anaerobically on a heating block at 37 °C. Different concentrations of L-cysteine were added, incubated for 6 min, and quenched with 20 mM *N*,*N*′-diphenyl-*p*-phenylenediamine (DPD) (in 7.2 M HCl) and 30 mM $FeCl_3$ (in 1.2 M HCl). The samples were centrifuged after 20 min and the absorbance was measured at 670 nm. The amount of sulfide produced was determined for each data point using a standard curve. Rates ($[S^{2-}]$/([NFS1]*min)) were plotted against the amount of L-cysteine added and fit to the Michaelis-Menten equation using Kaleidagraph to obtain k_{cat} and K_M parameters. For determining binding constant of monomer subunits by cysteine desulfurase activity measurement, concentration of IscS or $IscS^{S10Q}$ were varied keeping cysteine and D,L-DTT concentration fixed at 1 mM and 4 mM respectively. For 5 and 10 µM IscS, 2.5 mM cysteine and 10 mM D,L-DTT was used. Everything else about the methylene blue assay was kept the same. For samples with A670 >1, samples were remeasured after diluting 10 times with blank solution (800 µL assay buffer + 100 µL of 20 mM *N*,*N*′-diphenyl-*p*-phenylenediamine (DPD) (in 7.2 M HCl) + 100 µL of 30 mM $FeCl_3$ (in 1.2 M HCl). Rate (µM

[S^{2-}]/min) were plotted against protein concentration (μM) and the data were fitted to Equation (4) with the assumption that all the activity is due to dimer and monomer has no activity. The fit gave us binding constant of the two monomer subunits. This calculated binding constant and Equation (2), (3) were used to estimate monomer and dimer concentrations at a given protein concentration respectively[178].

Analytical size exclusion (S200) chromatography. IscS and $IscS^{S10Q}$ proteins were diluted to 600 μL final volume (in assay buffer) to a final concentration of 0.5, 1 2.5, 5 and 10 μM in presence of 2 mM TCEP (at pH 8.0). 500 μL from this sample was injected into an S200 column (Superdex 200 10/300 GL, GE Healthcare Life Sciences) and eluted with a flow rate of 0.5 mL/min). The area under the monomer and dimer peak was estimated using UNICORN software (default software of Acta FPLC, GE Healthcare Life Science).

Stopped-flow kinetics of quinonoid intermediate. Kinetics of quinonoid intermediate was monitored and analyzed as previously. In short,100 μM protein complex in assay buffer (50 mM HEPES, 250 mM NaCl, pH 7.5) was placed in one of the syringes of the stopped-flow apparatus (KinTek Corporation). The other syringe contained 10 mM L-cysteine. The samples were mixed by simultaneously pressing both syringes. Formation and decay of quinonoid intermediate were followed by monitoring changes in absorbance at 508 nm. 508 nm absorbance trace with time were fitted with Origin software (OriginLab) to a consecutive B equation [$y = y_0 + (k_1*[A]_0/(k_2-k_1))*(\exp(-k_1*t)-\exp(-k_2*t))$], where k_1 and k_2 are rate constants of the formation and decay of intermediates respectively.

$$D \overset{Kd}{\leftrightarrow} 2M$$

……..…

(1)

$$[M] = \frac{\left\{-\frac{Kd}{2} + \sqrt{(\frac{Kd^2}{4} + 2.Kd.Et}\right\}}{2}$$

……...

(2)

$$[D] = \frac{\{Kd + 4.Et - \sqrt{(Kd^2 + 8.Kd.Et}\}}{8}$$

……...

(3)

$$Observed\ rate = As.[D] = As.\frac{\{Kd + 4.Et - \sqrt{(Kd^2 + 8.Kd.Et}\}}{8}$$

…….....(4)

As = Specific activity ([product]/([enzyme]*time)), Et = total enzyme concentration, Kd = binding constant

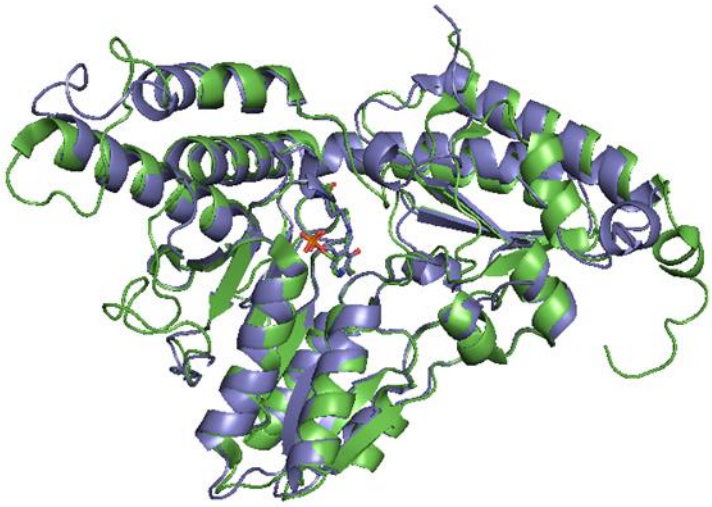

Figure IV-1. Alignment of IscS and NFS1 monomer subunits. Overall the tertiary structures are very similar.

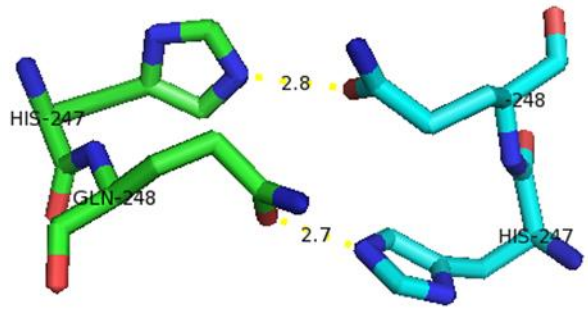

Figure IV-2. Bridging histidine glutamine pair. Green and cyan denotes different subunit.

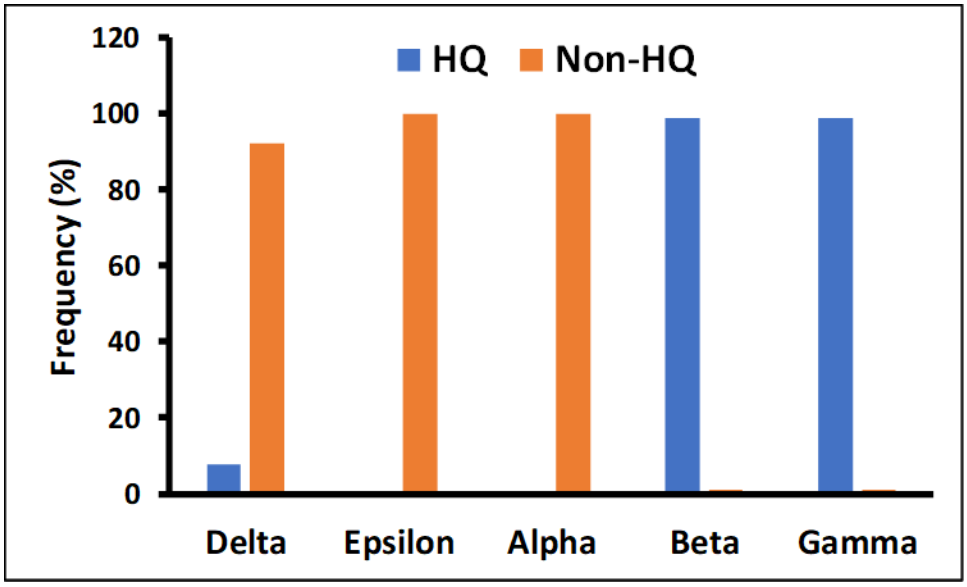

Figure IV-3. Distribution of amino acid residues in the position equivalent to 247, 248 of IscS among proteobacteria. Beta and Gamma proteobacteria (e.g. E coli) has mostly HQ pair in these positions whereas Delta, Epsilon and Alpha proteobacteria (which share last common ancestor with mitochondria) has other amino acids (Non-HQ) that cannot form hydrogen bonds at the dimer interface. Eukaryotes also has non-HQ residues exclusively.

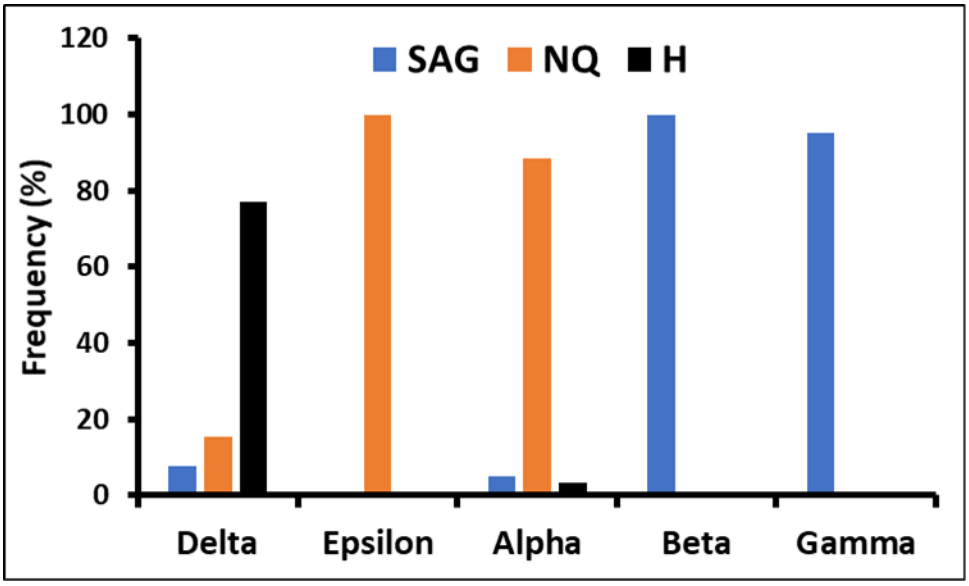

Figure IV-4. Distribution of amino acid residues in the position equivalent to 10 of IscS among proteobacteria. Beta and Gamma proteobacteria (e.g. E coli) has smallest amino acids such as serine (S), alanine (A) and glycine (G) in this position whereas Epsilon and Alpha proteobacteria (which share last common ancestor with mitochondria) has asparagine or glutamine. Eukaryotes has glutamine exclusively.

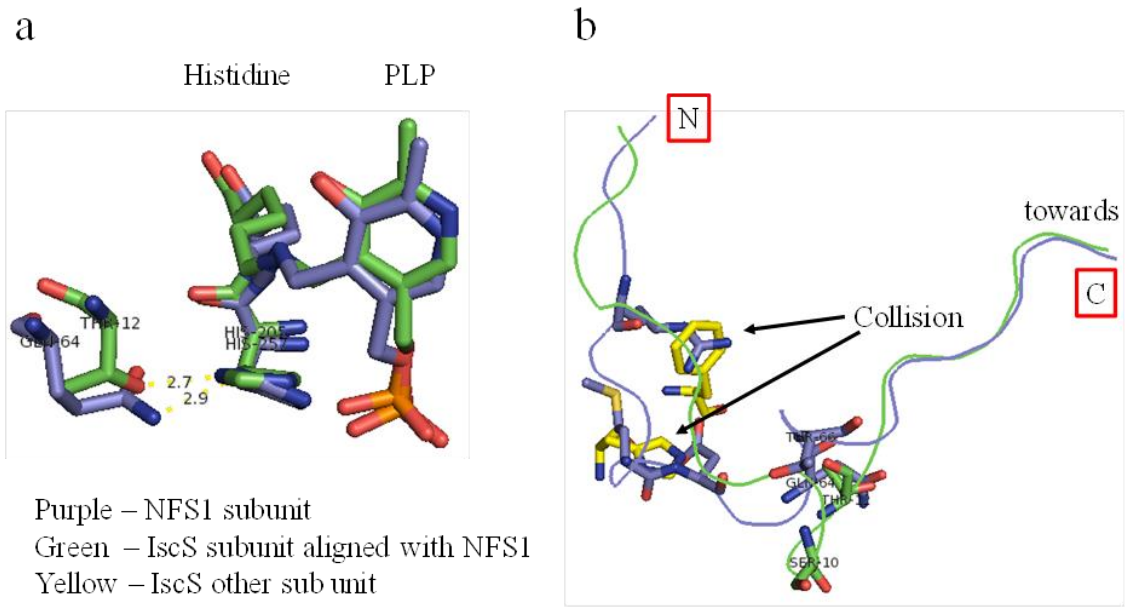

Figure IV-5. Effect of serine to glutamine mutation at position 10 of IscS. (a) Conserved histidine interacts with PLP phosphate group. That histidine is hold in place by either threonine (closed architecture) or glutamine (open architecture). **(b)** Shows the effect of the serine to glutamine switch. Towards C-terminus both IscS and NFS1 shows very good alignment. After the switch, there is big conformational change in N-terminus. When glutamine is the residue interacting with conserved histidine (Purple), the conformation that N-terminus adopts would cause collision with some residues of the other subunit of IscS (shown in yellow).

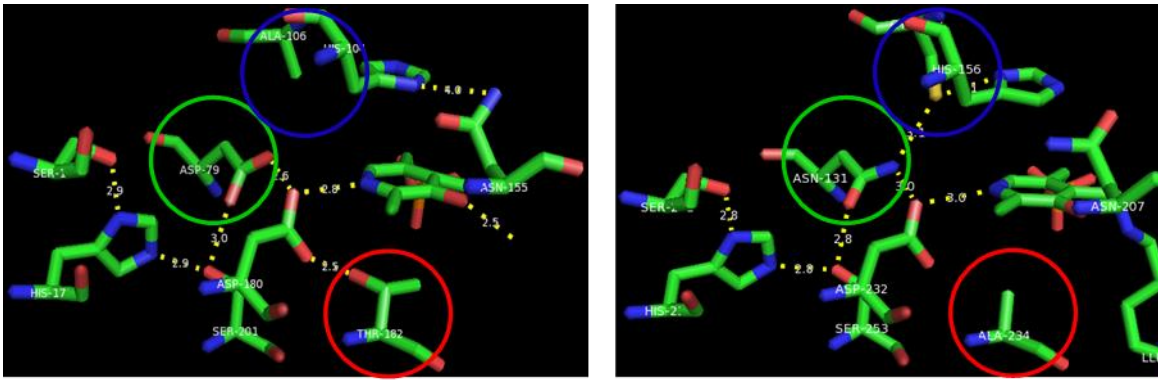

Figure IV-6. Comparison of active sites of IscS and NFS1. The active site looks very similar. Most of the residues are identical and they can be aligned in 3D very well. Blue, green and red circles pointing towards residues that are different between IscS and NFS1.

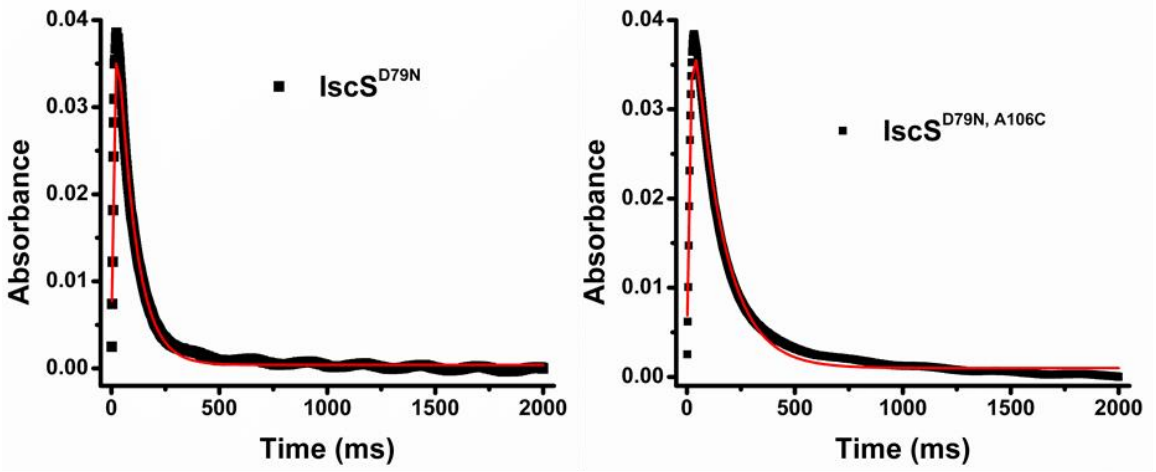

Figure IV-7. Comparison of quinonoid decay kinetics. Both D79N and D79N-A106C variants shows quinonoid decay kinetics similar to IscS and much faster than that of $SDA_{ec}UF$.

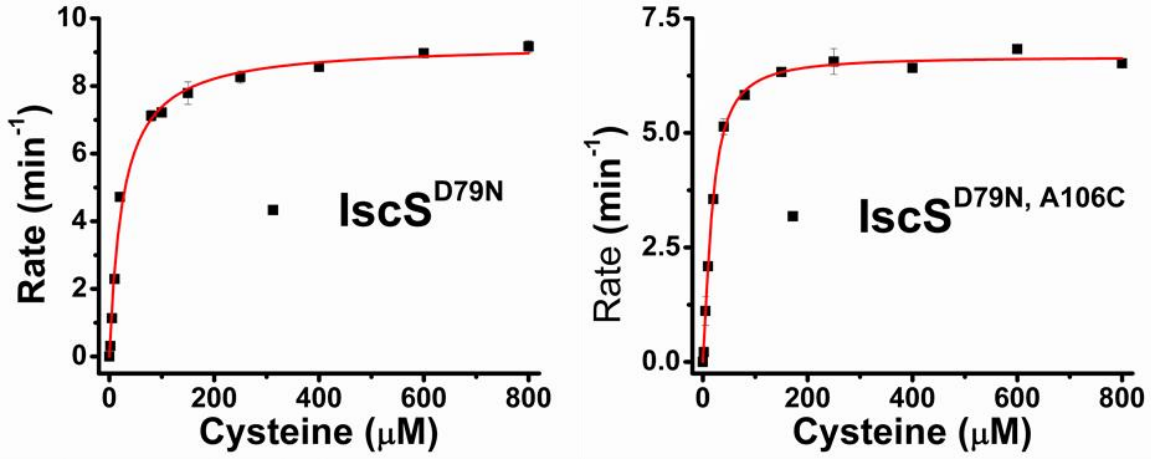

Figure IV-8. Comparison of cysteine desulfurase activity. $IscS^{D79N}$ has similar activity as wt whereas $IscS^{D79N, A106C}$ has slightly low activity but still much more active that SDA_{ec}, which has k_{cat} of ~1 per min.

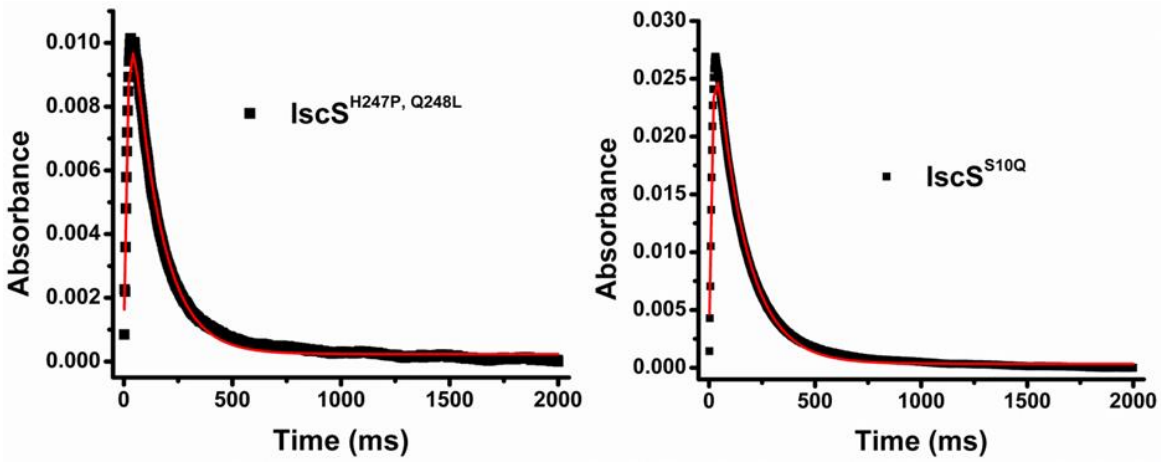

Figure IV-9. Comparison of quinonoid decay kinetics. Both H247P-Q248L and S10Q variants shows quinonoid decay kinetics similar to IscS and much faster than that of $SDA_{ec}UF$.

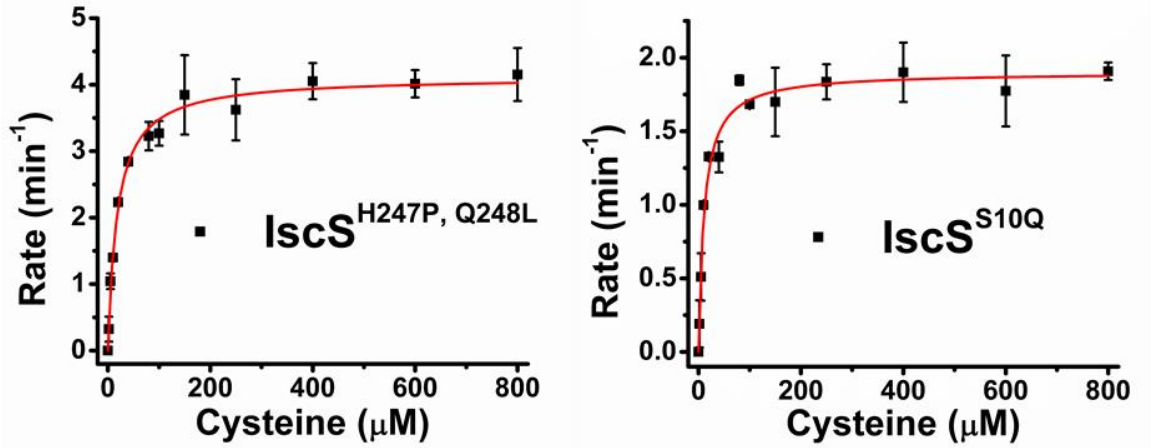

Figure IV-10. Comparison of cysteine desulfurase activity. Both IscS$^{H247P, Q248L}$ and IscS^{S10Q} has low activity compared to wt. The activity of IscS^{S10Q} is very close to that SDA_{ec}, which has k_{cat} of ~1 per min.

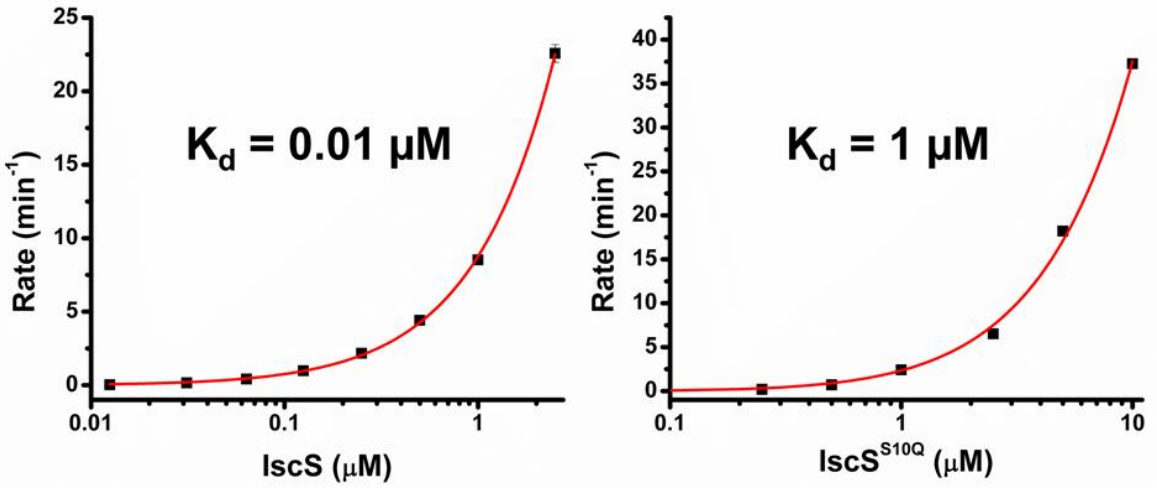

Figure IV-11. Binding constant determination by dependence of enzyme concentration on cysteine desulfurase activity. The data were fitted to Equation (4) to obtain binding constants of monomer subunits.

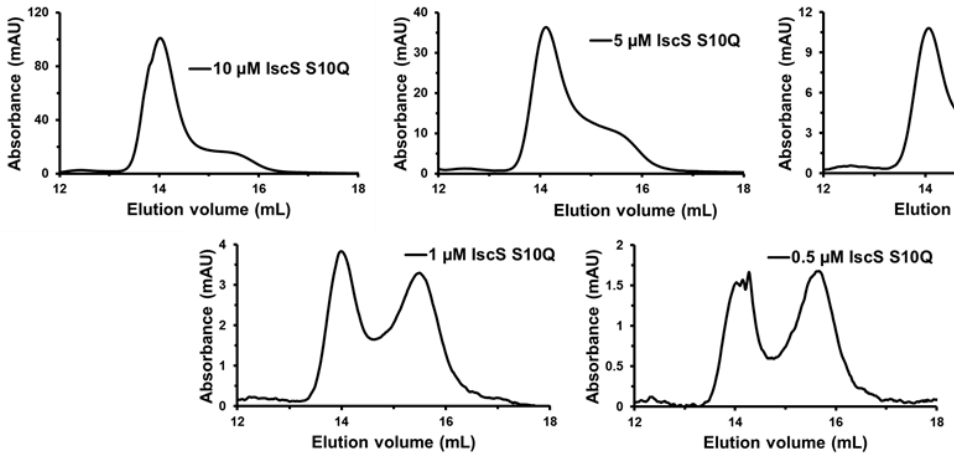

Figure IV-12. Chromatogram of analytical size exclusion chromatography of IscS^{S10Q}. As the protein concentration is lowered, monomer peak (~15.5 mL) grows while the dimer peak (~ 14 mL) shrinks indicating a monomer dimer equilibrium.

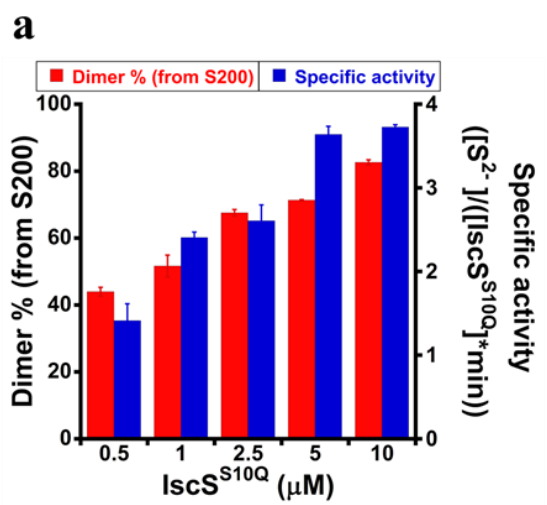

Figure IV-13. Specific activity correlates well with dimer concentration. Dimer % was estimated from analytical size exclusion chromatography. It was then plotted against protein concentration along with specific activity. This shows dimer concentration dictates specific activity.

Table IV-1. Effect of PLP second shell interacting residues on k_{cat} and quinonoid decay

Organism	Complex	k_{cat} (min^{-1})	K_M (μM)	Quinonoid decay (s^{-1})
E. coli	IscS	8.2 ± 0.1	20 ± 1	9.77 ± 0.09
	$IscS^{D79N}$	9.2 ± 0.2	26 ± 2	12.44 ± 0.12
	$IscS^{D79N, A106C}$	6.66 ± 0.07	17.6 ± 0.7	7.46 ± 0.07
Human	$SDA_{ec}UF$	10.07 ± 0.15	11.6 ± 0.9	4.8 ± 0.06
	$S^{N131D}DA_{ec}UF$	ND	ND	ND
	$S^{N131D, A234T}DA_{ec}UF$	7.1 ± 0.2	58 ± 7	ND
	$S^{N131D, A234T, C158A}DA_{ec}UF$	0.26 ± 0.01	188 ± 37	ND

Table IV-2. Effect of dimer interface residues of IscS on k_{cat} and quinonoid decay

Organism	Complex	k_{cat} (min^{-1})	K_M (μM)	Quinonoid decay (s^{-1})
E. coli	IscS	8.2 ± 0.1	20 ± 1	9.77 ± 0.09
	$IscS^{H247P, Q248L}$	4.12 ± 0.07	18 ± 2	7.87 ± 0.06
	$IscS^{S10Q}$	1.90 ± 0.05	11 ± 2	7.13 ± 0.05

CHAPTER VI

CONCLUSION AND FUTURE DIRECTION

Iron sulfur cluster is one of the smallest cofactors and plays an essential role in human health. Defect in iron sulfur cluster biosynthesis is responsible for several diseases such as Friedreich's ataxia (FRDA), ISCU myopathy, X-linked sideroblastic anemia[179]. However, the biosynthetic mechanism has remained mostly obscured. Over last 25 years there have been considerable progress in identifying different pathways and proteins involved in iron sulfur cluster biosynthesis. But the molecular details are still missing. This project started to figure out exactly how iron and sulfurs are assembled to make iron sulfur cluster and the function of each and every protein involved in this pathway. More specifically we wanted to know the exact function of frataxin and ferredoxin. Frataxin was discovered in 1996 in the process of discovering the cause of Friedreich's ataxia[38]. Since then, much progress was made through cell biology studies, but those studies also generated much controversies. Frataxin was initially assigned iron-based function (iron storage, iron chaperon, iron donor etc.) based on the phenotypes of iron accumulation in mitochondria and elevated amounts of ROS production by Fenton chemistry[56, 61-62, 64]. Majority of these studies were conducted on yeast and it was later revealed that yeast frataxin is unusually unstable (T_m = 35.8°C) and these effects are not observed with mature human frataxin (81-210)[66]. Next three very important studies changed the course of frataxin's function discovery. First, in 2009, frataxin (CyaY) was shown to inhibit iron sulfur cluster biosynthesis in *E. coli* contrary to observed acceleration by eukaryotic frataxin[75]. This raised serious question about the iron donor role as one would expect frataxin to accelerate and not inhibit iron sulfur cluster biosynthesis if its function is indeed to provide iron. Second, in 2010, human frataxin was shown

to accelerate cysteine desulfurase activity, thereby providing an alternate hypothesis to explain the observed acceleration in iron sulfur cluster biosynthesis[70]. Third, it was later revealed that the acceleration and inhibition by human and *E. coli* frataxin respectively actually depend on the type of cysteine desulfurase used[76]. So, when *E. coli* (prokaryotic) cysteine desulfurase was used both frataxin and CyaY would inhibit whereas when human (eukaryotic) cysteine desulfurase was used, both of them would activate. This tied up the function of frataxin with cysteine desulfurase activity and raised the fundamental question how exactly the function of frataxin is tied with cysteine desulfurase mechanism and how the same frataxin activating human cysteine desulfurase whereas inhibiting iron sulfur cluster synthesis in *E. coli*? These questions set up the foundation of this Ph.D. work.

To address these questions, a thorough investigation was undertaken where we would determine the effect of frataxin in each and every step of iron sulfur cluster biosynthesis up to the generation of holo-glutaredoxin, which is intermediate cluster carrier for target proteins. For this purpose, we divided the whole pathway into four major steps – 1) cysteine desulfurase activity (persulfide formation on cysteine desulfurase), 2) sulfur transfer (transfer of sulfane sulfur from cysteine desulfurase to scaffold protein generating a persulfide on scaffold protein), 3) cluster synthesis (on scaffold protein by combining persulfide, ferrous iron and electron) and 4) cluster transfer (from scaffold protein to glutaredoxin). A novel assay (involving use of radioactive cysteine as substrate, acid quenching, separation of proteins by HPLC and quantification of persulfide) was designed to determine the amounts of persulfide formed on cysteine desulfurase and scaffold protein with time. Fit of the data gave us new insight into frataxin function. We found in human system, frataxin accelerated both persulfide formation on NFS1 and ISCU2 whereas in *E. coli* system CyaY inhibited persulfide formation on IscU and didn't affect persulfide formation

on IscS. This gave the explanation of frataxin based activation and inhibition. When monitored iron sulfur cluster formation on scaffold protein, the effect of activation/inhibition in the upstream step(s) were evident. Further analysis into the effect of frataxin in the downstream revealed that both frataxin and CyaY had no effect on cluster transfer from scaffold protein to glutaredoxin in both *E. coli* and human system. However, under one-pot experimental setting, cluster formation on glutaredoxin was accelerated/inhibited in human/*E. coli* system respectively as a result of upstream activation/inhibition. Further analysis of the upstream steps to understand the molecular basis of the effect of frataxin/CyaY on persulfide formation on cysteine desulfurase revealed that both frataxin and CyaY accelerates quinonoid decay in human whereas CyaY has no effect in *E. coli*. This raised two important questions -1) what is the source of proton for quinonoid decay? 2) how frataxin facilitates proton donation to accelerate quinonoid decay? It has been previously hypothesized that the conserved S-transfer loop cysteine may be the proton donor[126-127]. When this residue was mutated to alanine, quinonoid decay was inhibited significantly (almost no decay) in both human and E. coli cysteine desulfurase indicating that cysteine residue in indeed the proton donor. Interestingly, the cysteine to alanine mutation also caused marked reduction in the maximum amount of quinonoid formed. To account for this, we reasoned that S-transfer loop cysteine must also be facilitating aldimine formation, which translates into greater quinonoid accumulation. Measurement of aldimine and ketimine kinetics of the cysteine to alanine mutants revealed this to be true i.e. aldimine formation was significantly reduced and ketimine formation was significantly affected as a result of very slow quinonoid decay. This established S-transfer loop cysteine as the main player of cysteine desulfurase mechanism where it 1) facilitates aldimine formation, 2) supply proton for quinonoid decay, 3) cleave C-S bond to generate persulfide and 4) carries the sulfane sulfur to sulfur acceptors. Interestingly all these steps were accelerated by

frataxin. Furthermore, all these steps were faster in *E. coli* IscS than SDAUF. A recent crystal structure of human cysteine desulfurase (PDB 5USR) revealed a very different quaternary architecture where the cysteine desulfurase subunits are interacting with each other through ISD11 subunits (instead of directly as in the case of IscS). In this architecture, although a dimer, the active site of SDA is solvent exposed (hence we call it open architecture) and very differently than IscS. These factors led to the hypothesis that cysteine desulfurase activity depends on the availability of the S-transfer loop thiol. In the case of SDAU, in the open architecture, S-transfer loop is free to adopt any number of trajectories resulting in very low probability of adopting the productive loop trajectory (which enables S-transfer loop cysteine to perform all four functions). As a result, SDAU has very low activity in all steps. In case of IscS, the closed architecture prevents most of the non-productive loop trajectories, thereby increasing the probability of adopting productive loop trajectory. This accelerates all four steps performed by S-transfer loop cysteine and results in high activity. We hypothesize that in human frataxin functions as a pseudo subunit of NFS1, binds where the other subunit would have bound and increase activity similar to IscS but to a lesser extent. This also means that frataxin binding to cysteine desulfurase is fundamentally different, which can explain different activation/inhibition properties of FXN/CyaY depending on cysteine desulfurase.

This then raises some important questions – 1) why human (most likely all eukaryotic) cysteine desulfurase has open architecture, 2) if cysteine desulfurase with open architecture indeed has low activity (comparable to SDAU), 3) whether frataxin would be able to rescue activity of the monomer in case it has low activity, 4) whether the eukaryotic-specific accessory protein ISD11 plays any additional role in frataxin based activation and finally 5) how did ancestors cope with this transition? Especially, alpha-proteobacteria (which share common ancestors with

mitochondria), which is expected to be monomer (hence have open architecture) based on sequence and does not contain ISD11. To address these questions, we first decided to find residues in the dimer interface which may explain open architecture of NFS1 and when altered, would break IscS dimer into the monomer. We found three potential residues, changed them into the corresponding residues of NFS1 and found that one mutation (S→Q) indeed caused weaker dimer interface, large amounts of the monomer at assay condition and decreased activity which corresponds very well with the proportion of dimer. Other double mutation (H→P, Q→L) also reduced k_{cat} by half indicating it also may contribute towards dimer stability. Further analysis of this double mutant and the triple mutant (S→Q, H→P, Q→L) is underway.

Very recently a second crystal structure of human cysteine desulfurase revealed an IscS type architecture (closed architecture) complicating our understanding. We then looked into some active site residues that may explain the low activity of human cysteine desulfurase. We exchanged the residues between IscS and NFS1 and none of the variants in IscS showed activity similar to SDA. This strongly suggests this architecture may an artifact of crystallization and may not be physiologically relevant.

REFERENCES

1. Vorholt, J. A.; Vaupel, M.; Thauer, R. K., A polyferredoxin with eight [4Fe-4S] clusters as a subunit of molybdenum formylmethanofuran dehydrogenase from Methanosarcina barkeri. *European Journal of Biochemistry* **1996,** *236* (1), 309-317.

2. Steigerwald, V. J.; Pihl, T. D.; Reeve, J. N., Identification and Isolation of the Polyferredoxin from Methanobacterium-Thermoautotrophicum Strain Delta-H. *P Natl Acad Sci USA* **1992,** *89* (15), 6929-6933.

3. Jacobson, M. R.; Brigle, K. E.; Bennett, L. T.; Setterquist, R. A.; Wilson, M. S.; Cash, V. L.; Beynon, J.; Newton, W. E.; Dean, D. R., Physical and Genetic-Map of the Major Nif Gene-Cluster from Azotobacter-Vinelandii. *J Bacteriol* **1989,** *171* (2), 1017-1027.

4. Jacobson, M. R.; Cash, V. L.; Weiss, M. C.; Laird, N. F.; Newton, W. E.; Dean, D. R., Biochemical and Genetic-Analysis of the Nifusvwzm Cluster from Azotobacter-Vinelandii. *Mol Gen Genet* **1989,** *219* (1-2), 49-57.

5. Zheng, L. M.; White, R. H.; Cash, V. L.; Jack, R. F.; Dean, D. R., Cysteine Desulfurase Activity Indicates a Role for Nifs in Metallocluster Biosynthesis. *P Natl Acad Sci USA* **1993,** *90* (7), 2754-2758.

6. Fu, W. G.; Jack, R. F.; Morgan, T. V.; Dean, D. R.; Johnson, M. K., Nifu Gene-Product from Azotobacter-Vinelandii Is a Homodimer That Contains 2 Identical [2fe-2s] Clusters. *Biochemistry* **1994,** *33* (45), 13455-13463.

7. Tokumoto, U.; Takahashi, Y., Genetic analysis of the isc operon in Escherichia coli involved in the biogenesis of cellular iron-sulfur protein. *J Biochem-Tokyo* **2001,** *130* (1), 63-71.

8. Zheng, L. M.; Cash, V. L.; Flint, D. H.; Dean, D. R., Assembly of iron-sulfur clusters - Identification of an iscSUA-hscBA-fdx gene cluster from Azotobacter vinelandii. *Journal of Biological Chemistry* **1998,** *273* (21), 13264-13272.

9. Takahashi, Y.; Nakamura, M., Functional assignment of the ORF2-iscS-iscU-iscA-hscB-hscA-fdx-ORF3 gene cluster involved in the assembly of Fe-S clusters in Escherichia coli. *J Biochem-Tokyo* **1999,** *126* (5), 917-926.

10. Schwartz, C. J.; Djaman, O.; Imlay, J. A.; Kiley, P. J., The cysteine desulfurase, IscS, has a major role in in vivo Fe-S cluster formation in Escherichia coli. *P Natl Acad Sci USA* **2000,** *97* (16), 9009-9014.

11. Krebs, C.; Agar, J. N.; Smith, A. D.; Frazzon, J.; Dean, D. R.; Huynh, B. H.; Johnson, M. K., IscA, an alternate scaffold for Fe-S cluster biosynthesis. *Biochemistry* **2001,** *40* (46), 14069-14080.

12. Kaut, A.; Lange, H.; Diekert, K.; Kispal, G.; Lill, R., Isa1p is a component of the mitochondrial machinery for maturation of cellular iron-sulfur proteins and requires conserved cysteine residues for function. *Journal of Biological Chemistry* **2000,** *275* (21), 15955-15961.

13. Ollagnier-de-Choudens, S.; Mattioli, T.; Tagahashi, Y.; Fontecave, M., Iron-sulfur cluster assembly - Characterization of IscA and evidence for a specific and functional complex with ferredoxin. *Journal of Biological Chemistry* **2001,** *276* (25), 22604-22607.

14. Wollenberg, M.; Berndt, C.; Bill, E.; Schwenn, J. D.; Seidler, A., A dimer of the FeS cluster biosynthesis protein IscA from cyanobacteria binds a [2Fe2S] cluster between two protomers and transfers it to [2Fe2S] and [4Fe4S] apo proteins. *Eur J Biochem* **2003,** *270* (8), 1662-71.

15. Tan, G.; Lu, J.; Bitoun, J. P.; Huang, H.; Ding, H., IscA/SufA paralogues are required for the [4Fe-4S] cluster assembly in enzymes of multiple physiological pathways in Escherichia coli under aerobic growth conditions. *The Biochemical journal* **2009,** *420* (3), 463-72.

16. Hoff, K. G.; Silberg, J. J.; Vickery, L. E., Interaction of the iron-sulfur cluster assembly protein IscU with the Hsc66/Hsc20 molecular chaperone system of Escherichia coli. *P Natl Acad Sci USA* **2000,** *97* (14), 7790-7795.

17. Kim, J. H.; Fuzery, A. K.; Tonelli, M.; Ta, D. T.; Westler, W. M.; Vickery, L. E.; Markley, J. L., Structure and Dynamics of the Iron-Sulfur Cluster Assembly Scaffold Protein IscU and Its Interaction with the Cochaperone HscB. *Biochemistry* **2009,** *48* (26), 6062-6071.

18. Chandramouli, K.; Johnson, M. K., HscA and HscB stimulate [2Fe-2S] cluster transfer from IscU to apoferredoxin in an ATP-dependent reaction. *Biochemistry* **2006,** *45* (37), 11087-11095.

19. Nakamura, M.; Saeki, K.; Takahashi, Y., Hyperproduction of recombinant ferredoxins in Escherichia coli by coexpression of the ORF1-ORF2-iscS-iscU-iscA-hscB-hscA-fdx-ORF3 gene cluster. *J Biochem-Tokyo* **1999,** *126* (1), 10-18.

20. Kispal, G.; Csere, P.; Prohl, C.; Lill, R., The mitochondrial proteins Atm1p and Nfs1p are essential for biogenesis of cytosolic Fe/S proteins. *Embo J* **1999,** *18* (14), 3981-3989.

21. Adam, A. C.; Bornhovd, C.; Prokisch, H.; Neupert, W.; Hell, K., The Nfs1 interacting protein Isd11 has an essential role in Fe/S cluster biogenesis in mitochondria. *Embo J* **2006,** *25* (1), 174-183.

22. Lange, H.; Kaut, A.; Kispal, G.; Lill, R., A mitochondrial ferredoxin is essential for biogenesis of cellular iron-sulfur proteins. *P Natl Acad Sci USA* **2000,** *97* (3), 1050-1055.

23. Lambeth, J. D.; Mccaslin, D. R.; Kamin, H., Adrenodoxin Reductase Adrenodoxin Complex - Catalytic and Thermodynamic Properties. *Journal of Biological Chemistry* **1976,** *251* (23), 7545-7550.

24. Uhrigshardt, H.; Singh, A.; Kovtunovych, G.; Ghosh, M.; Rouault, T. A., Characterization of the human HSC20, an unusual DnaJ type III protein, involved in iron-sulfur cluster biogenesis. *Human molecular genetics* **2010,** *19* (19), 3816-3834.

25. Song, D. S.; Tu, Z.; Lee, F. S., Human ISCA1 Interacts with IOP1/NARFL and Functions in Both Cytosolic and Mitochondrial Iron-Sulfur Protein Biogenesis. *Journal of Biological Chemistry* **2009,** *284* (51), 35297-35307.

26. Bekri, S.; Kispal, G.; Lange, H.; Fitzsimons, E.; Tolmie, J.; Lill, R.; Bishop, D. F., Human ABC7 transporter: gene structure and mutation causing X-linked sideroblastic anemia with ataxia with disruption of cytosolic iron-sulfur protein maturation. *Blood* **2000,** *96* (9), 3256-3264.

27. Muhlenhoff, U.; Balk, J.; Richhardt, N.; Kaiser, J. T.; Sipos, K.; Kispal, G.; Lill, R., Functional characterization of the eukaryotic cysteine desulfurase Nfs1p from Saccharomyces cerevisiae. *Journal of Biological Chemistry* **2004,** *279* (35), 36906-36915.

28. Wiedemann, N.; Urzica, E.; Guiard, B.; Muller, H.; Lohaus, C.; Meyer, H. E.; Ryan, M. T.; Meisinger, C.; Muhlenhoff, U.; Lill, R.; Pfanner, N., Essential role of Isd11 in mitochondrial iron-sulfur cluster synthesis on Isu scaffold proteins. *Embo J* **2006,** *25* (1), 184-195.

29. Shi, Y. B.; Ghosh, M. C.; Tong, W. H.; Rouault, T. A., Human ISD11 is essential for both iron-sulfur cluster assembly and maintenance of normal cellular iron homeostasis. *Human molecular genetics* **2009,** *18* (16), 3014-3025.

30. Pandey, A.; Yoon, H.; Lyver, E. R.; Dancis, A.; Pain, D., Isd11p protein activates the mitochondrial cysteine desulfurase Nfs1p protein. *The Journal of biological chemistry* **2011,** *286* (44), 38242-52.

31. Pandey, A.; Gordon, D. M.; Pain, J.; Stemmler, T. L.; Dancis, A.; Pain, D., Frataxin directly stimulates mitochondrial cysteine desulfurase by exposing substrate-binding sites, and a mutant Fe-S cluster scaffold protein with frataxin-bypassing ability acts similarly. *The Journal of biological chemistry* **2013,** *288* (52), 36773-86.

32. Pandey, A.; Golla, R.; Yoon, H.; Dancis, A.; Pain, D., Persulfide formation on mitochondrial cysteine desulfurase: enzyme activation by a eukaryote-specific interacting protein and Fe-S cluster synthesis. *The Biochemical journal* **2012,** *448* (2), 171-87.

33. Cory, S. A.; Van Vranken, J. G.; Brignole, E. J.; Patra, S.; Winge, D. R.; Drennan, C. L.; Rutter, J.; Barondeau, D. P., Structure of human Fe-S assembly subcomplex reveals unexpected cysteine desulfurase architecture and acyl-ACP-ISD11 interactions. *Proc Natl Acad Sci U S A* **2017,** *114* (27), E5325-E5334.

34. Brancaccio, D.; Gallo, A.; Mikolajczyk, M.; Zovo, K.; Palumaa, P.; Novellino, E.; Piccioli, M.; Ciofi-Baffoni, S.; Banci, L., Formation of [4Fe-4S] Clusters in the Mitochondrial Iron-Sulfur Cluster Assembly Machinery. *Journal of the American Chemical Society* **2014,** *136* (46), 16240-16250.

35. Sheftel, A. D.; Wilbrecht, C.; Stehling, O.; Niggemeyer, B.; Elsasser, H. P.; Muhlenhoff, U.; Lill, R., The human mitochondrial ISCA1, ISCA2, and IBA57 proteins are required for [4Fe-4S] protein maturation. *Molecular biology of the cell* **2012,** *23* (7), 1157-1166.

36. Ding, H.; Clark, R. J., Characterization of iron binding in IscA, an ancient iron-sulphur cluster assembly protein. *The Biochemical journal* **2004,** *379* (Pt 2), 433-40.

37. Lu, J. X.; Bitoun, J. P.; Tan, G. Q.; Wang, W.; Min, W. G.; Ding, H. G., Iron-binding activity of human iron-sulfur cluster assembly protein hIscA1. *Biochemical Journal* **2010,** *428*, 125-131.

38. Campuzano, V.; Montermini, L.; Molto, M. D.; Pianese, L.; Cossee, M.; Cavalcanti, F.; Monros, E.; Rodius, F.; Duclos, F.; Monticelli, A.; Zara, F.; Canizares, J.; Koutnikova, H.; Bidichandani, S. I.; Gellera, C.; Brice, A.; Trouillas, P.; DeMichele, G.; Filla, A.; DeFrutos, R.; Palau, F.; Patel, P. I.; DiDonato, S.; Mandel, J. L.; Cocozza, S.; Koenig, M.; Pandolfo, M., Friedreich's ataxia: Autosomal recessive disease caused by an intronic GAA triplet repeat expansion. *Science* **1996,** *271* (5254), 1423-1427.

39. Durr, A.; Cossee, M.; Agid, Y.; Campuzano, V.; Mignard, C.; Penet, C.; Mandel, J. L.; Brice, A.; Koenig, M., Clinical and genetic abnormalities in patients with Friedreich's ataxia. *New Engl J Med* **1996,** *335* (16), 1169-1175.

40. Filla, A.; DeMichele, G.; Cavalcanti, F.; Pianese, L.; Monticelli, A.; Campanella, G.; Cocozza, S., The relationship between trinucleotide (GAA) repeat length and clinical features in friedreich ataxia. *Am J Hum Genet* **1996,** *59* (3), 554-560.

41. Cossee, M.; Durr, A.; Schmitt, M.; Dahl, N.; Trouillas, P.; Allinson, P.; Kostrzewa, M.; Nivelon-Chevallier, A.; Gustavson, K. H.; Kohlschutter, A.; Muller, U.; Mandel, J. L.; Brice, A.; Koenig, M.; Cavalcanti, F.; Tammaro, A.; De Michele, G.; Filla, A.; Cocozza, S.; Labuda, M.; Montermini, L.; Poirier, J.; Pandolfo, M., Friedreich's ataxia: Point mutations and clinical presentation of compound heterozygotes. *Annals of Neurology* **1999,** *45* (2), 200-206.

42. Priller, J.; Scherzer, C. R.; Faber, P. W.; MacDonald, M. E.; Young, A. B., Frataxin gene of Friedreich's ataxia is targeted to mitochondria. *Ann Neurol* **1997,** *42* (2), 265-9.

43. Koutnikova, H.; Campuzano, V.; Foury, F.; Dolle, P.; Cazzalini, O.; Koenig, M., Studies of human, mouse and yeast homologues indicate a mitochondrial function for frataxin. *Nat Genet* **1997,** *16* (4), 345-51.

44. Koutnikova, H.; Campuzano, V.; Koenig, M., Maturation of wild-type and mutated frataxin by the mitochondrial processing peptidase. *Human molecular genetics* **1998,** *7* (9), 1485-9.

45. Cavadini, P.; Adamec, J.; Taroni, F.; Gakh, O.; Isaya, G., Two-step processing of human frataxin by mitochondrial processing peptidase - Precursor and intermediate forms are cleaved at different rates. *Journal of Biological Chemistry* **2000,** *275* (52), 41469-41475.

46. Schmucker, S.; Argentini, M.; Carelle-Calmels, N.; Martelli, A.; Puccio, H., The in vivo mitochondrial two-step maturation of human frataxin. *Human molecular genetics* **2008,** *17* (22), 3521-3531.

47. Branda, S. S.; Cavadini, P.; Adamec, J.; Kalousek, F.; Taroni, F.; Isaya, G., Yeast and human frataxin are processed to mature form in two sequential steps by the mitochondrial processing peptidase. *Journal of Biological Chemistry* **1999,** *274* (32), 22763-22769.

48. Geissler, A.; Krimmer, T.; Schonfisch, B.; Meijer, M.; Rassow, J., Biogenesis of the yeast frataxin homolog Yfh1p. Tim44-dependent transfer to mtHsp70 facilitates folding of newly imported proteins in mitochondria. *Eur J Biochem* **2000,** *267* (11), 3167-80.

49. Cavadini, P.; Gellera, C.; Patel, P. I.; Isaya, G., Human frataxin maintains mitochondrial iron homeostasis in Saccharomyces cerevisiae. *Human molecular genetics* **2000,** *9* (17), 2523-30.

50. Radisky, D. C.; Babcock, M. C.; Kaplan, J., The yeast frataxin homologue mediates mitochondrial iron efflux. Evidence for a mitochondrial iron cycle. *The Journal of biological chemistry* **1999,** *274* (8), 4497-9.

51. Park, S.; Gakh, O.; O'Neill, H. A.; Mangravita, A.; Nichol, H.; Ferreira, G. C.; Isaya, G., Yeast frataxin sequentially chaperones and stores iron by coupling protein assembly with iron oxidation. *Journal of Biological Chemistry* **2003,** *278* (33), 31340-31351.

52. Foury, F.; Talibi, D., Mitochondrial control of iron homeostasis - A genome wide analysis of gene expression in a yeast frataxin-deficient strain. *Journal of Biological Chemistry* **2001,** *276* (11), 7762-7768.

53. YamaguchiIwai, Y.; Stearman, R.; Dancis, A.; Klausner, R. D., Iron-regulated DNA binding by the AFT1 protein controls the iron regulon in yeast. *Embo J* **1996,** *15* (13), 3377-3384.

54. Blaiseau, P. L.; Lesuisse, E.; Camadro, J. M., Aft2p, a novel iron-regulated transcription activator that modulates, with Aft1p, intracellular iron use and resistance to oxidative stress in yeast. *Journal of Biological Chemistry* **2001,** *276* (36), 34221-34226.

55. Gakh, O.; Park, S.; Liu, G.; Macomber, L.; Imlay, J. A.; Ferreira, G. C.; Isaya, G., Mitochondrial iron detoxification is a primary function of frataxin that limits oxidative damage and preserves cell longevity. *Human molecular genetics* **2006,** *15* (3), 467-479.

56. O'Neill, H. A.; Gakh, O.; Park, S.; Cui, J.; Mooney, S. M.; Sampson, M.; Ferreira, G. C.; Isaya, G., Assembly of human frataxin is a mechanism to detoxify redox-active iron. *Free Radical Bio Med* **2004,** *37*, S21-S22.

57. Rotig, A.; deLonlay, P.; Chretien, D.; Foury, F.; Koenig, M.; Sidi, D.; Munnich, A.; Rustin, P., Aconitase and mitochondrial iron-sulphur protein deficiency in Friedreich ataxia. *Nature Genetics* **1997,** *17* (2), 215-217.

58. Huynen, M. A.; Snel, B.; Bork, P.; Gibson, T. J., The phylogenetic distribution of frataxin indicates a role in iron-sulfur cluster protein assembly. *Human molecular genetics* **2001,** *10* (21), 2463-2468.

59. Muhlenhoff, U.; Richhardt, N.; Ristow, M.; Kispal, G.; Lill, R., The yeast frataxin homolog Yfh1p plays a specific role in the maturation of cellular Fe/S proteins. *Human molecular genetics* **2002,** *11* (17), 2025-36.

60. Stehling, O.; Elsasser, H. P.; Bruckel, B.; Muhlenhoff, U.; Lill, R., Iron-sulfur protein maturation in human cells: evidence for a function of frataxin. *Human molecular genetics* **2004,** *13* (23), 3007-3015.

61. Cook, J. D.; Bencze, K. Z.; Jankovic, A. D.; Crater, A. K.; Busch, C. N.; Bradley, P. B.; Stemmler, A. J.; Spaller, M. R.; Stemmler, T. L., Monomeric yeast frataxin is an iron-binding protein. *Biochemistry* **2006,** *45* (25), 7767-7777.

62. Bulteau, A. L.; O'Neill, H. A.; Kennedy, M. C.; Ikeda-Saito, M.; Isaya, G.; Szweda, L. I., Frataxin acts as an iron chaperone protein to modulate mitochondrial aconitase activity. *Science* **2004,** *305* (5681), 242-245.

63. Kondapalli, K. C.; Kok, N. M.; Dancis, A.; Stemmler, T. L., Drosophila frataxin: an iron chaperone during cellular Fe-S cluster bioassembly. *Biochemistry* **2008,** *47* (26), 6917-27.

64. Yoon, T.; Cowan, J. A., Iron-sulfur cluster biosynthesis. Characterization of frataxin as an iron donor for assembly of [2Fe-2S] clusters in ISU-type proteins. *Journal of the American Chemical Society* **2003,** *125* (20), 6078-6084.

65. Pastore, C.; Franzese, M.; Sica, F.; Temussi, P.; Pastore, A., Understanding the binding properties of an unusual metal-binding protein - a study of bacterial frataxin. *Febs Journal* **2007,** *274* (16), 4199-4210.

66. Adinolfi, S.; Trifuoggi, M.; Politou, A. S.; Martin, S.; Pastore, A., A structural approach to understanding the iron-binding properties of phylogenetically different frataxins. *Human molecular genetics* **2002,** *11* (16), 1865-77.

67. Cavadini, P.; O'Neill, H. A.; Benada, O.; Isaya, G., Assembly and iron-binding properties of human frataxin, the protein deficient in Friedreich ataxia. *Human molecular genetics* **2002,** *11* (3), 217-227.

68. Seguin, A.; Sutak, R.; Bulteau, A. L.; Garcia-Serres, R.; Oddou, J. L.; Lefevre, S.; Santos, R.; Dancis, A.; Camadro, J. M.; Latour, J. M.; Lesuisse, E., Evidence that yeast frataxin is not an iron storage protein in vivo. *Biochim Biophys Acta* **2010,** *1802* (6), 531-8.

69. Schmucker, S.; Martelli, A.; Colin, F.; Page, A.; Wattenhofer-Donze, M.; Reutenauer, L.; Puccio, H., Mammalian Frataxin: An Essential Function for Cellular Viability through an Interaction with a Preformed ISCU/NFS1/ISD11 Iron-Sulfur Assembly Complex. *PloS one* **2011,** *6* (1).

70. Tsai, C. L.; Barondeau, D. P., Human Frataxin Is an Allosteric Switch That Activates the Fe-S Cluster Biosynthetic Complex. *Biochemistry* **2010,** *49* (43), 9132-9139.

71. Shan, Y. X.; Napoli, E.; Cortopassi, G., Mitochondrial frataxin interacts with ISD11 of the NFS1/ISCU complex and multiple mitochondrial chaperones. *Human molecular genetics* **2007,** *16* (8), 929-941.

72. Colin, F.; Martelli, A.; Clemancey, M.; Latour, J. M.; Gambarelli, S.; Zeppieri, L.; Birck, C.; Page, A.; Puccio, H.; Ollagnier de Choudens, S., Mammalian frataxin controls sulfur production and iron entry during de novo Fe4S4 cluster assembly. *Journal of the American Chemical Society* **2013,** *135* (2), 733-40.

73. Tsai, C. L.; Bridwell-Rabb, J.; Barondeau, D. P., Friedreich's ataxia variants I154F and W155R diminish frataxin-based activation of the iron-sulfur cluster assembly complex. *Biochemistry* **2011,** *50* (29), 6478-87.

74. Bridwell-Rabb, J.; Winn, A. M.; Barondeau, D. P., Structure-function analysis of Friedreich's ataxia mutants reveals determinants of frataxin binding and activation of the Fe-S assembly complex. *Biochemistry* **2011,** *50* (33), 7265-74.

75. Adinolfi, S.; Iannuzzi, C.; Prischi, F.; Pastore, C.; Iametti, S.; Martin, S. R.; Bonomi, F.; Pastore, A., Bacterial frataxin CyaY is the gatekeeper of iron-sulfur cluster formation catalyzed by IscS. *Nat Struct Mol Biol* **2009,** *16* (4), 390-396.

76. Bridwell-Rabb, J.; Iannuzzi, C.; Pastore, A.; Barondeau, D. P., Effector role reversal during evolution: the case of frataxin in Fe-S cluster biosynthesis. *Biochemistry* **2012,** *51* (12), 2506-14.

77. Bridwell-Rabb, J.; Fox, N. G.; Tsai, C. L.; Winn, A. M.; Barondeau, D. P., Human frataxin activates Fe-S cluster biosynthesis by facilitating sulfur transfer chemistry. *Biochemistry* **2014,** *53* (30), 4904-13.

78. Parent, A.; Elduque, X.; Cornu, D.; Belot, L.; Le Caer, J. P.; Grandas, A.; Toledano, M. B.; D'Autreaux, B., Mammalian frataxin directly enhances sulfur transfer of NFS1 persulfide to both ISCU and free thiols. *Nat Commun* **2015,** *6*.

79. Yoon, H.; Golla, R.; Lesuisse, E.; Pain, J.; Donald, J. E.; Lyver, E. R.; Pain, D.; Dancis, A., Mutation in the Fe-S scaffold protein Isu bypasses frataxin deletion. *The Biochemical journal* **2012,** *441* (1), 473-80.

80. Kato, S.; Mihara, H.; Kurihara, T.; Takahashi, Y.; Tokumoto, U.; Yoshimura, T.; Esaki, N., Cys-328 of IscS and Cys-63 of IscU are the sites of disulfide bridge formation in a covalently bound IscS/IscU complex: implications for the mechanism of iron-sulfur cluster assembly. *Proc Natl Acad Sci U S A* **2002,** *99* (9), 5948-52.

81. Smith, A. D.; Frazzon, J.; Dean, D. R.; Johnson, M. K., Role of conserved cysteines in mediating sulfur transfer from IscS to IscU. *FEBS letters* **2005,** *579* (23), 5236-5240.

82. Muhlenhoff, U.; Richhardt, N.; Gerber, J.; Lill, R., Characterization of iron-sulfur protein assembly in isolated mitochondria - A requirement for ATP, NADH, and reduced iron. *Journal of Biological Chemistry* **2002,** *277* (33), 29810-29816.

83. Sheftel, A. D.; Stehling, O.; Pierik, A. J.; Elsasser, H. P.; Muhlenhoff, U.; Webert, H.; Hobler, A.; Hannemann, F.; Bernhardt, R.; Lill, R., Humans possess two mitochondrial ferredoxins, Fdx1 and Fdx2, with distinct roles in steroidogenesis, heme, and Fe/S cluster biosynthesis. *P Natl Acad Sci USA* **2010,** *107* (26), 11775-11780.

84. Shi, Y. B.; Ghosh, M.; Kovtunovych, G.; Crooks, D. R.; Rouault, T. A., Both human ferredoxins 1 and 2 and ferredoxin reductase are important for iron-sulfur cluster biogenesis. *Bba-Mol Cell Res* **2012,** *1823* (2), 484-492.

85. Webert, H.; Freibert, S. A.; Gallo, A.; Heidenreich, T.; Linne, U.; Amlacher, S.; Hurt, E.; Muhlenhoff, U.; Banci, L.; Lill, R., Functional reconstitution of mitochondrial Fe/S cluster synthesis on Isu1 reveals the involvement of ferredoxin. *Nat Commun* **2014,** *5*.

86. Yan, R.; Adinolfi, S.; Pastore, A., Ferredoxin, in conjunction with NADPH and ferredoxin-NADP reductase, transfers electrons to the IscS/IscU complex to promote iron-sulfur cluster assembly. *Bba-Proteins Proteom* **2015,** *1854* (9), 1113-1117.

87. Kim, J. H.; Frederick, R. O.; Reinen, N. M.; Troupis, A. T.; Markley, J. L., [2Fe-2S]Ferredoxin Binds Directly to Cysteine Desulfurase and Supplies an Electron for Iron-Sulfur Cluster Assembly but Is Displaced by the Scaffold Protein or Bacterial Frataxin. *Journal of the American Chemical Society* **2013,** *135* (22), 8117-8120.

88. Cai, K.; Tonelli, M.; Frederick, R. O.; Markley, J. L., Human Mitochondrial Ferredoxin 1 (FDX1) and Ferredoxin 2 (FDX2) Both Bind Cysteine Desulfurase and Donate Electrons for Iron-Sulfur Cluster Biosynthesis. *Biochemistry* **2017**.

89. Agar, J. N.; Zheng, L. M.; Cash, V. L.; Dean, D. R.; Johnson, M. K., Role of the IscU protein in iron-sulfur cluster biosynthesis: IscS-mediated assembly of a [Fe2S2] cluster in IscU. *Journal of the American Chemical Society* **2000,** *122* (9), 2136-2137.

90. Pagnier, A.; Nicolet, Y.; Fontecilla-Camps, J. C., IscS from Archaeoglobus fulgidus has no desulfurase activity but may provide a cysteine ligand for [Fe2S2] cluster assembly. *Bba-Mol Cell Res* **2015,** *1853* (6), 1457-1463.

91. Foster, M. W.; Mansy, S. S.; Hwang, J.; Penner-Hahn, J. E.; Surerus, K. K.; Cowan, J. A., A mutant human IscU protein contains a stable [2Fe-2S](2+) center of possible functional significance. *Journal of the American Chemical Society* **2000,** *122* (28), 6805-6806.

92. Agar, J. N.; Krebs, C.; Frazzon, J.; Huynh, B. H.; Dean, D. R.; Johnson, M. K., IscU as a scaffold for iron-sulfur cluster biosynthesis: Sequential assembly of [2Fe-2S] and [4Fe-4S] clusters in IscU. *Biochemistry* **2000,** *39* (27), 7856-7862.

93. Lill, R., Function and biogenesis of iron-sulphur proteins. *Nature* **2009,** *460* (7257), 831-8.

94. Johnson, D. C.; Dean, D. R.; Smith, A. D.; Johnson, M. K., Structure, function, and formation of biological iron-sulfur clusters. *Annu Rev Biochem* **2005,** *74*, 247-81.

95. Van Vranken, J. G.; Jeong, M. Y.; Wei, P.; Chen, Y. C.; Gygi, S. P.; Winge, D. R.; Rutter, J., The mitochondrial acyl carrier protein (ACP) coordinates mitochondrial fatty acid synthesis with iron sulfur cluster biogenesis. *Elife* **2016,** *5*, e17828.

96. Wiedemann, N.; Urzica, E.; Guiard, B.; Muller, H.; Lohaus, C.; Meyer, H. E.; Ryan, M. T.; Meisinger, C.; Muhlenhoff, U.; Lill, R.; Pfanner, N., Essential role of Isd11 in mitochondrial iron-sulfur cluster synthesis on Isu scaffold proteins. *EMBO J* **2006,** *25* (1), 184-95.

97. Adam, A. C.; Bornhovd, C.; Prokisch, H.; Neupert, W.; Hell, K., The Nfs1 interacting protein Isd11 has an essential role in Fe/S cluster biogenesis in mitochondria. *EMBO J* **2006,** *25* (1), 174-83.

98. Shi, Y.; Ghosh, M. C.; Tong, W. H.; Rouault, T. A., Human ISD11 is essential for both iron-sulfur cluster assembly and maintenance of normal cellular iron homeostasis. *Hum Mol Genet* **2009,** *18* (16), 3014-25.

99. Terali, K.; Beavil, R. L.; Pickersgill, R. W.; van der Giezen, M., The effect of the adaptor protein Isd11 on the quaternary structure of the eukaryotic cysteine desulphurase Nfs1. *Biochem Biophys Res Commun* **2013,** *440* (2), 235-40.

100. Fox, N. G.; Chakrabarti, M.; McCormick, S. P.; Lindahl, P. A.; Barondeau, D. P., The Human Iron-Sulfur Assembly Complex Catalyzes the Synthesis of [2Fe-2S] Clusters on ISCU2 That Can Be Transferred to Acceptor Molecules. *Biochemistry* **2015,** *54* (25), 3871-9.

101. Stehling, O.; Elsasser, H. P.; Bruckel, B.; Muhlenhoff, U.; Lill, R., Iron-sulfur protein maturation in human cells: evidence for a function of frataxin. *Hum Mol Genet* **2004,** *13* (23), 3007-15.

102. Gerber, J.; Muhlenhoff, U.; Lill, R., An interaction between frataxin and Isu1/Nfs1 that is crucial for Fe/S cluster synthesis on Isu1. *EMBO Rep* **2003,** *4* (9), 906-11.

103. Campuzano, V.; Montermini, L.; Molto, M. D.; Pianese, L.; Cossee, M.; Cavalcanti, F.; Monros, E.; Rodius, F.; Duclos, F.; Monticelli, A.; Zara, F.; Canizares, J.; Koutnikova, H.; Bidichandani, S. I.; Gellera, C.; Brice, A.; Trouillas, P.; De Michele, G.; Filla, A.; De Frutos, R.; Palau, F.; Patel, P. I.; Di Donato, S.; Mandel, J. L.; Cocozza, S.; Koenig, M.; Pandolfo, M., Friedreich's ataxia: autosomal recessive disease caused by an intronic GAA triplet repeat expansion. *Science* **1996,** *271* (5254), 1423-7.

104. Schmucker, S.; Puccio, H., Understanding the molecular mechanisms of Friedreich's ataxia to develop therapeutic approaches. *Hum Mol Genet* **2010,** *19* (R1), R103-10.

105. Adamec, J.; Rusnak, F.; Owen, W. G.; Naylor, S.; Benson, L. M.; Gacy, A. M.; Isaya, G., Iron-dependent self-assembly of recombinant yeast frataxin: implications for Friedreich ataxia. *Am J Hum Genet* **2000,** *67* (3), 549-62.

106. Schagerlof, U.; Elmlund, H.; Gakh, O.; Nordlund, G.; Hebert, H.; Lindahl, M.; Isaya, G.; Al-Karadaghi, S., Structural basis of the iron storage function of frataxin from single-particle reconstruction of the iron-loaded oligomer. *Biochemistry* **2008,** *47* (17), 4948-54.

107. Gakh, O.; Adamec, J.; Gacy, A. M.; Twesten, R. D.; Owen, W. G.; Isaya, G., Physical evidence that yeast frataxin is an iron storage protein. *Biochemistry* **2002,** *41* (21), 6798-804.

108. Park, S.; Gakh, O.; Mooney, S. M.; Isaya, G., The ferroxidase activity of yeast frataxin. *J Biol Chem* **2002,** *277* (41), 38589-95.

109. Nichol, H.; Gakh, O.; O'Neill, H. A.; Pickering, I. J.; Isaya, G.; George, G. N., Structure of frataxin iron cores: an X-ray absorption spectroscopic study. *Biochemistry* **2003,** *42* (20), 5971-6.

110. Gakh, O.; Bedekovics, T.; Duncan, S. F.; Smith, D. Y. t.; Berkholz, D. S.; Isaya, G., Normal and Friedreich ataxia cells express different isoforms of frataxin with complementary roles in iron-sulfur cluster assembly. *The Journal of biological chemistry* **2010,** *285* (49), 38486-501.

111. Schmucker, S.; Martelli, A.; Colin, F.; Page, A.; Wattenhofer-Donze, M.; Reutenauer, L.; Puccio, H., Mammalian frataxin: an essential function for cellular viability through an interaction with a preformed ISCU/NFS1/ISD11 iron-sulfur assembly complex. *PLoS One* **2011,** *6* (1), e16199.

112. Zaidi, A.; Singh, K. P.; Anwar, S.; Suman, S. S.; Equbal, A.; Singh, K.; Dikhit, M. R.; Bimal, S.; Pandey, K.; Das, P.; Ali, V., Interaction of frataxin, an iron binding protein, with IscU of Fe-S clusters biogenesis pathway and its upregulation in AmpB resistant Leishmania donovani. *Biochimie* **2015,** *115*, 120-35.

113. Schmucker, S.; Argentini, M.; Carelle-Calmels, N.; Martelli, A.; Puccio, H., The in vivo mitochondrial two-step maturation of human frataxin. *Hum Mol Genet* **2008,** *17* (22), 3521-31.

114. Zhang, Y.; Lyver, E. R.; Knight, S. A.; Pain, D.; Lesuisse, E.; Dancis, A., Mrs3p, Mrs4p, and frataxin provide iron for Fe-S cluster synthesis in mitochondria. *J Biol Chem* **2006,** *281* (32), 22493-502.

115. Li, H.; Gakh, O.; Smith, D. Y. t.; Isaya, G., Oligomeric yeast frataxin drives assembly of core machinery for mitochondrial iron-sulfur cluster synthesis. *J Biol Chem* **2009,** *284* (33), 21971-80.

116. Yoon, T.; Cowan, J. A., Iron-sulfur cluster biosynthesis. Characterization of frataxin as an iron donor for assembly of [2Fe-2S] clusters in ISU-type proteins. *J Am Chem Soc* **2003,** *125* (20), 6078-84.

117. Yoon, T.; Dizin, E.; Cowan, J. A., N-terminal iron-mediated self-cleavage of human frataxin: regulation of iron binding and complex formation with target proteins. *J Biol Inorg Chem* **2007,** *12* (4), 535-42.

118. Huang, J.; Dizin, E.; Cowan, J. A., Mapping iron binding sites on human frataxin: implications for cluster assembly on the ISU Fe-S cluster scaffold protein. *J Biol Inorg Chem* **2008,** *13* (5), 825-36.

119. Rotig, A.; de Lonlay, P.; Chretien, D.; Foury, F.; Koenig, M.; Sidi, D.; Munnich, A.; Rustin, P., Aconitase and mitochondrial iron-sulphur protein deficiency in Friedreich ataxia. *Nat Genet* **1997,** *17* (2), 215-7.

120. Parent, A.; Elduque, X.; Cornu, D.; Belot, L.; Le Caer, J. P.; Grandas, A.; Toledano, M. B.; D'Autreaux, B., Mammalian frataxin directly enhances sulfur transfer of NFS1 persulfide to both ISCU and free thiols. *Nat Commun* **2015,** *6*, 5686.

121. Yoon, H.; Knight, S. A.; Pandey, A.; Pain, J.; Zhang, Y.; Pain, D.; Dancis, A., Frataxin-bypassing Isu1: characterization of the bypass activity in cells and mitochondria. *Biochem J* **2014,** *459* (1), 71-81.

122. Cai, K.; Frederick, R. O.; Tonelli, M.; Markley, J. L., Mitochondrial Cysteine Desulfurase and ISD11 Coexpressed in Escherichia coli Yield Complex Containing Acyl Carrier Protein. *Acs Chem Biol* **2017,** *12* (4), 918-921.

123. Fox, N. G.; Das, D.; Chakrabarti, M.; Lindahl, P. A.; Barondeau, D. P., Frataxin Accelerates [2Fe-2S] Cluster Formation on the Human Fe-S Assembly Complex. *Biochemistry* **2015,** *54* (25), 3880-9.

124. Bailey, T. S.; Zakharov, L. N.; Pluth, M. D., Understanding hydrogen sulfide storage: probing conditions for sulfide release from hydrodisulfides. *J Am Chem Soc* **2014,** *136* (30), 10573-6.

125. Zheng, L.; White, R. H.; Cash, V. L.; Jack, R. F.; Dean, D. R., Cysteine desulfurase activity indicates a role for NIFS in metallocluster biosynthesis. *Proc Natl Acad Sci U S A* **1993,** *90* (7), 2754-8.

126. Behshad, E.; Bollinger, J. M., Jr., Kinetic analysis of cysteine desulfurase CD0387 from Synechocystis sp. PCC 6803: formation of the persulfide intermediate. *Biochemistry* **2009,** *48* (50), 12014-23.

127. Zheng, L.; White, R. H.; Cash, V. L.; Dean, D. R., Mechanism for the desulfurization of L-cysteine catalyzed by the nifS gene product. *Biochemistry* **1994,** *33* (15), 4714-20.

128. Campuzano, V.; Montermini, L.; Lutz, Y.; Cova, L.; Hindelang, C.; Jiralerspong, S.; Trottier, Y.; Kish, S. J.; Faucheux, B.; Trouillas, P.; Authier, F. J.; Durr, A.; Mandel, J. L.; Vescovi, A.; Pandolfo, M.; Koenig, M., Frataxin is reduced in Friedreich ataxia patients and is associated with mitochondrial membranes. *Hum Mol Genet* **1997,** *6* (11), 1771-80.

129. Willis, J. H.; Isaya, G.; Gakh, O.; Capaldi, R. A.; Marusich, M. F., Lateral-flow immunoassay for the frataxin protein in Friedreich's ataxia patients and carriers. *Mol Genet Metab* **2008,** *94* (4), 491-7.

130. Deutsch, E. C.; Santani, A. B.; Perlman, S. L.; Farmer, J. M.; Stolle, C. A.; Marusich, M. F.; Lynch, D. R., A rapid, noninvasive immunoassay for frataxin: utility in assessment of Friedreich ataxia. *Mol Genet Metab* **2010,** *101* (2-3), 238-45.

131. Steinkellner, H.; Scheiber-Mojdehkar, B.; Goldenberg, H.; Sturm, B., A high throughput electrochemiluminescence assay for the quantification of frataxin protein levels. *Anal Chim Acta* **2010,** *659* (1-2), 129-32.

132. Sacca, F.; Puorro, G.; Antenora, A.; Marsili, A.; Denaro, A.; Piro, R.; Sorrentino, P.; Pane, C.; Tessa, A.; Brescia Morra, V.; Cocozza, S.; De Michele, G.; Santorelli, F. M.; Filla, A., A combined nucleic acid and protein analysis in Friedreich ataxia: implications for diagnosis, pathogenesis and clinical trial design. *PLoS One* **2011,** *6* (3), e17627.

133. Erwin, G. S.; Grieshop, M. P.; Ali, A.; Qi, J.; Lawlor, M.; Kumar, D.; Ahmad, I.; McNally, A.; Teider, N.; Worringer, K.; Sivasankaran, R.; Syed, D. N.; Eguchi, A.; Ashraf, M.; Jeffery, J.; Xu, M.; Park, P. M. C.; Mukhtar, H.; Srivastava, A. K.; Faruq, M.; Bradner, J. E.; Ansari, A. Z., Synthetic transcription elongation factors license transcription across repressive chromatin. *Science* **2017,** *358* (6370), 1617-1622.

134. Marmolino, D., Friedreich's ataxia: past, present and future. *Brain Res Rev* **2011,** *67* (1-2), 311-30.

135. Lill, R.; Hoffmann, B.; Molik, S.; Pierik, A. J.; Rietzschel, N.; Stehling, O.; Uzarska, M. A.; Webert, H.; Wilbrecht, C.; Muhlenhoff, U., The role of mitochondria in cellular iron-sulfur protein biogenesis and iron metabolism. *Biochim Biophys Acta* **2012,** *1823* (9), 1491-508.

136. Lindahl, P. A.; Moore, M. J., Labile Low-Molecular-Mass Metal Complexes in Mitochondria: Trials and Tribulations of a Burgeoning Field. *Biochemistry* **2016,** *55* (30), 4140-4153.

137. Turowski, V. R.; Busi, M. V.; Gomez-Casati, D. F., Structural and functional studies of the mitochondrial cysteine desulfurase from Arabidopsis thaliana. *Mol Plant* **2012,** *5* (5), 1001-10.

138. Webert, H.; Freibert, S. A.; Gallo, A.; Heidenreich, T.; Linne, U.; Amlacher, S.; Hurt, E.; Muhlenhoff, U.; Banci, L.; Lill, R., Functional reconstitution of mitochondrial Fe/S cluster synthesis on Isu1 reveals the involvement of ferredoxin. *Nat Commun* **2014,** *5*, 5013.

139. Manicki, M.; Majewska, J.; Ciesielski, S.; Schilke, B.; Blenska, A.; Kominek, J.; Marszalek, J.; Craig, E. A.; Dutkiewicz, R., Overlapping binding sites of the frataxin homologue assembly factor and the heat shock protein 70 transfer factor on the isu iron-sulfur cluster scaffold protein. *The Journal of biological chemistry* **2014,** *289* (44), 30268-78.

140. Boniecki, M. T.; Freibert, S. A.; Muhlenhoff, U.; Lill, R.; Cygler, M., Structure and functional dynamics of the mitochondrial Fe/S cluster synthesis complex. *Nat Commun* **2017,** *8* (1), 1287.

141. Adinolfi, S.; Iannuzzi, C.; Prischi, F.; Pastore, C.; Iametti, S.; Martin, S. R.; Bonomi, F.; Pastore, A., Bacterial frataxin CyaY is the gatekeeper of iron-sulfur cluster formation catalyzed by IscS. *Nat Struct Mol Biol* **2009,** *16* (4), 390-6.

142. Kaiser, J. T.; Clausen, T.; Bourenkow, G. P.; Bartunik, H. D.; Steinbacher, S.; Huber, R., Crystal structure of a NifS-like protein from Thermotoga maritima: implications for iron sulphur cluster assembly. *J Mol Biol* **2000,** *297* (2), 451-64.

143. Cupp-Vickery, J. R.; Urbina, H.; Vickery, L. E., Crystal structure of IscS, a cysteine desulfurase from Escherichia coli. *J Mol Biol* **2003,** *330* (5), 1049-59.

144. Marelja, Z.; Stocklein, W.; Nimtz, M.; Leimkuhler, S., A novel role for human Nfs1 in the cytoplasm: Nfs1 acts as a sulfur donor for MOCS3, a protein involved in molybdenum cofactor biosynthesis. *J Biol Chem* **2008,** *283* (37), 25178-85.

145. Miyazaki, K., MEGAWHOP cloning: a method of creating random mutagenesis libraries via megaprimer PCR of whole plasmids. *Methods Enzymol* **2011,** *498*, 399-406.

146. Vranish, J. N.; Russell, W. K.; Yu, L. E.; Cox, R. M.; Russell, D. H.; Barondeau, D. P., Fluorescent probes for tracking the transfer of iron-sulfur cluster and other metal cofactors in biosynthetic reaction pathways. *J Am Chem Soc* **2015,** *137* (1), 390-8.

147. Gill, S. C.; von Hippel, P. H., Calculation of protein extinction coefficients from amino acid sequence data. *Anal Biochem* **1989,** *182* (2), 319-26.

148. Siegel, L. M., A Direct Microdetermination for Sulfide. *Anal Biochem* **1965,** *11*, 126-32.

149. Fish, W. W., Rapid colorimetric micromethod for the quantitation of complexed iron in biological samples. *Methods Enzymol* **1988,** *158*, 357-64.

150. Beinert, H., Semi-micro methods for analysis of labile sulfide and of labile sulfide plus sulfane sulfur in unusually stable iron-sulfur proteins. *Anal Biochem* **1983,** *131* (2), 373-8.

151. Brzoska, K.; Meczynska, S.; Kruszewski, M., Iron-sulfur cluster proteins: electron transfer and beyond. *Acta Biochim Pol* **2006,** *53* (4), 685-91.

152. Py, B.; Barras, F., Building Fe-S proteins: bacterial strategies. *Nat Rev Microbiol* **2010,** *8* (6), 436-446.

153. Takahashi, Y.; Tokumoto, U., A third bacterial system for the assembly of iron-sulfur clusters with homologs in archaea and plastids. *Journal of Biological Chemistry* **2002,** *277* (32), 28380-28383.

154. Outten, F. W.; Djaman, O.; Storz, G., A suf operon requirement for Fe-S cluster assembly during iron starvation in Escherichia coli. *Molecular Microbiology* **2004,** *52* (3), 861-872.

155. Yang, J.; Bitoun, J. P.; Ding, H., Interplay of IscA and IscU in biogenesis of iron-sulfur clusters. *The Journal of biological chemistry* **2006,** *281* (38), 27956-63.

156. Ding, H.; Yang, J.; Coleman, L. C.; Yeung, S., Distinct iron binding property of two putative iron donors for the iron-sulfur cluster assembly: IscA and the bacterial frataxin ortholog CyaY under physiological and oxidative stress conditions. *The Journal of biological chemistry* **2007,** *282* (11), 7997-8004.

157. Kim, J. H.; Tonelli, M.; Frederick, R. O.; Chow, D. C.; Markley, J. L., Specialized Hsp70 chaperone (HscA) binds preferentially to the disordered form, whereas J-protein (HscB) binds preferentially to the structured form of the iron-sulfur cluster scaffold protein (IscU). *The Journal of biological chemistry* **2012,** *287* (37), 31406-13.

158. Knoell, H. E.; Knappe, J., Escherichia coli ferredoxin, an iron-sulfur protein of the adrenodoxin type. *Eur J Biochem* **1974,** *50* (1), 245-52.

159. Kim, J. H.; Bothe, J. R.; Frederick, R. O.; Holder, J. C.; Markley, J. L., Role of IscX in iron-sulfur cluster biogenesis in Escherichia coli. *Journal of the American Chemical Society* **2014,** *136* (22), 7933-42.

160. Roche, B.; Huguenot, A.; Barras, F.; Py, B., The iron-binding CyaY and IscX proteins assist the ISC-catalyzed Fe-S biogenesis in Escherichia coli. *Mol Microbiol* **2015,** *95* (4), 605-23.

161. Babcock, M.; de Silva, D.; Oaks, R.; Davis-Kaplan, S.; Jiralerspong, S.; Montermini, L.; Pandolfo, M.; Kaplan, J., Regulation of mitochondrial iron accumulation by Yfh1p, a putative homolog of frataxin. *Science* **1997,** *276* (5319), 1709-12.

162. Li, D. S.; Ohshima, K.; Jiralerspong, S.; Bojanowski, M. W.; Pandolfo, M., Knock-out of the cyaY gene in Escherichia coli does not affect cellular iron content and sensitivity to oxidants. *Febs Lett* **1999,** *456* (1), 13-6.

163. Vivas, E.; Skovran, E.; Downs, D. M., Salmonella enterica strains lacking the frataxin homolog CyaY show defects in Fe-S cluster metabolism in vivo. *J Bacteriol* **2006,** *188* (3), 1175-1179.

164. Pohl, T.; Walter, J.; Stolpe, S.; Soufo, J. H.; Grauman, P. L.; Friedrich, T., Effects of the deletion of the Escherichia coli frataxin homologue CyaY on the respiratory NADH:ubiquinone oxidoreductase. *BMC Biochem* **2007,** *8*, 13.

165. Roche, B.; Agrebi, R.; Huguenot, A.; de Choudens, S. O.; Barras, F.; Py, B., Turning Escherichia coli into a Frataxin-Dependent Organism. *Plos Genet* **2015,** *11* (5).

166. Iannuzzi, C.; Adinolfi, S.; Howes, B. D.; Garcia-Serres, R.; Clemancey, M.; Latour, J. M.; Smulevich, G.; Pastore, A., The role of CyaY in iron sulfur cluster assembly on the E. coli IscU scaffold protein. *PloS one* **2011,** *6* (7), e21992.

167. di Maio, D.; Chandramouli, B.; Yan, R.; Brancato, G.; Pastore, A., Understanding the role of dynamics in the iron sulfur cluster molecular machine. *Bba-Gen Subjects* **2017,** *1861* (1), 3154-3163.

168. Skovran, E.; Lauhon, C. T.; Downs, D. M., Lack of YggX results in chronic oxidative stress and uncovers subtle defects in Fe-S cluster metabolism in Salmonella enterica. *J Bacteriol* **2004,** *186* (22), 7626-7634.

169. Gralnick, J. A.; Downs, D. M., The YggX protein of Salmonella enterica is involved in Fe(II) trafficking and minimizes the DNA damage caused by hydroxyl radicals - Residue Cys-7 is essential for YggX function. *Journal of Biological Chemistry* **2003,** *278* (23), 20708-20715.

170. Boyd, J. M.; Lewis, J. A.; Escalante-Semerena, J. C.; Downs, D. M., Salmonella enterica requires apbC function for growth on tricarballylate: Evidence of functional redundancy between apbC and iscU. *J Bacteriol* **2008,** *190* (13), 4596-4602.

171. Boyd, J. M.; Pierik, A. J.; Netz, D. J. A.; Lill, R.; Downs, D. M., Bacterial ApbC can bind and effectively transfer iron-sulfur clusters. *Biochemistry* **2008,** *47* (31), 8195-8202.

172. Boyd, J. M.; Drevland, R. M.; Downs, D. M.; Graham, D. E., Archaeal ApbC/Nbp35 Homologs Function as Iron-Sulfur Cluster Carrier Proteins. *J Bacteriol* **2009,** *191* (5), 1490-1497.

173. Boyd, J. M.; Sondelski, J. L.; Downs, D. M., Bacterial ApbC Protein Has Two Biochemical Activities That Are Required for in Vivo Function. *Journal of Biological Chemistry* **2009,** *284* (1), 110-118.

174. Kim, S. H.; Lee, B. Y.; Lau, G. W.; Cho, Y. H., IscR Modulates Catalase A (KatA) Activity, Peroxide Resistance, and Full Virulence of Pseudomonas aeruginosa PA14. *J Microbiol Biotechn* **2009,** *19* (12), 1520-1526.

175. Yoon, H.; Knight, S. A. B.; Pandey, A.; Pain, J.; Turkarslan, S.; Pain, D.; Dancis, A., Turning Saccharomyces cerevisiae into a Frataxin-Independent Organism. *Plos Genet* **2015,** *11* (5).

176. Vranish, J. N.; Das, D.; Barondeau, D. P., Real-Time Kinetic Probes Support Monothiol Glutaredoxins As Intermediate Carriers in Fe-S Cluster Biosynthetic Pathways. *Acs Chem Biol* **2016,** *11* (11), 3114-3121.

177. Van Vranken, J. G.; Jeong, M. Y.; Wei, P.; Chen, Y. C.; Gygi, S. P.; Winge, D. R.; Rutter, J., The mitochondrial acyl carrier protein (ACP) coordinates mitochondrial fatty acid synthesis with iron sulfur cluster biogenesis. *Elife* **2016,** *5*.

178. Margosiak, S. A.; Vanderpool, D. L.; Sisson, W.; Pinko, C.; Kan, C. C., Dimerization of the human cytomegalovirus protease: kinetic and biochemical characterization of the catalytic homodimer. *Biochemistry* **1996,** *35* (16), 5300-7.

179. Rouault, T. A.; Tong, W. H., Iron-sulfur cluster biogenesis and human disease. *Trends Genet* **2008,** *24* (8), 398-407.